UNIVERSITÀ CAMPUS BIO-MEDICO DI ROMA

PhD in SCIENCE AND ENGINEERING FOR HUMANS AND THE ENVIRONMENT

XXXIV cycle A.Y. 2018-2019

Curriculum: Bioengineering

PHYSICAL AND CHEMICAL FUNCTIONALIZATION OF HYDROGEL SYSTEMS TO IMPROVE CONTROLLED DRUG DELIVERY

PhD Candidate

Aurora Salvati

Supervisors

Prof. Marcella Trombetta

Dott. Francesco Basoli

Abstract

In this Ph.D. thesis we investigate macro and nano-hydrogels for controlled drug delivery. In particular, we first focus the attention on macro hydrogels physically functionalized with graphene, and then we consider nanogels chemically functionalized with different aromatic groups.

Indeed, new trends in drug delivery strategies have seen lately a considerable interest in the synthesis of graphene-based materials in order to design biomaterials promoting tunable drug release via electric or stretching stimuli. However, the design of a thermosensitive scaffold using pristine graphene has not been investigated yet, and it can be considered a promising approach for several therapeutic treatments, including hyperthermia. We present the fabrication of thermosensitive hydrogels where pristine nano-layered graphene (few layered graphene, FLG) is used as a nanofiller to investigate the graphene thermal effect in the drug release scenario. Hydrogels are synthesized in two steps: i) esterification between polyacrylic acid and agarose, under microwave irradiation, to activate the sol gel transition, and ii) incorporation of drug loaded FLG during sol-gel transition. Following a first check over hydrogel non-toxicity, according to ASTM 10399-5 standard, the drug release profile of the gels at different temperatures is investigated. The chosen drug is Diclofenac, an anti-inflammatory molecule used to treat musculoskeletal inflammations. The drug release profile is investigated at three different temperatures: 25, 37 and 44 °C. Results show that is possible to tune diclofenac release over time by modifying temperature. This response is not observed in polymeric scaffolds without FLG, suggesting that pristine graphene, due to its thermal conductivity and pi-conjugated chemical structure, is able to generate electronic interactions with both the polymeric matrix and the drug molecules, modulating the release profile of diclofenac.

Moreover, the anti-inflammatory performance of the released drug is evaluated in terms of cyclooxygenase (COX) inhibition, resulting in an efficiency comparable to the administration of free diclofenac in aqueous medium, which proves that the graphene interactions do not affect the therapeutic properties. Furthermore, the high biocompatibility of the synthesized graphene-laden hydrogels confirms their potential use as 3D scaffolds for thermally triggered drug release.

Regarding NGs the goal is to evaluate how NGs with different aromatic coatings may affect biocompatibility, chemical-physical properties, drug loading, drug release and cell uptake in a specific disease scenario. In particular, NGs are tested

on representative renal cell carcinoma T-786O in order to evaluate NGs cellular internalization with the purpose of developing an innovative approach based on the microfluidic system to mimic the effective condition on a potential *in vivo* administration. In detail, NGs synthesis is performed in batch by cross-linking reaction via emulsion-evaporation method and subsequently an aromatic surface functionalization is realized by three different aromatic layers. The obtained NGs are compared in terms of size, polydispersity index, biocompatibility and drug encapsulation efficiency. Regarding the latter, NGs are tested as nanocarriers for drug delivery using Sunitinib malate an FDA-approved drug for the treatment of kidney cancer. The NGs-drug interaction is investigated in terms of drug release varying the aromatic coating. In particular, different drug release profiles are obtained for each aromatic coating confirming the possibility of using the nanomaterial for intracellular controlled drug delivery. On the other hand, the NGs internalization, following a preliminary evaluation through the conventional flow cytometry analysis, is evaluated in vitro using the microfluidic system. The microfluidic-assisted NGs cell uptake is evaluated with two different approaches: static and dynamic conditions. In the first instance, NGs internalization is performed in static conditions to compared it with the conventional approach due to cell seeding occurs in a different environment and then under dynamic to estimate cell uptake in injection-like condition. The collected results showed how the selected aromatic coatings on NGs surface ensure a tunable drug delivery of Sunitinib and modulate the cellular internalization in T-786O cell line. Regarding the latter, the evaluation of NGs cell uptake in flow condition through the microfluidic system has revealed a different trend from the traditional approach, more similar to the effective injection-like conditions, suggesting the potential of this approach. Overall, these results demonstrated that through surface decoration with specific aromatic moieties it's possible to tune NG-cell interactions and the drug delivery performances, designing versatile nanosystems suitable for the definition of future therapeutic approaches.

The present thesis is divided into two different parts:

- Part I consists of three chapters and it focuses on the current state of the art on hydrogel for drug delivery (Chapter 1), on hydrogels with graphene (Chapter 2) and on nanocarriers for drug delivery (Chapter 3).

- Part II is devoted to the research activities, presenting the experimental methodology conducted for hydrogel with physical functionalization (Chapter 4)

and Nanogels with chemical functionalization (Chapter 5). Finally, the last Chapter 6 sums up and collects all the conclusions and proposes future developments to the present work.

Contents

Part I

State of the art

Chapter 1

Hydrogels for drug delivery and drug Release mechanism

1.1 Drug delivery

Drug delivery is becoming a whole interdisciplinary and independent field of research and is gaining the attention of pharmaceutical makers, medical doctors and industry.

The term "drug delivery" means the development of technologies for the transport of drugs, the drug delivery systems (DDS) [1]. DDS represent a milestone in the development of efficient therapeutic strategies for the modern healthcare scenario given their capacity to:

- target the release in a specific area of interest,
- improve effectiveness,
- reduce potential cytotoxic effects,
- check the times of administration of the drug,

The crucial role of DDS, is to convey the active agent to the target without variations in terms of structure and function and maintaining drug concentration into the therapeutic window to guarantee a therapeutic effect. The therapeutic window is defined between the minimum effective concentration (MEC) and the minimum toxic concentration (MTC). When a drug is administered in a single large dose, the level of the drug exceeds the MEC, causing toxic side-effects, and then rapidly falls below the MEC (Figure 1.1.1).

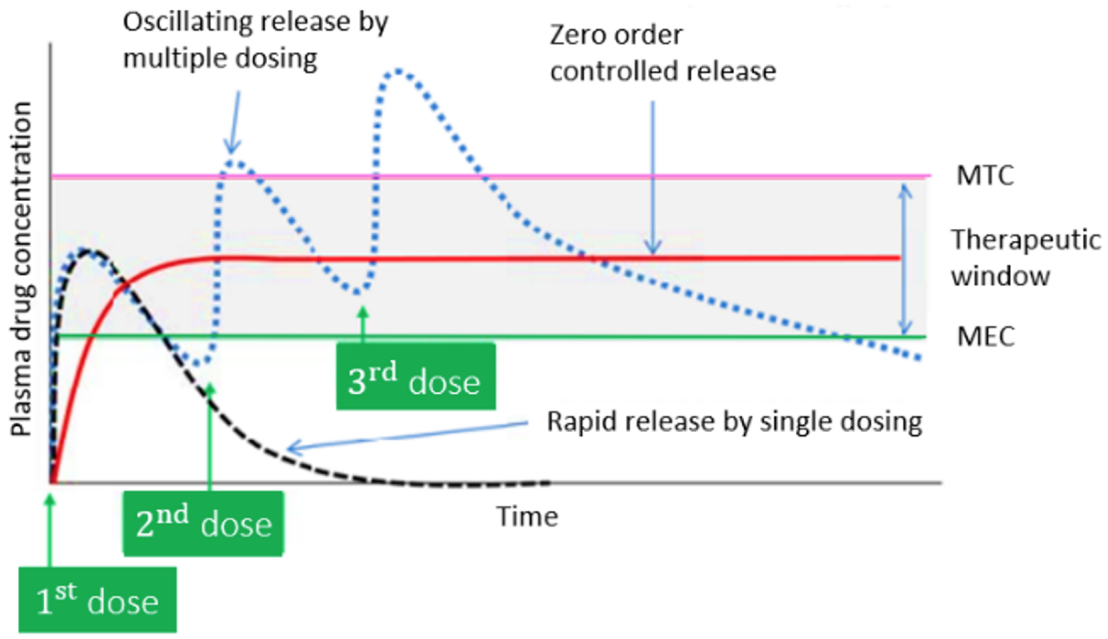

Figure 1.1.1: Plasma drug concentration profile obtained by single dosing, multiple dosing and zero order controlled release. The therapeutic window is where drug is effective without displaying toxicity. [2]

Undoubtedly multiple dosing with a certain interval can reduce the fluctuation of drug levels, but it may not be patient-compliance. Therefore, it is desirable to develop drug-carriers that provide sustained or controlled drug release with a low frequency. To this end, a constant drug release rate (zero order drug release profile) is often pursued [2, 3]. On the other hand, excessive attenuation in drug release can compromise the therapeutic efficacy. Controlled release systems have been proposed to improve drug efficacy. In these systems, drugs can be protected from premature elimination, facilitated to cross physiological barriers, and released in a controlled manner to maintain their effective concentration; therefore, pulsatile or stimuli-responsive drug release [4] is also used to achieve timely drug release.

Therefore, controlled drug delivery represents one of the most relevant opportunities for drug administration aiming to overcome the limitations of conventional drug somministration. In particular, the advantages of a DDS are:

- the protection and the stability of bioactive substances,
- the control of the kinetics and of the quantity released,

- the possibility of having a cellular selectivity,
- the reduction of side effects (invasiveness and overdose),
- the possibility of directing the release of the drug in a specific area avoiding contact between the drug and organs not involved, also known as "drug targeting": the drug is conveyed exclusively to the site of interest. In drug targeting, nanometric-sized devices, such as nanogels, are of particular interest, as they can identify the pathogenic cells, avoiding the healthy cells and tissues.

1.2 Hydrogels for drug delivery

Studying the DDS, researches have focused on systems allowing tunable pharmacokinetics and the efficacy of released active principles, generating a wide range of polymer-based biomaterials, such as hydrogels.

Hydrogels are commonly recognized as tailored three-dimensional (3D) cross-linked polymer networks. Their unique physical-chemical properties are essentially correlated to the porous structure and the high-water imbibing capacity: they guarantee the diffusion of drug payload and the exchange of ions and metabolites with tissues to maintain the biological chemical balance with the surrounding environment [5].

Hydrogels are made up of a cross-linked network of hydrophilic polymers chains that chemically bind to create a three dimensional structure, obtained from the simple reaction of monomers, forming a polymeric crosslink [6, 7]. They have been successful as drug delivery systems thanks to their swelling behaviour, their porous structure, high water imbimbing capacity, which allows an excellent ability to encapsulate hydrophilic drugs, and the introduction of filler materials in the polymer matrix, that improve their functions and properties. Most of them are non-toxic and biocompatible [8].

Their large water imbimbing capacity is due to terminal groups (e.g. $-OH$, $-CONH-$, $-CONH_2$, and $-SO_3H$) present in their structure [9].

Also, hydrogels are known as stimuli-responsive materials (SRMs), thanks to their tendency to modify their structure in response to external stimuli, such as exposure to magnetic fields, light, pressure, pH or temperature variation. Such stimuli-sensitive materials find applications in electrochemical, biomimetic, sound-absorbing devices,

actuators and sensors, smart medicine instruments. Several factors, such as the loss of hydrogen bonds and the progressive ionization in the polymeric matrix, influence the responses of hydrogels to external stimuli [10]. For biomedical applications, these materials must be biocompatible, biodegradable and must not cause any immune response under biological conditions [11].

1.2.1 Physico-chemical properties

The distinctive features of these smart materials are correlated to their physical-chemical properties that characterize them.

1.2.1.1 Swelling behaviour

The ability of hydrogels to absorb water derives from the hydrophilic functional groups, while their resistance to dissolution derives from the cross-linking between the network chains [12]. The high water content (typically 70-99%) provides a physical resemblance to human tissue, and can give hydrogels excellent biocompatibility and the ability to easily encapsulate hydrophilic drugs. Furthermore, the risk of drug denaturation and aggregation causing exposure to organic solvents is minimized [13]. The remarkable swelling capacity of hydrogels has been attributed to the disruption of hydrogen bonds between the polymeric matrix, resulting in increased chain mobility and network expansion [7].

1.2.1.2 Mechanical properties

Another attractive aspect of hydrogels is that the crosslinked chains in the gel are linked together to form a large molecule on a macroscopic scale. The gel is in a state that is neither completely liquid nor completely solid. These intermediate properties are responsible for many interesting behaviours not found in either a pure solid or liquid [12]. The stiffness is adjustable, and can vary [14] from 0.5 kPa to 5 MPa, allowing to exploit their physical properties to different soft tissues in the human body [15]. Furthermore, the mechanical and structural properties of hydrogels provide protection for drugs, preventing the penetration of various proteins [16] that could prematurely degrade the bioactive molecules.

1.2.1.3 Sensitivity to external stimuli

Hydrogels show changes in their volume in response to specific external stimuli, both physical and chemical. Among the physical ones we find temperature, electric or magnetic field, light, pressure and sound. While chemical stimuli include pH, solvent composition, ionic strength, molecular species, etc. (Figure 1.2.1). They have the capability of detect small changes in environmental conditions and they respond to the latter with a consequent swelling and de-swelling [17], through reversible changes in volume. Such volumetric variation behaviours of hydrogels have attracted considerable interest in the last three decades [12]. Functionalization is often required to increase the responsiveness of hydrogels to stimuli.

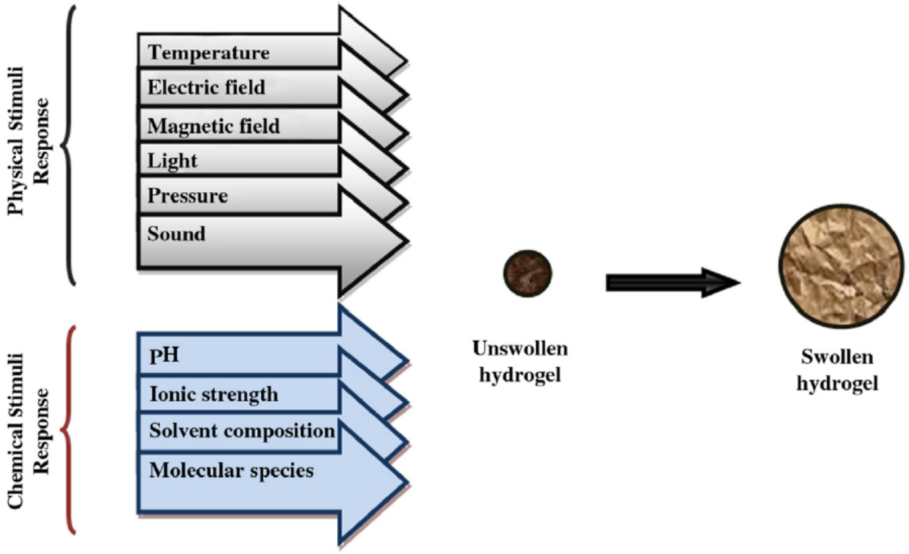

Figure 1.2.1: Volumetric response to physical and chemical stimuli of a hydrogel. [6]

1.2.1.4 Shape and size

Hydrogels differ in size and function; together, these characteristics determine how drugs are delivered. The hydrogels dimensions range from centimeters to sub-nanometers (Figure 1.2.2). Depending on their size, they can be classified in three categories: macroscopic hydrogels, microgels and nanogels. Microgels and nanogels are hydrogels with dimensions in the order of micrometers and nanometers, respectively. They can be designed in almost any size and shape. Micro-pores, with pore sizes of 10–500 μm, will greatly affect the physical properties (e.g., deformability)

(Figure 1.2.2A), while allowing the transport of drugs. The polymer network can have different mesh sizes, adjustable from about 5 to about 100 nm. Importantly, the mesh size regulates drug diffusion within the hydrogel network (Figure 1.2.2B). Finally, at the molecular and atomic scales, various chemical interactions can occur between drugs and polymer chains (Figure 1.2.2C). Polymer chains can have numerous sites for drug binding, and these can be functionalized using a variety of physical and chemical methods. The characteristics of the mesh scale and the molecular and atomic scale are essential for the controlled release of drugs. This multiscale nature can serve as a versatile platform to meet specific requirements based on the desired application [13].

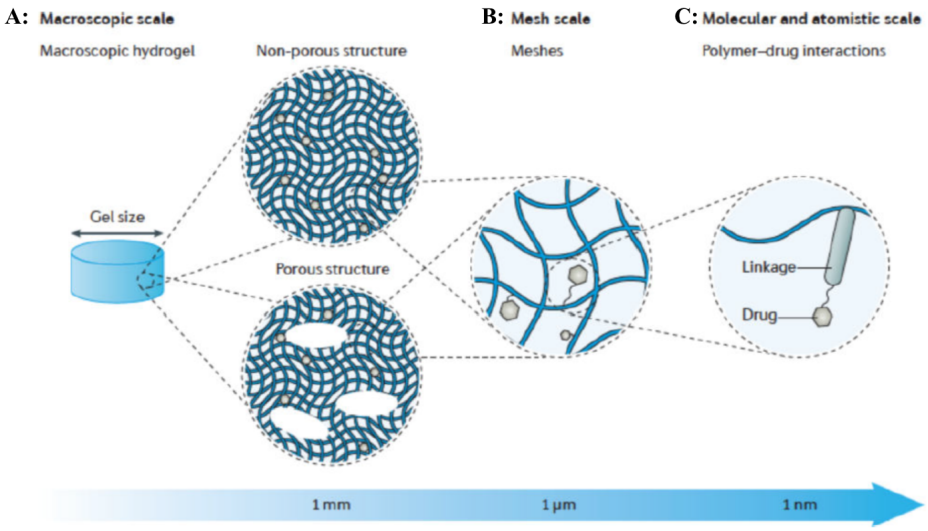

Figure 1.2.2: Multiscale properties of hydrogels. A: Macroscopic design: size and porous structure; B: Mesh size; C: Molecular (or atomic) scale [13]

1.2.2 Polymeric matrix composition

Different classes of hydrogels are distinguished depending on polymerization method. These can be divided into:

1. *Homopolymer hydrogels*: the polymeric matrix derived from a single monomer species, which is a basic structural unit constituting all the polymeric network [18]. The crosslinked structure of homopolymers is influenced by the nature of the monomer and the polymerization technique;

2. *Copolymeric hydrogels.* They are composed of two or more different monomer species with at least one hydrophilic component, arranged in a random, blocky or alternating configuration along the polymer network chain [19];

3. *Hydrogels with interpenetrating polymer network (IPN).* They are a kind of hydrogel which includes two or more polymeric units in the network in which the polymers are cross-linked with each other. In the semi-IPN hydrogel, one component is a crosslinked polymer and another component is a non-crosslinked polymer [20].

1.2.3 Hydrogel functionalization

Hydrogel functionalization offers new tools to both tune the mechanical properties and tailor the biomimetic properties, which is useful for tissue engineering, regenerative medicine and other applications.

In their natural environment, cells are surrounded by an intricate network of extracellular molecules, called the Extracellular Matrix (ECM), that ensures cell adhesion, functionalization, proliferation, morphology and gene expression. Hydrogel networks have attracted a greatest interest to mimic the ECM. Owing to their high water content, as well as their amenability to mechanical and biochemical optimization, hydrogels lend themselves as excellent microenvironments for cell colonization. However, before their applications may be expanded, some limitations of hydrogel properties remain to be overcome, including the fact that they are still far from the mechanical or biological properties of native tissues. For innumerable biological applications, such as for example to favour the interaction between the polymeric chains and the cellular component, a functionalization of the hydrogel is required, in order to emulate the behaviour of the ECM and to guarantee the vitality of the cells [21]. Functionalization consists in the introduction of protein or peptide sequences into the matrix structure. The technique can be done with physical or chemical methods. The most common procedure involves the addition of bioactive binding sites in synthetic hydrogels through the encapsulation of extra-cellular matrix proteins (such as collagen, fibronectin, etc.) within the polymeric structure. Among the complications that may occur, we find the denaturation of the hydrogel after the introduction of proteins, or a non-uniform distribution of the polypeptides within the matrix [22]. The functionalization of a hydrogel has proved to be a promising technique also with regard to drug targeting. The term *active targeting* refers to the

functionalization of the drug carrier surface with ligands that are selectively recognized by receptors located on the surface of the target cells. In this way, the drug release, in not just controlled but will also take place exclusively at the site of interest [23]. These prevent side effects such as dispersion of the drug to areas of no interest during transport through the mechanism of endocytosis. For example, to combat a tumor, the effectiveness of this technique relies on the antigen-antibody interaction, or on the addition of thermosensitive or pH sensitive functional groups, depending on the biological characteristics of the tumor tissue.

1.2.3.1 Problems related with Polymer functionalization

Post-polymerization modification is an attractive approach for the synthesis of functional polymers that overcomes problems related to the limited functional-group tolerance of a number of polymerization strategies. Polymer functionalization can be applied in bulk materials (like hydrogels) and in colloid ones with the main aims to allow biomaterial tracking, cell adhesion and improve drug delivery performances.

Two main problems can take place when polymer functionalization is applied in drug delivery field:

1. the use of precursors or catalysts or initiator or solvent that can compromise materials biocompatibility, leading to various adverse effects such as cytotoxicity and inflammation;

2. chemical functionalization that can reduce or change the activity of the solute loaded within the polymeric network.

One of the primary concerns when using polymer functionalization in drug delivery is the use of precursors, catalysts, initiators, or solvents that can be toxic or lead to the formation of toxic by-products. For example, some of the commonly used cross-linking agents, such as glutaraldehyde and formaldehyde, are known to be cytotoxic and can cause allergic reactions in patients [24]. Also other commonly used precursors and initiators such as azo compounds and peroxides can produce toxic by-products that can compromise the biocompatibility of the resulting polymers [25]. Moreover, the use of solvents such as chloroform, tetrahydrofuran (THF), dimethyl sulfoxide (DMSO) and dimethylformamide (DMF) can cause hemolysis, cytotoxicity, and affect the viability of cells [26, 27, 28]. Several studies have reported that the use of toxic precursors, catalysts, initiators, or solvents during polymer functionalization

can lead to adverse effects on biological systems [29]. To address this issue, researchers have explored alternative and safer precursors, catalysts, initiators, or solvents for polymer functionalization [30, 31, 32].

The loaded solute within the polymeric network can also be affected by chemical functionalization in different ways. In fact the activity of the solute is dependent on its interactions with the polymer matrix, and any modification to the polymer can affect these interactions. For instance, the introduction of functional groups on the polymer surface can alter the surface properties, such as hydrophobicity, which can affect the adsorption of drugs onto the polymer matrix [33, 34, 35]. Additionally, chemical functionalization can lead to changes in the chemical environment of the solute, which can affect its stability and release profile, impacting its efficacy [36]. Moreover, the introduction of reactive functional groups on the polymer surface can cause undesired chemical reactions with the loaded solute, leading to a decrease in its activity [37]. To address this issue, researchers have explored alternative approaches for polymer functionalization that do not affect the activity of the loaded solute [38, 39, 40]. Moreover, the use of responsive polymers that can respond to specific stimuli, such as pH or temperature, can be an effective strategy to avoid the undesired chemical reactions between the polymer and the loaded solute.

In summary, polymer functionalization is an important technique in the drug delivery field, but it is important to carefully consider the precursor, catalyst, initiator, or solvent used to ensure biocompatibility of the resulting materials. Additionally, chemical functionalization can affect the activity of the solute loaded within the polymeric network, and this should also be considered when selecting a functionalization method. As the field of drug delivery continues to evolve, it is important to continue to explore new methods of functionalization that are both effective and safe for use in clinical settings.

1.3 Drug release mechanism

Several approaches can be induced on hydrogel to release the drug in a controlled manner. Drug release is influenced by drug type, hydrogel chemical composition, hydrogel functionalization, physical interaction between drug, matrices and release environment or can be mediated by stimuli. In general, more than one mechanism contributes to the drug release from the matrices, although one may be more influ-

ential than the other. For instance, in drug-loaded hydrogel coated with a polymer membrane, drug release is controlled by swelling as well as diffusion through the membrane [41].

According to the mechanism by which a drug is released, it can be classified into four categories: diffusion, solvent, degradation and stimuli-controlled release.

1.3.1 Diffusion controlled release

Diffusion-controlled drug release is driven by drug concentration gradient across the bulk matrix and it can occur in:

1. Capsule-type reservoir system
2. Matrix-type system

In capsule-type reservoir systems, the drug is dissolved or dispersed in a core surrounded by a polymeric membrane [42] and the drug dissolves in the core and then diffuses through the membrane providing a diffusion-controlled release profile [43]. Depending on drug-loading methods, capsule-type reservoir systems can be divided in non-constant drug source reservoir (a) and constant drug source reservoir (b) as shown in Figure 1.3.1.

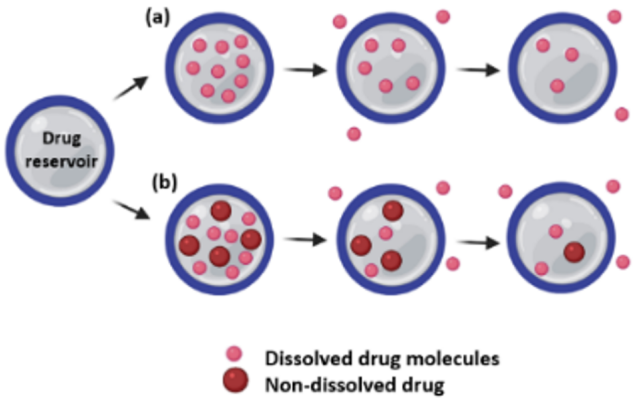

Figure 1.3.1: Capsule-type reservoir systems: non-constant drug source reservoir system (a), constant drug source reservoir system (b). Created with *BioRender.com*

In matrix-type systems, the drug is dispersed in the matrix and there is not a membrane that can function as a barrier to diffusion, nevertheless the drug release

is based on the concentration gradient [44]. Matrix-type systems can be divided in monolithic solution, and monolithic dispersion as shown Figure 1.3.2 .

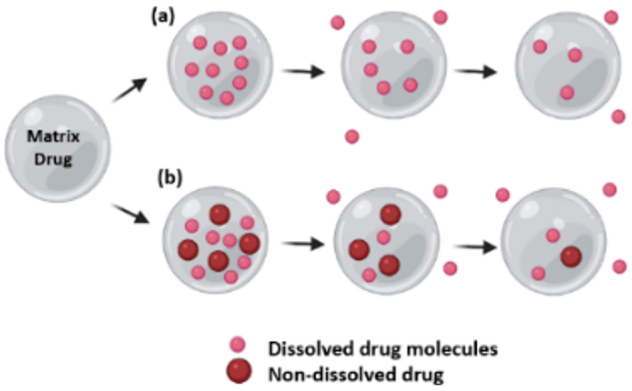

Figure 1.3.2: Matrix-type systems: monolithic solution (a) and monolithic dispersion (b). Created with *BioRender.com*

1.3.2 Solvent controlled release

Solvent-controlled release is mediated by a transport of a solvent into drug-delivery systems that induce the drug release. In this category, two different release mechanism are classified [46] :

1. Osmosis-controlled release
2. Swelling-controlled release

Osmotic-controlled release occurs in a carrier covered by a semipermeable polymer membrane and water flows, properly biological fluids, from the outside of the carrier, with a low concentration of drug, to the centre of the carrier, with a high concentration of drug (Figure 1.3.3). As a result of this mechanism, drug release with zero-order kinetics occurs along a concentration gradient that is constantly maintained across the carriers' membrane [47].

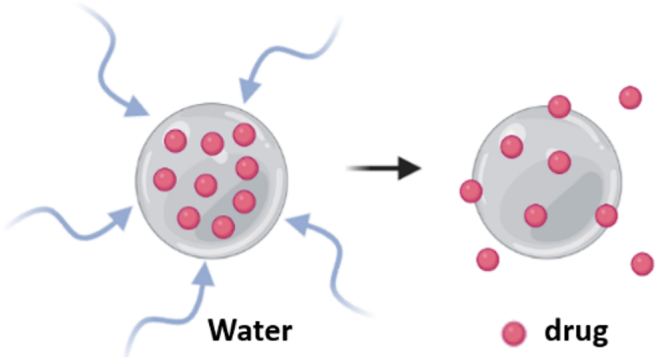

Figure 1.3.3: Osmosis-controlled release. Created with *BioRender.com*

Swelling-controlled release occurs in a system primarily composed of polymeric material with a three-dimensional cross-linked network structure, such as a hydrogel in which the mesh size controls the drug release as result of swelling (Figure 1.3.4). The drug release rate is determined by the diffusion rate of water and the chain relaxation rate of polymers [48, 49].

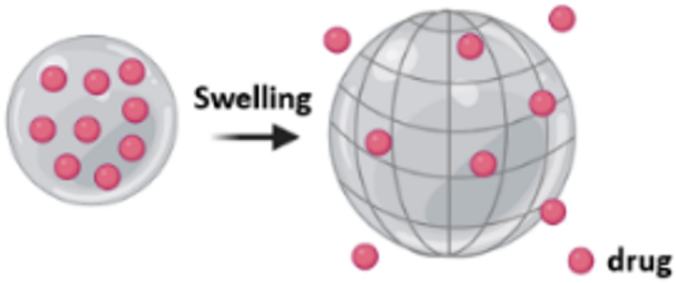

Figure 1.3.4: Swelling-controlled release. Created with *BioRender.com*

1.3.3 Degradation-controlled release

Degradation-controlled release occurs by degradation of the carrier structure (Figure 1.3.5). In particular, drug carriers composed of biodegradable polymers such as polyesters, polyamides, and polysaccharides release the drug through enzymatic decomposition, which degrades ester or amide bonds, or causes hydrolysis [50]. Nevertheless, matrix, made of polymer anhydrides or orthoesters, typically erodes from

the surface to the centre causing degradation of the polymer at a faster rate than water diffuses into the matrix.

However, a small matrix, has a very short diffusion length for water. The polymer degradation continues to accelerate with general degradation of the polymer rather than just surface erosion [51, 52]. Drug release kinetics is determined by the degradation rate of polymers, which depends on their molecular weight, groups, and monomer composition. Additionally, the drug can be contained in the polymeric matrix but also conjugated to the drug by chemical bonds. In the latter case, the drug is released from the carrier by hydrolytic or enzymatic cleavage of the bond between the drug and the polymer and the rate of cleavage controls the kinetics of drug release. Enzymatically cleavable drug-polymer conjugates can be used for target-specific drug delivery if the enzyme is concentrated in the target tissues [53].

Figure 1.3.5: Degradation-controlled release. Created with *BioRender.com*

Biodegradable polymer systems are preferable in biomedical applications because they are degraded in the body without causing long-term side-effects.

1.3.4 Stimuli-controlled release

Stimuli-responsive hydrogels can be promising smart drug delivery platforms for the selective drug release at the desirable sites [54, 55]. In fact in recent years, biomedical researchers acquired great consideration to introduce smart or stimuli–responsive polymeric drug delivery systems. The release is driven by external or internal stimuli (Figure 1.3.6) such as temperature, pH, ionic strength, sound, and electric or magnetic fields [56]. This approach is adaptable, it can be used for both passive and specific-drug targeting because stimuli can be localized or be characteristic of a pathological condition [57].

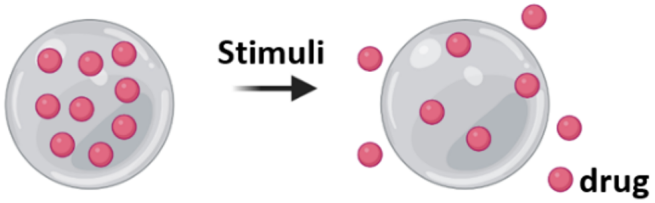

Figure 1.3.6: Stimuli-controlled release. Created with *BioRender.com*

Chapter 2

Hydrogel with graphene

In Chapter 1, we have talked about hydrogels and some different release mechanisms. However, often the drug release from these 3D scaffolds is mostly driven by a pure diffusion mechanism, due to the high clearance observed in vivo and it can difficulty be modulated through external stimuli. To overcome these limitations, hybrid composites are being developed and the scientific community has shown great interest in the use of graphene as a nanoscale filler [58, 59]. In fact one of the way to achieve the electrical conduction goal in hydrogel is the addiction of graphene in different forms (carbon nanotubes, pristine graphene or graphene oxide)[60, 61, 62]. Graphene is defined as a single layer of sp^2-hybridized carbon atoms arranged in a honeycomb two-dimensional (2D) lattice array [63, 64]. The application of graphene in the synthesis of drug carriers is justified by its peculiar feature, which include high Young's modulus, mechanical stability, excellent electrical and thermal conductivity, and combination of fast mobility of charge with a large specific surface area that provide multiple attachment sites for drug targeting [65, 66]. Indeed, the planar configuration represents an attractive substrate to immobilize different substances, such as drugs, biomolecules, chromophores and cells [67, 68, 69]. The main application of graphene in DDS is in its oxidized (graphene oxide, GO) or reduced (reduced graphene oxide, rGO) state to endow polymeric networks with improved mechanical consistence, self-healing ability, ultrasound or IR responsivity, which affect the drug release kinetics [70, 71]. In particular, the choice of graphene oxide is due to its water dispersibility, result of the epoxide and hydroxyl functionalities on the two sides of a single layer of graphene, and of the carboxylic terminal groups at the edges: the polarity of these chemical groups empowers the formation of hydrogen bonds with hy-

drophilic molecules and their chemical reactivity gives rise to covalent linkage with polymers or biomolecules [72, 73]. For example, Dembereldorj and coworkers [74] have been proposed the PEGylation of GO to optimize the biocompatible release of doxorubicin; Wang's group [75] discussed the covalent functionalization among GO and polyethyleneimine, polyethylene glycol, and folic acid to design a plasmid delivery system for targeting hepatocellular carcinoma; Cheng and coworkers [76] described the synthesis of a 3D printable GO-hydrogel as BMP7 protein delivery system and as protection of the cartilage by the pathway of Rank/Rankl/OPG in biomimetic tissue models in vitro and in vivo. On the other hand, the application of pristine graphene is investigated due to its specific conductivity (higher than oxidized derivative) and mechanical stability: recently, González-Domínguez and his group [77] have studied the response of a hybrid graphene-hydrogel to electrical and mechanical stimuli to modulate the release of a drug. However, the pristine graphene thermal behaviour within a polymeric matrix has not been fully investigated yet. The thermal triggering approach to drug delivery is common in cancer [78, 79, 80] and brain tumors [81, 82]. As we will see in Chapter 4, in this thesis we propose the synthesis of graphene-based hydrogels as thermo-sensitive carriers for controlled drug release. In the next sections we will analyze the main properties of graphene and its main applications in drug delivery.

2.1 Graphene

Graphene – a single layer of graphite – is a monolayer of sp2 hybridised carbon atoms patterned in a honeycomb lattice form [83]. The discovery of this revolutionary material took place in 2004 by two English physicists, Andre Geim and Konstantin Novoselov [84]. In this 2D material, all the carbon atoms are tightly bonded through in-plane σ-bonds and form a strong honeycomb layered network. Moreover each carbon atoms has a network of delocalized π-electrons. These π-electrons, which are oriented along perpendicular plane of the layers, provide a high electron density above and below the 2D planar structure of graphene [85].

A large number of experiments focus on the insertion of additional chemical species between the basal planes of graphite [86, 87]. However, the presence of these delocalized electrons' makes the graphene as an electrically conductive and chemically inert structure to gasses and vapors [88]. Pure graphene is hydrophobic

in nature and it often requires the dispersion of stabilizing agents or surfactants in water [89]. Graphene and its derivatives have been extensively explored in recent years for drug transport and delivery applications in the body by many research groups [90]. Some salient characteristics of graphene are reported in the following sections.

2.1.1 Graphene properties

Graphene was first isolated using mechanical exfoliation with the *scotch-tape* method. Each carbon atom of pristine graphene (that is the graphene in its original, pure, and deionized form) is bonded to three others in a planar structure (sp^2 hybridization). This structure is the basis of many carbon materials with different geometries (Figure 2.1.1): spherical structures (zero-dimensional fullerenes), carbon nano-tubes (CNTs) or stacking of three-dimensional structures (graphite) [91]. Graphene, fullerenes and CNTs vary in diameter, length and surface chemistry [92].

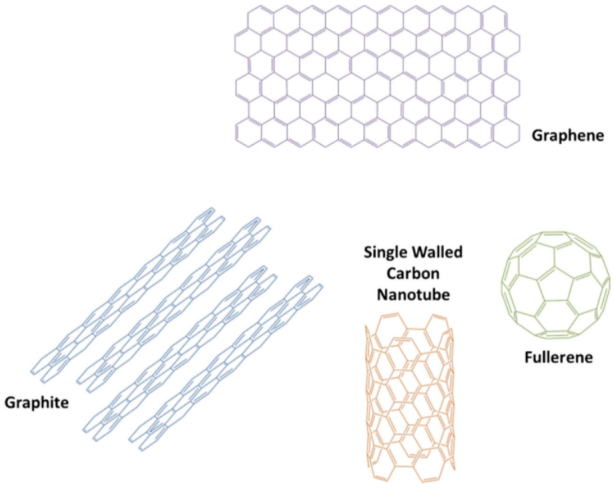

Figure 2.1.1: sp^2 hybridization in graphene and its allotropic forms [93]

2.1.1.1 Mechanical properties

Its excellent mechanical strength makes graphene the strongest material in nature, despite being the thinnest in the world and extremely light. The C-C bond, which is established in the plane thank to the sp^2 hybridization between an s orbital and two p orbitals, is considered the strongest of all chemical bonds; on the other hand, the

interplanar π-bond is extremely weak, which makes possible the separation of the graphite planes and it is the foundation of the mechanical microexfoliation technique. The Young's modulus, fracture toughness, and Poisson's ratio of defect-free, single-layer graphene are 1 TPa, 130 GPa, and 0.149 GPa, respectively [94, 95] ; it also turns out to be 200 times stronger than steel.

Due to its high mechanical properties, graphene has been used for enhancing strength of polymeric materials. Graphene reinforcement into polymeric matrix significantly increased the modulus and hardness of composites for biological applications [96]. High strength and ability to tune the mechanical properties using various forms/functionalization strategies imply potential applications of graphene as fillers or reinforcements in medical implants, hydrogels and scaffolds used in tissue engineering [97, 98, 99].

2.1.1.2 Thermal and Electrical Properties

The presence of a strong σ bond and delocalized π electrons makes graphene a highly conductive material both electrically and thermally, with a low coefficient of thermal expansion. [100] Single layer graphene has higher thermal and electrical conductivity due to low defect density in the crystal lattice. It is approximately of the order of $4.5-5.5\times10^3$ W/mK, while it is approximately 2×10^3, 3×10^3 and 3.5×10^3 W/mK for graphene oxide, multiwall carbon nanotubes, and single wall carbon nanotubes, respectively [107]. The thermal conductivity of GO is lower than that of graphene due to the presence of defects in its structure that hinder the conductivity. The thermal properties of graphene are also greatly affected by phenomenon such as defect edge scattering [101] and isotopic doping [102] due to scattering or localization of phonons at the defect sites. Exceptional electrical conductivity and thermal properties of graphene can be useful not only in electronic devices, in biomedical devices for measuring cell potential and as a substrate for conductive cell culture devices and biosensors [103, 104, 105, 106].

2.1.1.3 Optical properties

In addition to the exceptional mechanical strength and thermal and electrical properties, graphene has excellent optical properties. A single layer of graphene showed an incident light transmission of 97.7% over a wide range of wavelengths. This property is strongly influenced by the presence of impurities and the number of layers

of graphene [108]. The high optical transparency, conductivity, excellent mechanical strength and chemical stability make graphene a material for the design of transparent electrodes in solar cells or liquid crystals, as well as flexible transparent electrodes [109].

2.1.2 Graphene oxide, reduced graphene oxide, and pristine graphene

It is possible to obtain graphene from graphite with different techniques: micromechanical exfoliation, solvent exfoliation, epitaxial growth and chemical vapor deposition (CVD) [110]. Generally, graphene-based materials are classified into different types, such as pristine graphene, graphene oxide (GO), and reduced GO (rGO) [111]. Among these materials, GO and rGO have the greatest interest and potential in biomedical fields due to their modifiable physicochemical properties, high biocompatibility, and easy availability. Furthermore, the photothermal properties of GO and rGO give them great potential in targeted cancer therapy [112] (Figure 2.1.2).

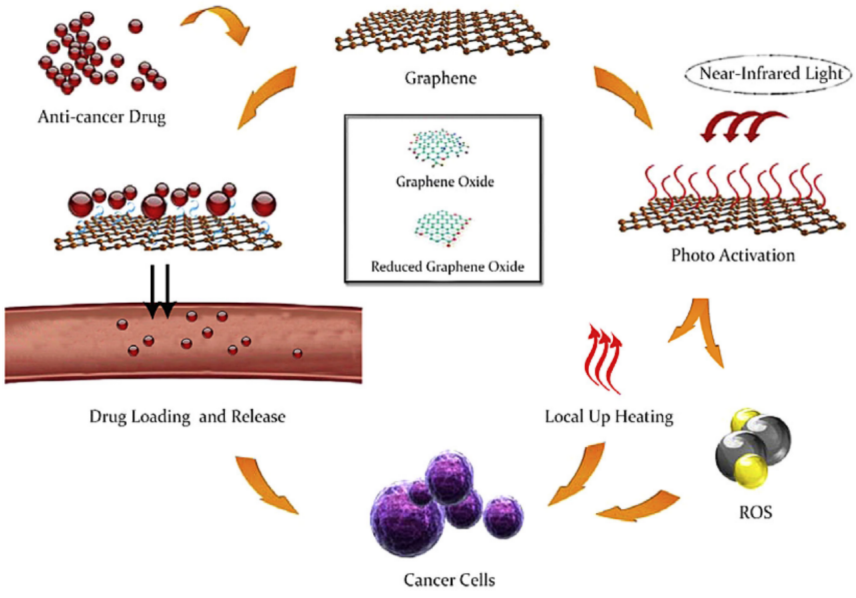

Figure 2.1.2: Graphene-based materials as drug carriers for anticancer systems [113].

Pristine graphene, having a hydrophobic nature, requires functionalization treatments in order to be used in biomedical applications.

The solubilization is achieved by exfoliation of graphite layers in the presence of a non-polar solvent or surfactants [114]. The hydrophobic regions cover much of the surface of the exfoliated flake, while the hydrophilic tails extend into the aqueous solution in which the flakes are suspended. Consequently, the geometry of the nanostructures will be significantly modified compared to a single sheet of untreated graphene. Furthermore, when surfactants are used, most of the surface of graphene is covered by surfactant molecules, which could cause steric interference with other functional molecules, and consequently modify the geometry of the flakes. (Figure 2.1.3) [115].

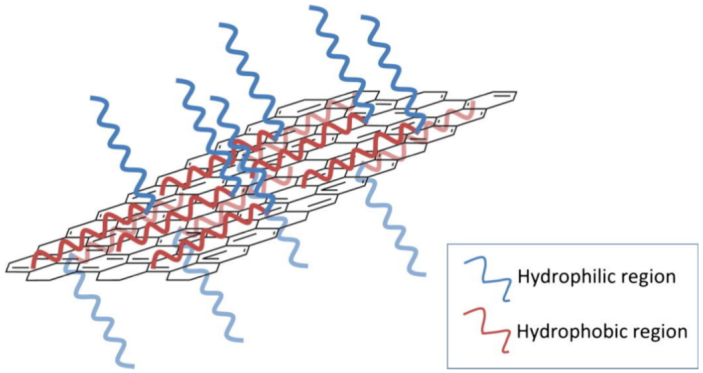

Figure 2.1.3: Graphene solubilization with surfactant molecules [115].

Finally, both the treatment with surfactants and the use of residual non-polar solvent molecules adsorbed on the surface, can significantly contribute to the toxicity of the preparation. These are the reasons why pristine graphene is less used for biomedical applications than the use of GO and rGO. These behaviours could provide insights for future developments, in order to analyze the cytotoxicity of pristine graphene in vivo.

2.1.3 Graphene for drug delivery

Graphene is made up of highly mobile electrons called π which are found above and below the graphene sheet. The electron clouds above and below each layer made up of carbon atoms overlap, creating a continuous π orbital that cover the entire graphene layer 2.1.4. This free movement of electrons makes graphene highly conductive. The structure can be conceptually seen as a planar achromatic macromolecule [116]. Even without further functionalization, this structure confers an excellent ability to trap a

large number of substances, including drugs and biomolecules: these molecules can bind through non-covalent interactions with the carbon rings (π-π stacking). For pristine graphene, π-π stacking and hydrophobic interactions are the main source of binding for drugs and other molecules. However, for other forms of graphene the additional presence of chemical functional groups provides a wider range of possible interactions. Thus, suitably modified graphene can serve as an excellent drug delivery platform for anticancer/gene delivery, for biosensing, bio-imaging, antibacterial applications, cell culture, and tissue engineering [117].

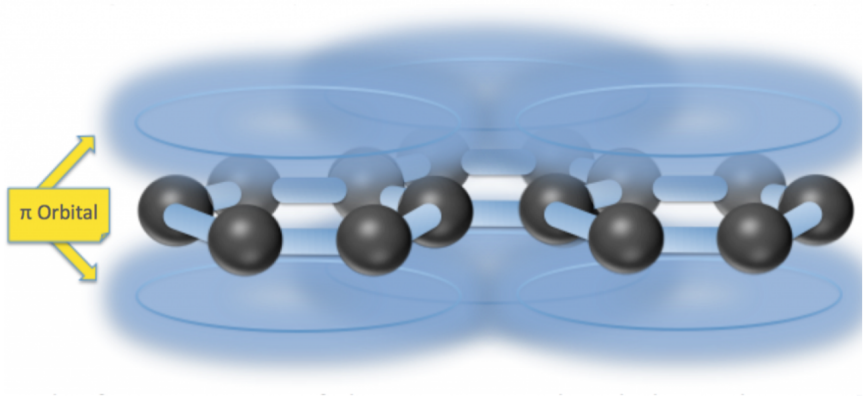

Figure 2.1.4: π orbitals in graphene [118].

2.1.3.1 Drug Loading

The way in which the drug is implanted on the surface or inside the transport vehicles determines its protection from degradation, the methods in which it is released, and its site of action. Drugs can interact in different ways with graphene. Some studies included the use of drugs that directly interacted with the graphene sheets by exploiting the aromatic and hydrophobic areas of the material [119]. For example, some drugs bind to graphene thanks to hydrophobic interactions and π-π stacking; while for others this bond occurs thanks to non-oxygenated hydrogen bonds [120]. In both cases, the efficacy of drug delivery is optimized. These transport mechanisms of molecules (such as genetic materials) are exploited to avoid premature degradation.

After attachment to graphene, the molecule of interest must be transported to the target cell or tissue. Passive targeting mechanisms via external agents are promising as they do not require excessive functionalization. For example, the high infrared absorption capacity of graphene or GO allows exploiting photothermal effects to

induce localized cell apoptosis through hyperthermia, applying the infrared light only to the affected area [121]. Localized heating by photothermia also improve cell permeability, further increasing the transfection efficiency of graphene complexes in the region where infrared light is applied [122].

2.1.3.2 Drug release

To achieve a targeted pharmacological effect, a transported therapeutic agent must be released at its site of action. The mechanism required to release the drug depends on the graphene preparation technique. For functionalized graphene, the drug is usually bound by hydrophobic interactions or π-π interactions; this can be released following the change of physicochemical properties within the environment, often making use of the physiological characteristics in place within the cell. Several research groups have encapsulated graphene-based nanoparticles in hydrogels to promote localized and controlled drug transport and release, often leading to significantly improved release profiles compared to hydrogels containing no filler in the polymer matrix [123].

Chapter 3

Nanocarriers for drug delivery

3.1 Historical background

The genesis of the concept of nanotechnology dates to 1959 and it is attributed to the American Nobel physicist Richard P. Feynman, who worked on the Manhattan Project at Los Alamos during World War II and later taught at the California Institute of Technology (Caltech) for most of his professorial career. In his historic lecture titled "There's plenty of room at the bottom", during the annual meeting of the American Physical Society, Feynman proposed using machine tools to make smaller machine tools, and so on all the way down to the atomic level [124]. Furthermore, Feynman prophetically concluded that such a development could not be avoided and that nanomachines, nanodevices and nanorobots could be used to develop microscopic instrumentation and manufacturing tools, what is known as nanotechnology.

In the following years, different definitions inspired by Feynman's vision have been given to the term nanotechnology, in the 2000, an accurate definition was given by the US National Nanotechnology Initiative: "*Nanotechnology is concerned with materials and systems whose structures and components exhibit novel and significantly improved physical, chemical and biological properties, phenomena and processes due to their nanoscale size*".

Feynman was not only the pioneer of nanotechnology development but also inspired the development of nanomedicine. In fact, clearly aware of the potential medical applications that nanotechnology could have, he discussed with his colleague and friend Albert R. Hibbs who predicted the advent of nanomedicine. Feynman reported about the "*wild idea*" of Albert R. Hibbs in his later work:

"A friend of mine suggests a very interesting possibility for relatively small machines. He says that, although it is a very wild idea, it would be interesting in surgery if you could swallow the surgeon. You put the mechanical surgeon inside the blood vessel and it goes into the heart and looks around. It finds out which valve is the faulty one and takes a little knife and slices it out. Other small machines might be permanently incorporated in the body to assist some inadequately functioning organ"[124].

Feynman awakened the interest of many scientists opening to a new research field and two directions of thought arose describing the possibilities for producing nanostructures:

1. The top-down approach

2. The bottom-up approach

The top-down approach is based on Feynman's vision of gradually reducing the size of existing materials, machines, and tools. It is essentially the reduction of bulk material to nano-sized particles. The second one, the bottom-up approach revolves around the construction of nanostructures atom-by-atom or molecule-by-molecule by physical and chemical methods and by controlled manipulation of the self-organizing forces of atoms and molecules. This theory of *"molecular engineering"* became popular in 1986 with the publication of the book *"Engines of Creation: The Coming Age of nanotechnology"* by K. Eric Drexler [125] in which he described the construction of complex machines capable of independently manipulating molecules and atoms and thereby producing things and self-replicating.

In later years, the possible uses of such *"nanobots"* or *"assemblers"* in medicine are described by K. Eric Drexler, Chris Peterson, and Gayle Pergamit in their book *"Unbounding the Future: The Nanotechnology Revolution*" published in 1991 [126] in which the term "nanomedicine" would have been used for the first time. The term became more established with the book *"Nanomedicine"* by Robert A. Freitas [127] published in 1999 and it has since been used in the technical literature. In December 2002, the US National Institutes of Health (NIH) announced a 4-year program for nanoscience and nanotechnology in medicine [128]. Burgeoning interest in the medical applications of nanotechnology has led to the emergence of a new field called nanomedicine [129]. Since then, over the years, interest and research in this new field has progressed until to reach a crucial role in medical field.

3.2 Nanomedicine

There are many ways of defining nanomedicine, the definition used by the European Technology Platform on nanomedicine states:

"Nanomedicine is the application of nanotechnology to health. It exploits the improved and often novel physical, chemical, and biological properties of materials at the nanometric scale".

In other hand, nanomedicine is the application of nanotechnology to medicine, it is the process of diagnosing, treating, and preventing disease and traumatic injury as well as relieving pain, preserving and improving human health by using molecular tools and molecular knowledge of the human body. Nanomedicine aims to overcome the limitations of traditional medicine by minimizing side effects, improving the effectiveness of medical treatments and reducing diagnostic time via nanoparticles.

Over the years, nanomedicine becomes more relevant both in research and on the market scene, expanding its fields of application [130, 131].

As reported by VDI Technologiezentrum in 2008 (Figure 3.2.1) and Nanomedicine European technology platform in 2021, nanomedicine is already accounting for approximatively 80 marketed products, ranging from drugs and drug delivery to gene therapy, in vivo medical imaging, in vitro diagnostics.

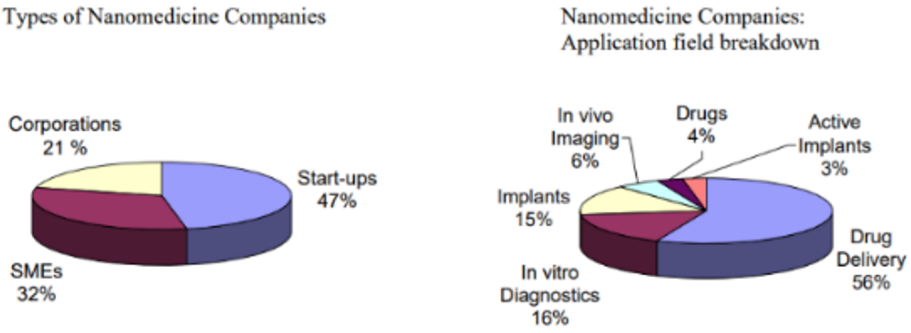

Figure 3.2.1: Types of companies and application field breakdown (2008)

Nowadays, drug delivery still accounts the largest share in both research and market scenario and consistently with the present developments, the following work on Chapter 5 is focused on drug delivery nanoparticles, specifically, synthesis of nanogels and evaluation of nanogels-cell interaction.

3.3 General features of nanocarriers

Nanocarriers as nanoparticles (NPs) for medical applications are defined as particles with a size between 1 and 1000 nm [132]. Depending on the overall shape these nanostructures can be *0D*, *1D*, *2D* or *3D* [133]. The nanometric size is also the scale of many biological mechanisms in the human body allowing nanoparticles to potentially cross natural barriers to access new sites of delivery and to interact with DNA or small proteins at different levels, in blood or within organs, tissues or cells, for that reason, nanomedicine uses nanoscale materials larger than 100 nm [134]. Besides, at the nanoscale the surface-to-volume ratio is very high such that surface properties influence the behaviour of the nanoparticle,

Other remarkable strengths related to nanoparticles are represented by the coating and superficial functionalization, even at multiple levels, which are extremely common to increase the biocompatibility, cellular uptake, its circulation time in the blood, drug release as well as to ensure a highly selective binding to the desired target. The wide variety of nanoparticles in terms of shape, size, coating and composition have allowed their inclusion in different applications such as drug delivery. Nanoparticles for drug delivery are commonly known as "nanocarriers" and they should be non-toxic, biocompatible, blood stable, non-immunogenic and non-thrombogenic, and eventually biodegradable. It has been demonstrated how nanocarriers can overcome side effects of free anti-cancer drugs in the tumor site. Nanocarriers are, basically, nanocages to protect bio-active substances, to maintain their stability providing spatiotemporal control of drug release avoiding side-effects during drug targeting and to target's adjacent areas. Spatiotemporal control of drug release from nanocarriers aims to maintain drug concentration in blood or target tissues at the efficacious level to maximize therapeutic effect. The therapeutic effect by drug delivery systems can be achieved by reaching the target site using two different approaches:

1. Selective targeting

2. Passive targeting

Selective targeting is accomplished by nanocarriers that actively recognize only receptors at the target site. Passive targeting is achieved by nanocarriers that reach the target site through the bloodstream.

Nano-drug delivery systems or nanocarriers are engineered technologies which could improve delivery of poorly water-soluble drugs; induce a targeted delivery of

one or more drugs in a cell or tissue-specific manner combining therapeutic agents; control drug release; visualize drug delivery sites by combining therapeutic agents with *in-vivo* imaging; achieve transcytosis of drugs across narrow epithelial and endothelial barriers; enable delivery of large macromolecules to intracellular sites of action intracellular sites of action or obtain an in vivo real-time analysis of efficacy for a therapeutic agent [135]. Latter and many others are the reasons why nanoparticles hold great promise for drug delivery.

Nanocarriers can be classified in different ways, the most widespread is based on the type of structure of which the nanocarrier is composed. Nanocarriers include organic and inorganic nanoparticles.

3.4 Organic nanoparticles

Organic nanoparticles are essentially composed of soft materials as polymers or small molecules and therefore they have potentially lower toxicity than inorganic nanoparticles made of metals or semiconductors. Organic nanoparticles include lipid-based NPs and polymeric NPs.

3.4.1 Lipid-based NPs

Lipid-based NPs include various subset structures including liposomes, micelles, and solid lipid Nps which are distinguished by the different arrangement of lipids that constitute the cage.

3.4.1.1 Liposomes and micelles

The first liposomes ware developed by Bangham in 1960s [136] and have widely been used as a drug carrier since then. Since Doxil, a PEGylated liposome with doxorubincin (DOX), was approved by the U.S. Food and Drug Administration (FDA) in 1995, several other liposomal drugs have been approved for clinical uses.

Liposomes are vesicles made of a lipid-bilayer of phospholipids in aqueous solution produced in large scale up to the size of 50-150 nm, which is a useful range for enhanced permeation and retention (EPR) highlighting their strong market impact. By means their structural composition can be used as carrier for water-soluble drugs which are encapsulated in the hydrophilic compartment surrounded by lipid

bilayers and hydrophobic drugs in the lipid layer. Although the common structure of liposomes is composed of two phospholipid layers, multilayer liposomes have been developed to combine the therapeutic effect of multiple drugs [137].

The main features of liposomes include easy fabrication, higher drug-to-lipid ratio loading efficiency, high biocompatibility, biodegradability in the intestinal tract and surficial functionalization to achieve selective targeting.

Similar considerations can be made about micelles that differ from liposomes because they are composed of a single layer of phospolipids oriented with hydrophilic heads outward and hydrophobic tails towards the core of the structure [138].

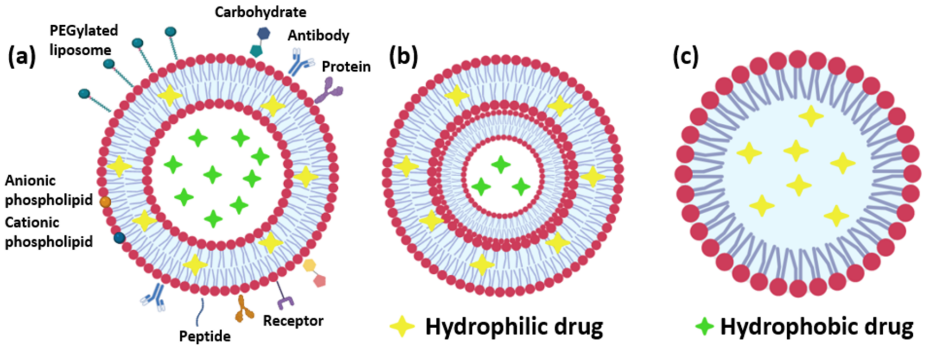

Figure 3.4.1: Liposomes, and micelles: bilayer and superficial functionalized liposomes (a), multi-layers liposome (b), micelle (c). Created with *BioRender.com*

3.4.1.2 Solid-lipid NPs

Solid-lipid NPs (SLN) are composed of a matrix, covered by a phospholipids layer, containing triglycerides, diglycerides, monoglycerides, solid fats, fatty acids, steroids or waxes stabilized by surfactant in which drug is dissolved and their size can be less than 1 μm. They were developed as an alternative to liposomal formulations in order to improve physical stability, modulate release of the loaded drug, reduce their cost, and simplify manufacturing. Current preclinical experiments show that solid lipid-based anticancer drug systems appear to be superior to conventional drug solutions and are at least comparable to other encapsulated systems in many aspects such as drug efficacy, pharmacokinetics, and drug delivery [139].

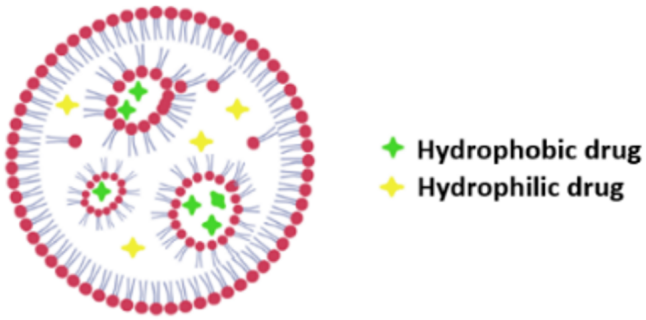

Figure 3.4.2: Example of Solid-lipid NP as nacorrarier. Created with *BioRender.com*

3.4.2 Polymeric NPs

Polymeric NPs are widely used for drug delivery applications. They can be formulated to enable precise control of multiple nanoparticles features and they are generally good delivery vehicles due to biocompatibility and simple formulation parameters. Polymeric NPs can be synthesized from natural or synthetic materials, as well as monomers or preformed polymers allowing for a wide variety of possible structures and characteristics. The commonly used natural polymers are Chitosan, Gelatine, Albumin and Sodium Alginate; instead, the commonly synthetic polymer are PLA (Polylactides), PGA (Polyglycolides), PLGA (Poly-lactide co-glycolides) and PEG (Poly-ethylene glycol). The main classification of polymeric NPs includes nanocapsules as polymeric micelles and polymersomes and nanospheres as dendrimers and nanogels.

3.4.2.1 Dendrimers

Dendrimers, also called "cascade molecules," are highly symmetric spherical compounds composed of repeatedly branched polymeric units ranging from 1 to 100 nm [140, 141]. These hyperbranched molecules were first discovered by Fritz Vogtle in 1978, by Donald Tomalia and co-workers in the early 1980s, and at the same time but independently by George R. Newkome. They differ from linear polymers by an architecture with tailored surface groups. Their properties are mainly determined by the functional groups on their surface, which made dendrimers suitable for surface functionalization [142]. Dendrimers can contain many types of cargo; they are commonly studied for delivery of nucleic acids, small molecules and drugs, which are

attached to dendrimers in complex forms or capsules [143].

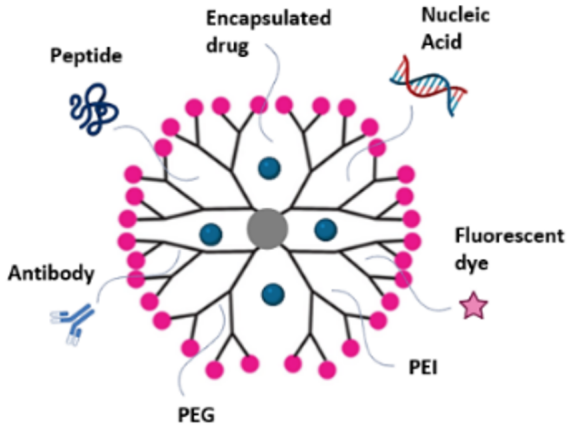

Figure 3.4.3: Dendrimer structure, drug load and superficial functionalization. Created with *BioRender.com*

Those nanostructures can be synthesized by two different approaches: convergent approach and divergent approach. Convergent approach consists in creating 3D-spherical structure starting from the central core, instead, divergent approach occurs synthetizing polymeric units from outside to the core [144].

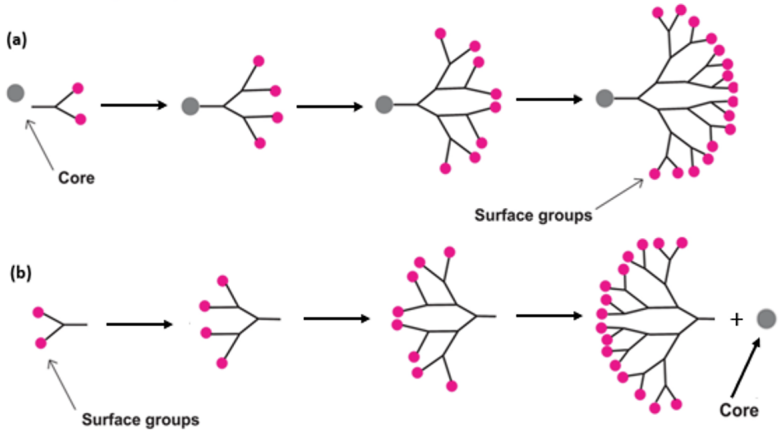

Figure 3.4.4: Synthesis of dendrimers: convergent approach (a), divergent approach (b). Created with *BioRender.com*

3.4.2.2 Polymeric micelles

Polymeric micelles, classified as nanocapsules, are self-assembled core-shell nanoparticles formed by amphiphilic copolymer dispersed in aqueous media which are able to hold hydrophobic drugs inside the core and hydrophilic bioactive molecules in outer shell. Polymeric micelles are created when the polymer concentration is higher than the critical micelle concentration (CMC) [145] and the size is ranging between 10-100 nm.

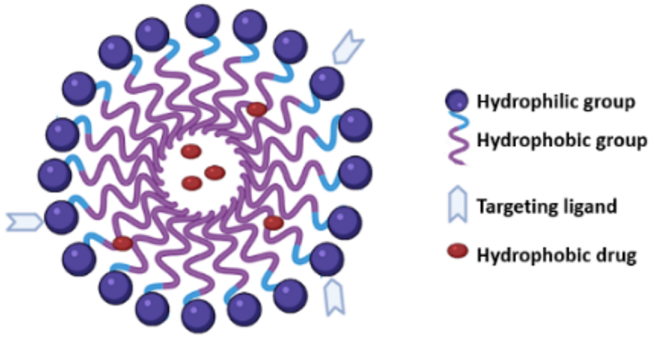

Figure 3.4.5: Structure of polymeric micelles. Created with *BioRender.com*

Those nanoparticles are characterized to have control drug-release property and tissue-penetration capability, high stability in physiological conditions, high and versatile loading capacity, high accumulation of drug at target site, and possibility of functionalization of end group for conjugation of targeting ligands [146, 147].

3.4.2.3 Polymersomes

Polymersomes as micelles are core-shell structure but, in contrast to micelles, the common shell is composed of amphiphilic copolymer double-layer. The polymeric chains are organized radially in order to obtain interposed hydrophobic and hydrophilic regions with an aqueous lumen [148]. Polymersomes can be engineered to make the delivery responsive to pH, temperature, light, enzymes, or any other stimuli. They are an alternative to liposomes due to their better physical and chemistry stability but worse cellular uptake. Additionally, the most polymersomes are reduced to less than 150 nm in diameter to encourage long circulation times. Those structures can be used to carrier both hydrophilic and hydrophobic drugs [149, 150].

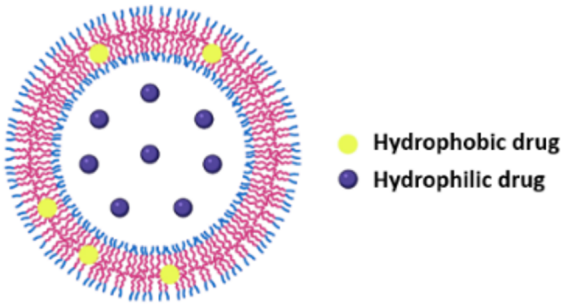

Figure 3.4.6: Structure of polymersome as nanocarrier. Created with *BioRender.com*

3.4.2.4 Nanogels

The term nanogel appeared for the first time in 1999 to describe a matrix-like structure obtained by polyethylene glycol (PEG) and PEI (polyethylimine) polymers [151], still used and investigated.

Nanogel (NGs) are 3D-hydrogel nanoparticles composed of cross-linked polymers as a result of chemical or physical interactions [152]. The main characteristic is the ability to swell and hold water, without dissolving in the aqueous medium [153]. This behaviour is related to hydrophilic functional groups, such as $-OH$ or $-CONH$, along the polymer chains [154]. Additionally, the ability to absorb large quantities of water makes them soft structures close to biological tissues, ensuring high biocompatibility and biodegradability [155]. Due to their hydrophilic characteristics, nanogels are inherently compatible to load a large part of molecules, of drugs and biomacromolecules as proteins and nucleic acids through appropriate alteration of the structure [156]. Although, nanogels have the unique ability to encapsulate more than one bioactive molecule in the same carrier through different physical activities. Their characteristic features such as size, charge, porosity, amphiphilicity, softness, degradability and stimuli-response can be tuned by chemical composition and cross-linking matrix level [157].

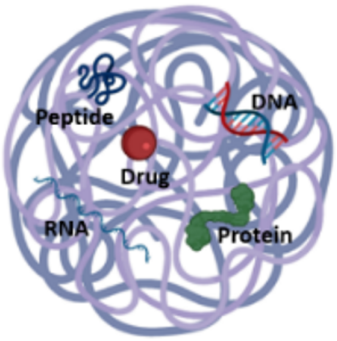

Figure 3.4.7: Structure of Nanogel and its cargo molecules. Created with *BioRender.com*

One of the most important features of nanogels is the possibility to realize superficial functionalization.

The same result can be achieved using two main different strategies: synthetizing nanogels from functionalized polymers or superficial functionalizing once nanogels are synthetized [158]. Functionalization may change also depending on nanogel applications. This step can influence the nanogel behaviour at different levels, can control the drug release, cellular uptake, cell selectivity, as well as it can induce specific targeting and ensure stability and integrity of carried molecules [159].

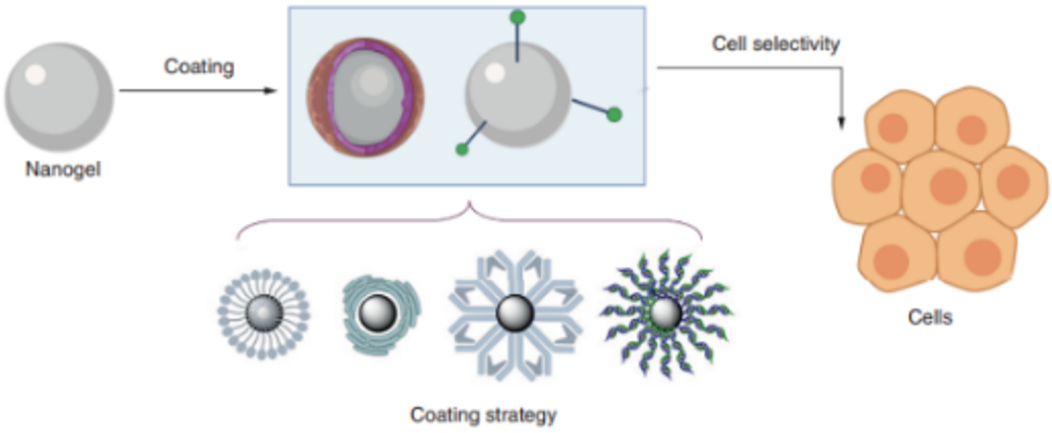

Figure 3.4.8: Main coating strategies for cell selectivity [159].

3.5 Inorganic Nanoparticle

Inorganic nanoparticles are structures with material and size-dependent physico-chemical properties, making them a potential resource in the biomedical field for several applications. Their thermal, mechanical, optical, magnetic, and other physical properties, as well as inertness, stability, and easy functionalization, make inorganic nanoparticles alternatives to organic nanoparticles for bio-imaging, diagnosis, drug delivery and tumour ablation via Photothermal therapy (PTT) [160, 161, 162]. Inorganic nanoparticles widely used for drug delivery are carbon-based NPs, gold NPs, Iron-oxide NPs and Silica NPs.

3.5.1 Carbon-based NPs

Carbon-based NPs are nanostructures made of different carbon allotropes such as carbon nanotubes and fullerene. The attention has been focused on those materials due to their thermal conductivity to trigger specific phenomena by external stimuli and rigid structure to encapsulate drug or molecules.

3.5.1.1 Carbon nanotubes

Carbon nanotubes (CNTs) was reported for the first time in 1976 by Oberlin et al. [163] as rolled graphene sheets with diameters in the nanometre range and lengths in the micrometre range. They can be structured as a single-wall (SW-CNTs) or multi-wall (MW-CNTs) depending on concentric graphene sheets. The main reason why research regarding carbon nanotubes for drug delivery has expanded in the last decade is their ability to penetrate cell membrane due to their morphology without damage cell structures and their high surface-volume ratio [164]. This latter peculiarity is suitable to functionalize superficially and make CNTs more specific in terms of targeting and delivering [165]. Although, the cylindrical shape ensures high drug load efficiency. Nevertheless the remarkable benefits of CTs in drug delivery, the disadvantages are not negligible such as water-insoluble, limited biodegradability that can induce toxicity and long-term retention that led inflammations [166, 167].

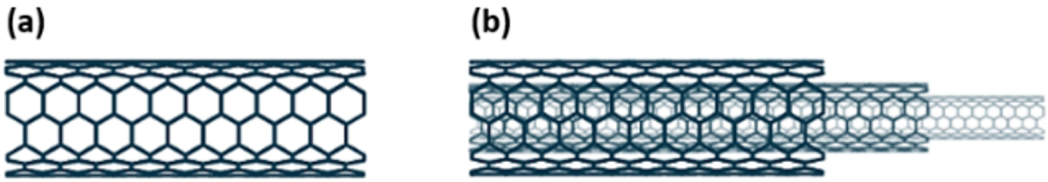

Figure 3.5.1: Structure of Carbon nanotubes: single-wall nanotube (a); multi-wall nanotube (b).

3.5.1.2 Fullerenes

Fullerenes (C60) are hollow spherical nanostructures composed of hexagonal networks of carbon atoms. They have chemical and physical properties close to carbon nanotubes but differ from each other structurally and used as drug or molecules carrier [168, 169], maintaining, perhaps, disadvantages of carbon-nanotubes. Nevertheless, as for carbon-tubes, it has been developing water-soluble structures that reduce the long-term accumulation and toxicity effects of carbon-based NPs [170]. Moreover, fullerenes can bind and inactivate radicals more efficiently than any other medical antioxidant. For that reason, those carbon-based nanoparticles can be used as a new class of nanodrug for specific diseases [171].

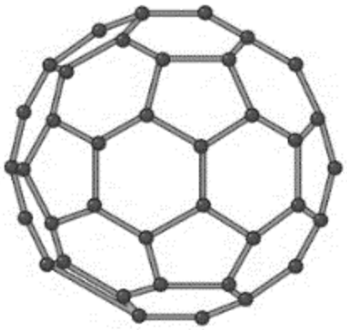

Figure 3.5.2: Structure of fullerene nanoparticle. Created with *BioRender.com*

3.5.2 Gold NPs

Gold NPs, due to their electrical, optical and photothermal properties, are used for different purposes in the biomedical field and for this reason they are among the most investigated nanoparticles. Mainly, Gold NPs are employed in drug delivery,

imaging and targeting [172]. This kind of metallic nanoparticles are commonly assembled using colloidal synthesis which allows high control of shapes and sizes, such as spherical, rod-like, cage-like and so on, ranging from 1 nm to more than 100 nm. Although, shape and size are strongly related to their physical proprieties.

Figure 3.5.3: Example of morphologies of gold nanoparticles. Created with *BioRender.com*

In addition to *in vivo* biocompatibility and non-toxicity, Gold NPs can be functionalized by all kinds of biomolecules due to the negative charge on outer surface. This peculiarity increases their performance as carriers, biosensors or contrast agents and induces an external stimulus-response behaviour such as in photothermal therapy (PTT) used as cancer treatment [173, 174, 175].

3.5.3 Magnetic iron-oxide NPs

Iron oxide is another common material for inorganic NP synthesis and iron oxide NPs are majority of FDA-approved inorganic nanodrugs [176]. Magnetic iron oxide NPs, composed of magnetite (Fe_3O_4) or maghemite (Fe_2O_3), are characterized to possess superparamagnetic properties at certain sizes and they can be used as contrast agents in magnetic resonance imagining (MRI) [177], drug delivery carriers and thermal-based therapeutics [178]. When the magnetic iron-oxide NPs reach small sizes, ranging from 10-20 nm, superparamagnetic proprieties appear, a relevant potential for medical applications such as drug delivery [179]. Using an external magnetic field, magnetic iron-oxide NPs can be guided towards the target site. Besides the sizes, also shape, coating and stability influence magnetic iron-oxide NPs. In fact, the main disadvantages related to this kind of nanoparticles are oxidation and cell toxicity which can be overcame though polymeric, golden or peptide surface-coating.

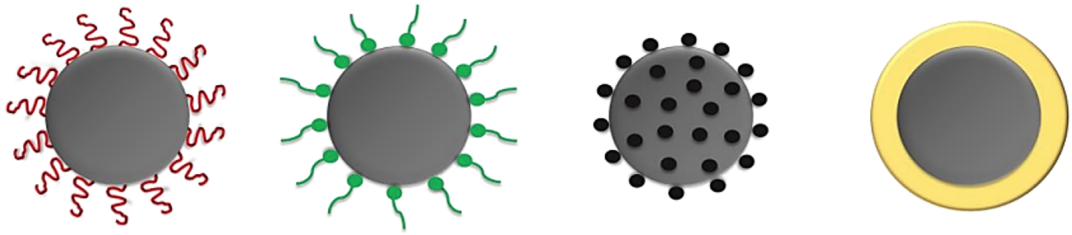

Figure 3.5.4: Schematic illustration of the main shells for functionalization of iron-oxide NPs: polymeric coating (a), organic coating (b), inorganic coating (c), golden coating (d) [179].

3.5.4 Silica-based NPs

Silica-based NPs have a dominant role in drug delivery due to their key characteristics, such as size ranging between 5 - 1000 nm, porous structure, optical properties, high specific surface area, low density, adsorption capacity, high encapsulation ability, biocompatibility, and low toxicity [180]. Those features induce Silica NPs to be widely utilized as an inert solid cage or entrapping matrix [181]. Silica-based NPs in drug delivery are primarily mesoporous Silica-NPs.

3.5.4.1 Mesoporous Silica NPs

Mesoporous Silica NPs, as nanocarrier, retain the drug through the pores and its release is mediated by other particles such as Gold NPs that keep pores occluded or open. This latter behaviour is called gatekeeping [182]. The chemical bond between caps NPs and pores of mesoporous Silica NPs is stimuli responsive [183].

This kind of NPs are highly efficient for drug delivery because they offer a stimuli-controlled drug release and different drugs can be loaded without structure modifications [184].

Figure 3.5.5: Structure of Mesoporous Silica-NP. Created with *BioRender.com*

Part II

Experimental section

Chapter 4

Hydrogel physically functionalized

In the previous chapters we talked about hydrogel systems for drug delivery and the use of graphene as a filler. In this first part of the PhD thesis, we propose the synthesis of graphene-based hydrogels as thermo-sensitive carriers for controlled drug release. In this work, hydrogels were obtained via microwave-assisted condensation reaction between branched polyacrylic acid and agarose, and pristine nano-layered graphene (few layered graphene, FLG) was used as a nanofiller to investigate the graphene thermal effect in the drug release scenario. The FLG stabilization was obtained through the dispersion of exfoliated graphite in isopropyl alcohol to induce the intercalation of the solvent molecules into the graphitic interlayer spaces, providing a material with increased water dispersibility. This approach ensures the sol-gel transition in aqueous media, avoiding the use of organic solvents. Moreover, the synthetized hybrid scaffolds preserve all the peculiar features of pristine graphene as the hydrogel are physically functionalized, without distortions related to the oxidation processes. We investigated the drug release profile at different temperatures: 25 °C, 37 °C and 44 °C. Diclofenac, an anti-inflammatory molecule commonly used to treat musculoskeletal and systemic inflammations, was chosen as a candidate drug. Results showed tunable diclofenac release over time, according to the temperature increase. This response is not observed in polymeric scaffolds without FLG, suggesting that the thermal conductivity and the π-conjugated structure affect the vibration frequency of the nanofiller [185, 186] and, consequently, the electrostatic interactions with drug and the release kinetic. In particular, increasing temperature, the diclofenac release becomes faster. Furthermore, we evaluated the anti-inflammatory performance of released drug, in terms of cyclooxygenase (COX) inhibition, report-

ing an efficiency comparable to diclofenac in aqueous medium, and proving that the interactions with FLG did not affect the properties of the drug. According to ISO 10993-5, these graphene hybrid hydrogels present high biocompatibility, that confirms their potential application for thermally triggered drug release in several biomedical applications.

4.1 Experimental

4.1.1 Materials

Branched polyacrylic acid (carbomer 974P, $MW = 1MDa$, by Fagron, The Netherlands) and ultrapure agarose ($MW = 200kDa$, by Invitrogen Corp., USA) were used as reagents for gel formulation. Commercially available intercalated graphite was provided by Asbury Carbons (Anthracite Industries, Inc.) and was used as the starting material for the synthesis of FLG. This graphite was intercalated with sulphates and nitrates, positioned between the various carbonaceous layers, and prepared in an acid environment (pH between 1 and 6). All other chemicals and diclofenac sodium salt were purchased from Merck (Merck KGaA, Darmstadt, Germany). The materials were used as received, without further purifications, and the solvents were of analytical grade.

4.1.2 Synthesis of few layered graphene (FLG)

FLG were fabricated through the exfoliation method assisted by microwave irradiation, according to a simple and industrially scalable procedure [187, 188] previously developed at the INFN NEXT Nanotechnology Laboratory in Frascati (Rome). Intercalated graphite (2 g) underwent a sudden thermal shock for 30 s, caused by microwave irradiation (800 W), and resulting in a growth temperature above 1000 °C. The resulting crystalline stacks of atomic graphene layers (200 mg, hereinafter FLG, in Figure4.1.1) were dispersed in isopropyl alcohol (200 mL) by stepwise additions (50 mg each) every 10 minutes under pulsed-mode sonication at room temperature (RT), to a final concentration of 1 mg/mL (Figure 4.1.2). The obtained system was dried at 90 °C to remove alcohol and the resulting conglomerate was dispersed in distilled water at 0.01% w/v and sonicated for 40 min, until complete suspension.

Figure 4.1.1: Few layered graphene.

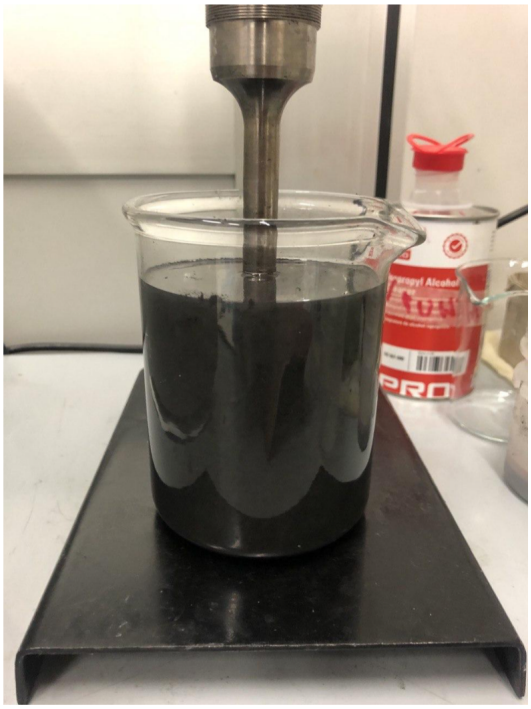

Figure 4.1.2: FLG dispersion in water.

4.1.3 Synthesis of graphene-laden hydrogels

The starting branched polyacrylic acid (PAA) solution was prepared as follows: carbomer 974P (50 mg) was dissolved in PBS solution (9.95 mL), then the mixture was left to settle for 30 min and pH was brought to 7.8 by 1M NaOH addition. Hence, graphene-laden hydrogels (FLG-HG) were synthetized: agarose (40 mg, 0.8% w/v) was added to PAA solution (5 mL) and the mixture was subjected to electromagnetic stimulation (500 W) for 30 s and heated to 80 °C to induce the condensation reaction between the carboxyl and hydroxyl groups. The reactor was kept closed to prevent solvent evaporation. The resulting system was cooled to 60 °C and mixed at 1:1 volume ratio with the FLG solution, obtaining a final FLG concentration of 0.5 mg/mL. Finally, the solution was poured in cylinders (0.25 mL of mixture in each cylinder with a diameter of 1.1 cm) upon cooling to achieve the complete gelation (Figure 4.1.3). Pristine hydrogels (HG) were also produced as a reference standard for the experimental validations. The latter were synthetized following the FLG-HG protocol using distilled water for the 1:1 dilution stage prior to casting.

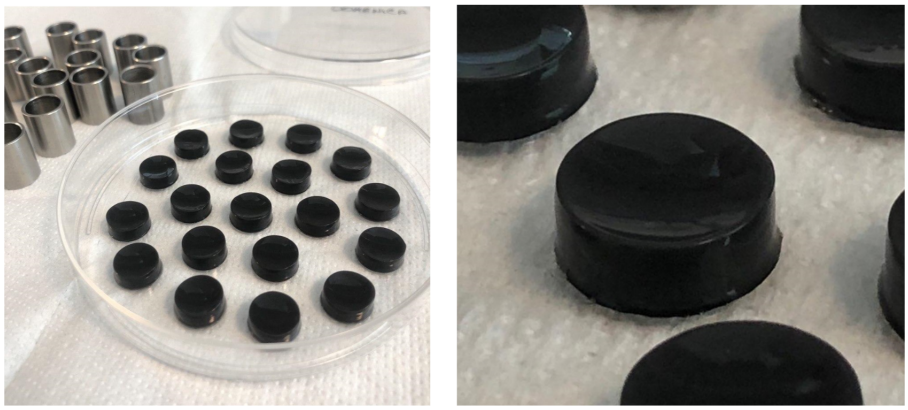

Figure 4.1.3: FLG-HG

4.1.4 Water uptake behavior

Water uptake capacities of FLG-HG and HG were evaluated gravimetrically. The hydrogel samples were first immersed in PBS for about 30 min, to remove potential unreacted components, and freeze-dried; then they were weighed (Wdry) incubated in excess PBS (about 3 mL) to reach complete swelling. At defined time points, each sample was removed from the PBS, wiped with moistened filter paper and weighed (Wwet). The water uptake percentage (Q) was calculated according to Eq. 4.1.1.

$$Q = \frac{W_{wet} - W_{dry}}{W_{dry}} \times 100\% \quad (4.1.1)$$

Data were recorded at temperatures of 25 °C, 37 °C and 44 °C and each condition was analyzed in triplicate.

4.1.5 Characterization techniques

4.1.5.1 Raman spectroscopy

Raman characterization was carried out using an Invia microscope (Renishaw) equipped with a 532 nm laser and two gratings (600 and 1800 l/mm). Spectra were acquired directly on the lyophilized samples. The power laser, the exposure time and the number of accumulations were optimized for each sample.

4.1.5.2 FT-IR analysis

FT-IR analysis was performed on an Agilent Cary 630 spectrometer, equipped with Diamond ATR-module, at a resolution of $2cm^{-1}$ and 128 acquisitions. Spectra were acquired placing the lyophilized samples on the diamond cell without any preparation and recorded in the $4000 - 650cm^{-1}$ wavenumber range.

4.1.5.3 Rheological studies

Measurements were performed on a MCR302 rheometer (Anton Paar GmbH) with a 25-mm plane plate configuration. Amplitude sweep and frequency sweep tests were conducted at 25 °C, 37 °C and 44 °C, after complete gelation of each sample. Amplitude tests were performed at 10 Hz, whereas G´ (elastic modulus) and G˝ (loss/viscous modulus) were determined at low strain values (0.1%) over the frequency range 0.5–50 Hz.

4.1.6 Drug loading

Drug loading was performed during the synthetic step. Diclofenac was respectively dissolved in FLG solution (FLG-HG group) or in distilled water (HG group) at 0.5 mg/mL. The drug solution was sonicated for 1 h at room temperature (RT) and used to dilute the polymeric mixture post microwave irradiation, following the

procedure reported in the hydrogel synthesis (section 4.1.3), leading to a final drug concentration of 0.25 mg/mL in hydrogel samples.

4.1.7 Drug release profiles

Drug release mechanism was investigated at pH 7.4, at different temperatures: 25 °C, 37 °C and 44 °C. In details, hydrogel specimens were incubated in PBS (1 mL) and 500 μL aliquots were collected at defined time points, restoring the buffer volume to avoid mass transfer equilibrium with the surrounding environment. The amount of released diclofenac was determined by UV-vis spectroscopy at λ= 276 nm against a calibration curve.

4.1.8 Cytotoxicity assay

The biocompatibility of HG and FLG-HG was assessed in vitro, according to ISO 10993-5, using BALB/3T3 cell line (American Tissue Culture Collection, ATCC; Rockville, MD). Lyophilized hydrogel specimens were sterilized by UV irradiation for 20 min and placed into a 24-well plate. Then, Dulbecco's Modified Eagle Medium (DMEM) supplemented with 10% fetal bovine serum (FBS), 1% L-glutamine, and 1% penicillin/streptomycin (Merck KGaA) were added to each sample (1 mL per 3.5 mg of hydrogel specimen) and incubated for 24 h at 37 °C. The resulting eluate was supplemented to cell cultures at different titers and cell viability was evaluated at 24 h by MTT assay, which is based on the reduction of tetrazolium salts by metabolically active cells. Briefly, 3-(4,5-dimethylthiazolyl-2)-2,5-diphenyltetrazolium bromide was added to each well to a final concentration of 0.5mg/mL. After incubation for 4 h at 37 °C, 5% CO2, medium was removed, and the resulting intracellular purple formazan salts were dissolved in DMSO (200 μL per well). Absorbance was measured at 590 nm on a microplate reader (TECAN M200 Pro plate reader). Non treated cells were used as a control for cell viability. Experiments were performed in triplicate.

4.1.9 Cyclooxygenase (COX) assay

The anti-inflammatory activity of diclofenac following its release from the hydrogels was tested in vitro in terms of COX inhibition on cell lysates. The THP-1 monocytic cell line was used as a cell model. Cells were maintained in RPMI 1640 (Merck KGaA) supplemented with 10% fetal bovine serum (FBS), 1% non-essential amino acids,

1% sodium pyruvate and 0.1 mg/ml penicillin/streptomycin/L-glutamine (Merck KGaA). Cell differentiation into macrophages was performed in 75 cm^2 flasks at a density of 1 x 10^6 cells/mL in complete RPMI containing 150 nM phorbol 12-myristate 13-acetate (PMA) (Merck KGaA). Medium was changed after 24 h, and cells were cultured for additional 48 h in complete RPMI. Inflammation was induced by administration of 10 ng/mL LPS (Merck KGaA) for 48 h. Cells were then washed with PBS and detached by trypsin. THP-1 macrophages were pelleted by centrifugation at 200 × g for 5 min and washed with PBS. The pellet was lysed in a lysis buffer consisting of ice-cold PBS, 1% NP-40 surfactant (Thermo Fisher Scientific) and Halt Protease Inhibitor Cocktail (1:1000, Thermo Fisher Scientific), and incubated on ice for 5 min. The lysate was centrifuged at 13,000 × g for 5 min at 4 °C and the supernatant was collected. Inhibitory effect of diclofenac was analyzed through a Fluorometric COX Activity Assay (Abcam, ab204699) that provides a sensitive method to detect the peroxidase activity of COX in biological samples. Eluates from FLG-HG were withdrawn after 24 h incubation, and diclofenac concentration was determined spectrophotometrically. A freshly prepared diclofenac solution, at the same concentration, was used as a positive control. Additionally, a no-drug group was used for data normalization. In our typical experiment, 20 µL of reaction buffer containing cell lysate, fluorometric probes and sample under investigation were spotted on a 96 well multiplate. After the addition of arachidonic acid (COX substrate) in NaOH solution, the enzymatic reaction led to the production of a fluorescent molecule (resorufin dye, $\lambda_{Ex/Em}$=535/587 nm), that could be monitored in kinetic mode (one read every 15 s) for 20 min at RT, using a TECAN M200 Pro plate reader. Data were plotted as Relative Fluorescence Units (RFU) over time and COX activity could be determined as the slope of the curve in its linear region, using a resorufin standard calibration curve: in particular, 1 COX unit is defined as the amount that leads to the production of $1\mu mol$ of resorufin per min, at physiological pH and 25 °C.

4.1.10 Statistical analysis

Where applicable, experimental data were analyzed using Analysis of Variance (one-way and two-way ANOVA). Statistical significance was at the 0.05 level. Results are presented as mean value ± standard deviation.

4.2 Results and discussion

4.2.1 FLG production

FLG was prepared using an expandable graphite characterized by intercalating sulfate and nitrate derivatives, localized among the graphite planes. The microwave-induced thermal shock promotes the intercalating substances vaporization, which modifies the air dielectric properties and causes a propagation of sparks that sustain the process, reaching temperatures around 1000 °C [189]. During the vaporization, the gases exert a pressure between two adjacent planes increasing the reciprocal distance and giving rise to the final exfoliated material. The resulting graphene presented a worm-like structure, with a higher surface area and a thickness in the range of 3-9 planes, according to the expansion process. Therefore, the material has the ability to increase the electronic interactions with other molecules, exploiting its cyclic nature and the electronic cloud that can merge with other rings or protonated/deprotonated chemical groups [190, 191]. Moreover, the use of microwave irradiation ensures a fast and cheaper procedure in terms of time (30 s) and energy needs (lower than a thermal approach carried out in an oven), and the experimental conditions are solvent-free, reducing potential side effects and secondary reactions. The subsequent formation of nanoplatelets occurred as dispersion in isopropyl alcohol, under ultrasound, that ensures the rearrangement of graphene layers to form nanostructures with the two-dimensional lateral sides having sizes of about 10 μm, as showed in Figure 4.2.1, and a thickness of 5 nm.

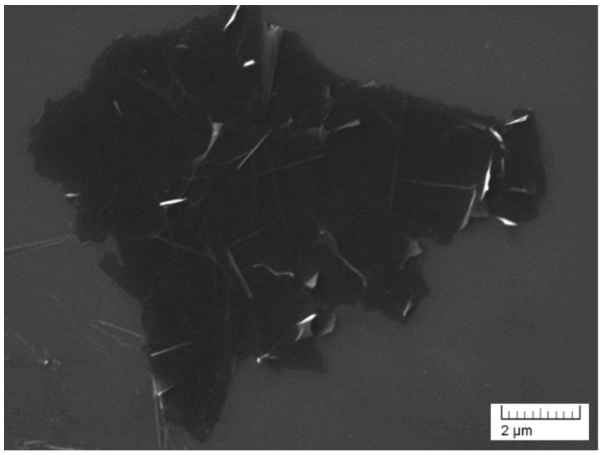

Figure 4.2.1: SEM image of graphene nanoplates

Isopropyl alcohol is less aggressive than other commonly used solvents, protects graphene against chemical modifications or aggregations and ensures the FLG stabilization in aqueous medium due to the interactions between its hydroxyl groups and the graphene $\pi-$surface or the edges, preserving the thermal properties of the material [192, 193, 194]. The resulting FLG was characterized by high graphitic sp^2 character and the presence of oxygenated groups was negligible [195, 196].

4.2.2 Hydrogel formation

The gelation mechanism of our material is due to the chemical cross-linking between the carboxyl groups of polyacrylic acid and the hydroxyl moieties of agarose. The microwave irradiation causes a temperature increase to ca. 80 °C, enhancing the macromer mobility, and thus the short-range interconnections among functional groups of the polymers. This leads to the production of local networks (also known as microgels) which, as polycondensation proceeds, give rise to the final hydrogel matrix. During the sol-gel transition, the viscosity progressively increases, decreasing the mobility of macromers and allows closer functional groups still react efficiently. The resulting physico-chemical condition promotes the 'welding' between microgel surfaces, giving rise to the three-dimensional macrostructure [197]. The choice to use carbomer and agarose was due to their well-known biocompatible features that make them good candidates in therapeutic protocols and tissue engineering: carbomer also possesses an anti-inflammatory action [198, 199], and agarose shows tunable properties suitable for medicine-oriented applications, such as permeation to oxygen and nutrients, resemblance to extracellular matrix components and low immunogenicity [200, 201]. Furthermore, the microwave-assisted approach ensures the design of hydrogels able of in situ forming, offering a major advantage over rigid scaffolds because they can easily adapt to any shape and can also be introduced using minimally invasive procedures. In this work, the hydrogel building blocks were made up mostly of C-C bonds, where FLG was entrapped through physical interactions, without affecting the peculiar properties of graphene, as shown in Figure 4.2.2. For these reasons, FLG was added after microwave irradiation, during the sol-gel transition. Similarly, the drug was firstly added to the FLG solution and added to the polymer solution following microwave irradiation, in order not to affect the reciprocal interactions ($\pi-\pi$ and physical bonds) between diclofenac and FLG. In particular, the drug molecules non-covalently adsorb onto or wrap around the graphene surface, due to the

π-π and physical bonds formation. Indeed, the covalent functionalization of graphene generally include two different routes: the formation of covalent bonds between free radicals or dienophiles and C=C bonds of the pristine graphene or between organic functional groups and the oxygen groups of graphene oxide [202].

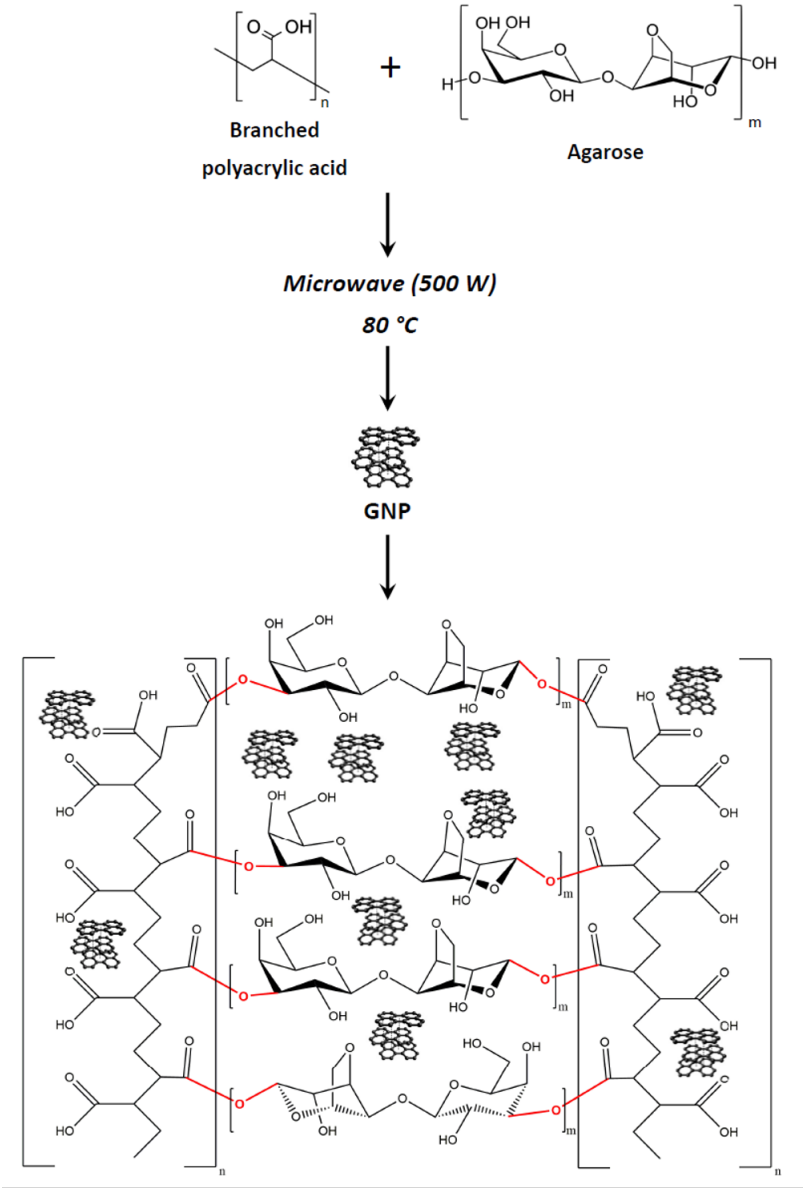

Figure 4.2.2: Synthesis of graphene-laden hydrogel and putative matrix chemical structure: ester bonds (cross-linking points) are highlighted in red

SEM analysis was performed on fracture surfaces of lyophilized samples confirming the homogeneous FLG dispersion in the HG matrix, ruling out the presence of

FLG agglomerates. HG and FLG-HG specimens were snap frozen and lyophilized for 24 h. Specimens were fractured and gold-sputtered (Cressington sputter coater) prior to SEM observation (Tescan Vega II). SEM observation allowed us to rule out agglomeration of FLG in the FLG-HG specimen. The presence of a porous texture (pore size 6-21 μm) in lyophilized samples is reliably associated to the thermally induced phase separation occurring during freezing, which is known to leave a sponge like morphology in hydrogel materials [203, 204], as shown in Figure 4.2.3.

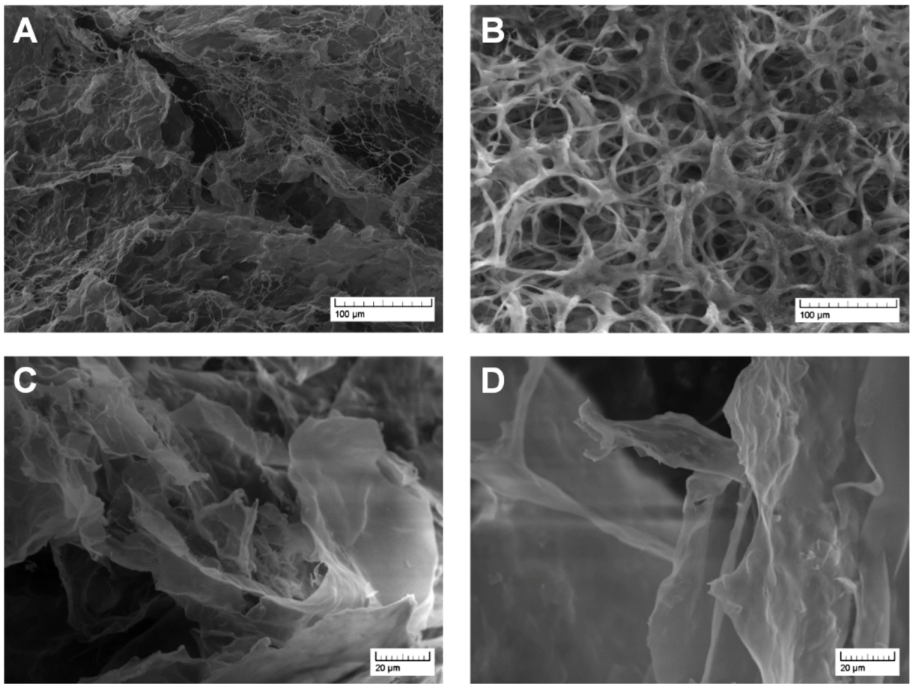

Figure 4.2.3: SEM images of FGL-HG scaffold (A,C) and neat hydrogel (B,D)

Raman analysis, in Figure 4.2.4, shows the spectra of neat and graphene-laden hydrogels. In pristine HG (Figure 4.2.4A), the signal at 3438 cm^{-1} can be ascribed to the stretching vibration of the residual O-H groups, whereas the peak at 2954 cm^{-1} is related to the C-H stretch of the polymer backbone. The formation of ester bonds can be traced back to the asymmetric CO_2 stretching at 1476 cm^{-1} and to the C-O-C stretch vibration in the range 900–1000 cm^{-1}, which can be ascribed to the glycosidic bond between the monosaccharide units of agarose and the formed ester groups. The Raman spectrum of FLG-HG (Figure 4.2.4B) shows all the peculiar peaks of pristine HG (the O-H stretching at 3471 cm^{-1}, the C-H stretching at 3000 and 2950 cm^{-1}, and the asymmetric CO_2 stretching of esterification at 1465 cm^{-1}), even if partially

covered by graphene bands (D band= 1353 cm^{-1}, G band= 1585 cm^{-1} and 2D band= 2718 cm^{-1}), suggesting that the FLG intercalation did not chemically modify the hydrogel matrix and the graphene layers were entrapped within the mesh size through physical bonds.

Figure 4.2.5 shows the whole Raman spectra in aqueous solution of FLG, diclofenac and the system FLG-diclofenac after sonication. In the latter, additional bands related to a potential hybridization sp3 C-C bonds in covalent bonds are not detectable, confirming the only physical interactions between the pristine graphene structure and the drug: D, G and 2D band of FLG are clearly recognizable.

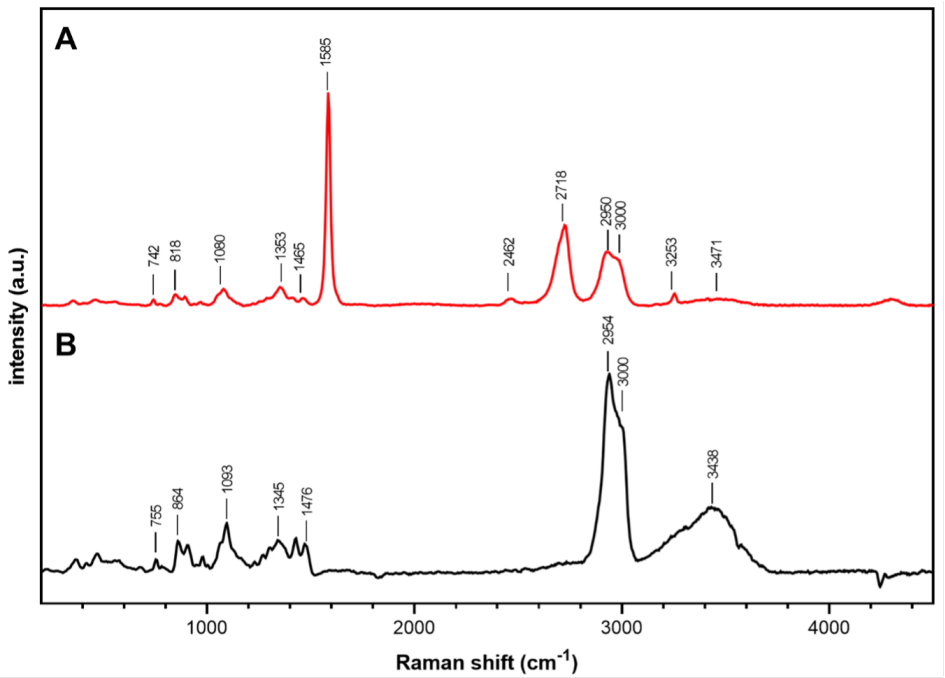

Figure 4.2.4: Raman spectrum of FLG-laden hydrogel (A) and of neat polymeric matrix (B)

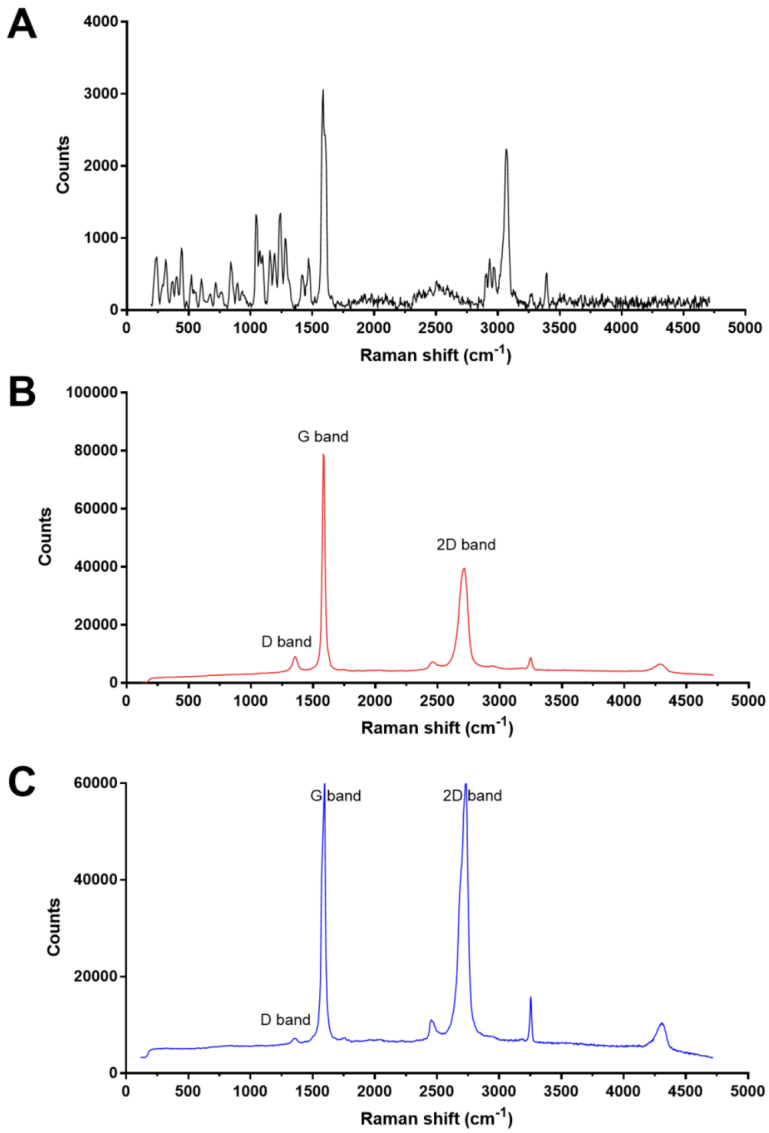

Figure 4.2.5: Raman spectra of diclofenac (A), FLG (B) and FLG-diclofenac (C) in aqueous solution.

An additional check was carried out through ATR/FT-IR analysis, that ensured a clear detection of the characteristic peaks of chemical cross-linking between carbomer and agarose, and the absence of chemical shift following the embedding of FLG.

In Figure 4.2.6, FT-IR spectrum of lyophilized FLG-diclofenac specimen after sonication in aqueous medium (before hydrogel synthesis) is compared to the spectra of pure FLG and diclofenac. In FLG spectrum the peak at 3296 cm^{-1} (***) can be ascribed to the aromatic C-H stretching, the signals at 1560 cm^{-1} and 1500

cm^{-1} (**) are related to the C=C stretching and the peak around 1450 cm^{-1} (*) is representative of the C-H bending [205, 206]. The spectrum of diclofenac shows the characteristic peaks of the N-H stretching of the secondary amine group at 3421 cm^{-1} (♦♦♦♦), the C=C stretch vibration of the phenyl moieties around 2950 cm^{-1} (♦♦♦), the C-H stretching of the aromatic structure at 1560 cm^{-1} (♦♦) and the stretch of the Cl-disubstituted phenyl group at 746 cm^{-1} (♦) [207]. The graphene and drug signals are detectable in the spectrum of the complex FLG-diclofenac and no additional peaks appear, confirming that the drug molecules are not covalently linked to the graphene lattice and the interactions between the two components are due to physical bonds and π-π stacking.

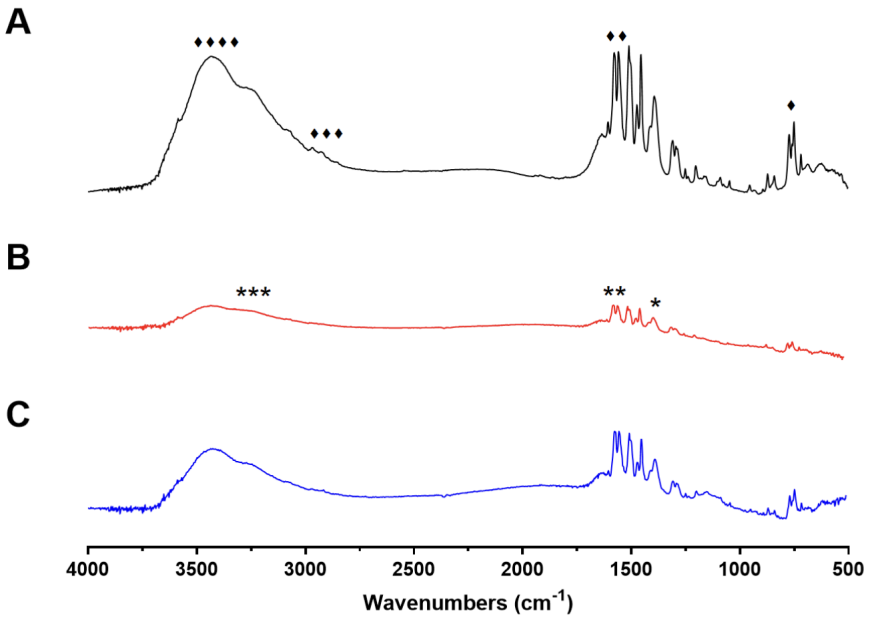

Figure 4.2.6: FT-IR spectra of diclofenac (A, black), FLG (B, red) and FLG-diclofenac system (C, blue). The characteristic peaks of the pristine graphene and the drug are highlighted.

Figure 4.2.7 shows the comparison between the ATR spectra of HG and FLG-HG. Referring [208] , the characteristic peaks of esterification are clearly detectable at 1650 cm^{-1} (symmetric CO2 stretching) and at 1400 cm^{-1} (asymmetric CO2 stretching). The addition of graphene in FLG-HG does not modify the peculiar signal of the polymer matrix, confirming the hypothesis that FLG was entrapped through physical interactions and not through chemical bonds. Furthermore, any additional

peaks of FLG are present, confirming the low presence of defects (oxidation) of the filler.

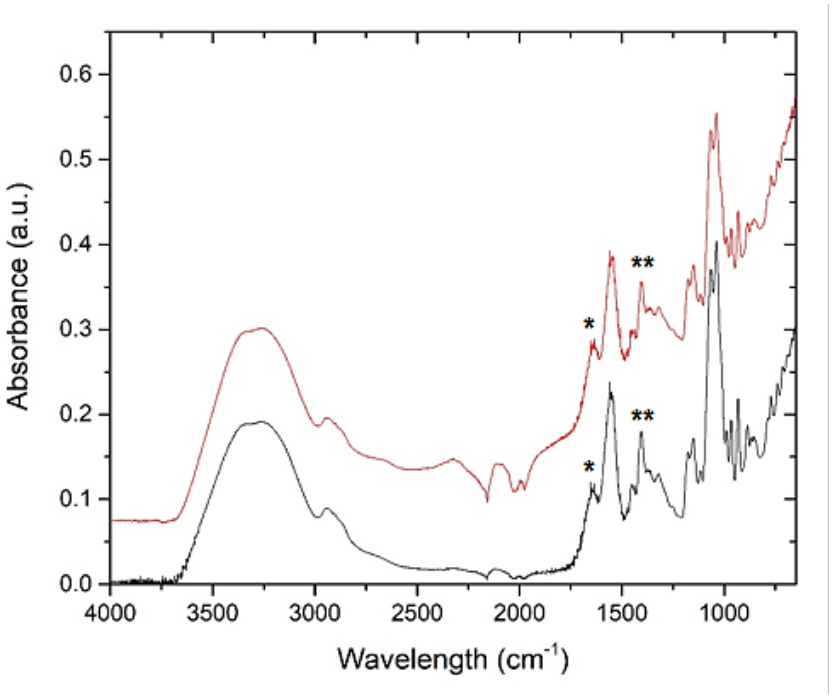

Figure 4.2.7: ATR spectra of HG (black) and of FLG-HG (red). The signals related to the symmetric (*) and asymmetric (**) stretching of CO_2 are highlighted.

Nevertheless, a furthered analysis of O-H and C-H bond stretching confirms the nature of interaction between FLG and hydrogel matrix. The intermolecular interactions occurring in the studied system can be divided into two main groups: site-specific polar (polar π interaction, in our case hydrogen bonding due to hydroxyl and carboxylic groups) and non-specific dispersive interactions (London–van der Waals interactions, related to C-H instantaneous dipole moments). The two types of interactions are highlighted by the change in relative intensity of O-H and C-H bond stretching. In Figure 4.2.8A, the normalized intensity (and peak area) of C-H stretching at 3000 cm^{-1} and O-H stretching at 3471 cm^{-1} are reported vs. peak at 2950cm^{-1} , which was set as a reference.

This evaluation demonstrated that FLG was physically entrapped in the hydrogel matrix generating intramolecular interaction with the polymer. The presence of FLG promoted the dispersive interaction, as detectable by the increased value of the 3000 cm^{-1} / 2950 cm^{-1} ratio, both in intensity and peak area, in FLG-HG (Fig. 4.2.8A, black columns) compared to the neat hydrogel matrix (Fig. 4.2.8A,

red columns), and hinder the polar interactions resulting in the decreasing of the value of the 3471 cm^{-1} /2950 cm^{-1} ratio, both in intensity and peak area, in FLG-HG (Fig. 4.2.8A, black columns) compared to HG (Fig. 4.2.8A, red columns).This is in agreement with previous literature (Belyaeva and coworkers [209]) that shows how the transparency of FLG to polar and dispersive interactions may vary upon the nature of the supporting substrate, as well as the number of graphene layers and the presence of contaminants and defects at the FLG/substrate interface. In particular, in the presence of corrugations in the FLG structure (as reliably occurring in our system), FLG is reported to screen polar interactions, while transmitting dispersive ones. The π-π and physical interactions between diclofenac and graphene are confirmed by a shift of the G band, as reported in Figure 4.2.8B. The G-band of pristine FLG, located at 1581.45 ± 0.06 cm^{-1} , experiences a shift of 1.3 cm^{-1} due to the interaction with diclofenac, proving the carrier-drug bond through π-π interactions.

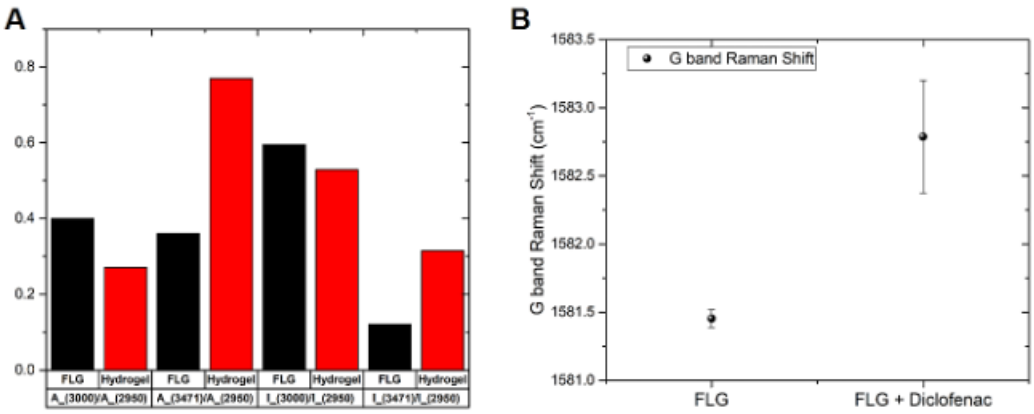

Figure 4.2.8: A: Signal intensity of C-H stretching and O-H stretching due to the intramolecular interaction between FLG and polymer matrix in FLG-HG (Hydrogel); B: Raman shift values of G-band in FLG and FLG-diclofenac system

4.2.3 Hydrogel physical properties

The peculiar feature of hydrogels is their capacity to retain a high amount of water and ensure exchange and diffusion of molecules with the surrounding environment. The water uptake capacity is a function of the network structure, in terms of concentration of the elastic chains, hydrophilicity, density of electronic charge of the functional groups, and pore size [210]. The addition of FLG could affect the polymer

chains stretching during the exposure to aqueous solvents, altering the swelling and the equilibrium water content. We investigated this aspect at different temperatures and compared the FLG-HG samples to those pristine HG. As shown in Figure 4.2.9, HG shows higher water uptake at equilibrium than FLG-HG at 25 °C (6300±200% vs. 5000±200% after 24 h). At 37 °C and 44 °C, instead, HG and FLG-HG show similar trends and reach the same swelling equilibrium, with FLG-HG only showing an increased water uptake vs. pristine HG in the initial phase of swelling. These results could be explained considering the nature of FLG: at RT, its hydrophobicity and the physical interaction between the π-system and the residual hydroxyl and carboxyl groups counterbalances the polymer chains elongation, resulting in an opposite force to the swelling; increasing the temperature, the mobility of cross-linked polymer tends to increase and the thermal transfer ability of FLG [211] supports the scaffold stretching, also inducing a more swollen configuration in the first minutes at 44 °C. Therefore, the presence of FLG results in a temperature-dependent modulation of the initial hydrogel swelling behavior. Generally, the equilibrium between the hydrophobic and hydrophilic polymer moieties controls the water uptake ability of the hydrogel [212, 213]: here, the presence of graphene nanofiller con- tributes to the definition of the equilibrium state in aqueous medium.

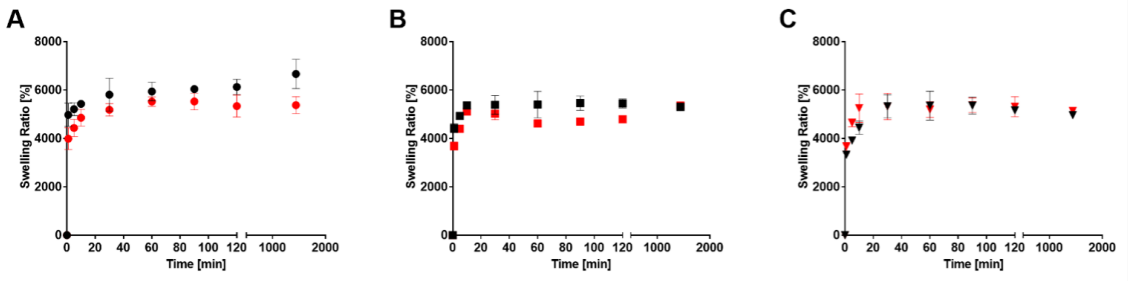

Figure 4.2.9: Swelling behavior of FLG-HG (red) and HG (black) hydrogel at different temperature: A) 25 °C, B) 37 °C, C) 44 °C.

Rheological studies were carried out to characterize the viscoelastic behavior of the hydrogel samples. Notably, the FLG loading could affect the scaffold capacity to store energy elastically, promoting a reinforcement in the mechanical properties or modulating the deformation of polymer chains due to the nanoplatelet physical hindrance. Figure 4.2.10A shows the recorded data for HG and FLG-HG. All samples presented a storage modulus G' approximately one order of magnitude higher than the corresponding loss modulus G", indicating that the hydrogels are elastic

rather than viscous materials, with an essentially frequency-independent behavior. Moreover, the physisorption of FLG modulates the G' and G" values at all investigated temperatures. At 25 °C, FLG led to an increase in the storage modulus compared to the HG reference: FLG-HG exhibited G'=1800 Pa, whereas HG was characterized by a value of G'=1200 Pa; this result could be attributed to the formed physical cross-linking points between graphene and the polymeric chains which may strengthen the gel network [214] and enhance its mechanical properties.

Indeed, after FLG incorporation during the microwave-assisted synthesis, the π-lattice is responsible for the physical complexation of graphene with polymer carboxyl and hydroxyl groups, mainly through electron-based interactions and hydrogen bonds [181], limiting the movement of polymeric chains. Regarding G", the viscous component was not significantly influenced by FLG.

On the other hand, at 37 °C and 44 °C, the graphene-laden hydrogels were characterized by lower G' and G" than the corresponding HG samples, showing an opposite trend compared to 25 °C. The decrease could be related to the rise of molecular mobility [215]: temperature increase promotes polymer chains elongation and the weak physical bonds (Van der Waals and hydrogen linkage) formed with FLG are minimized due to the enhanced thermal vibration mode of the π system and the consequent phonon dissipation that reduces the cross-linking feasibility in the hydrogel matrix [216]. For these reasons, FLG-HG at 37 °C and 44 °C showed comparable viscoelastic trend (G' varies in the range 400-340 Pa and 456-377 Pa, respectively), with a slightly higher deformability at 37 °C. The latter could be explained considering the agarose and polyacrylic acid thermal response: by increasing the temperature, the polymer chains become more elongated and in particular agarose, due to its helix conformation, tends to be entangled giving rise to micro-concentrated junctions area, assisted by formation of intramolecular hydrogen bonds [217, 218]. This behavior is also oriented by the presence of chemical cross-linking points (ester bonds) between the constituents of the hydrogel matrix [219], suppressing the stress concentration during the tensile measurement [220]. As a result, the sample carried out a higher value of viscous component at 44 °C.

Moreover, the FLG prevents effectively the polymeric flexibility due to its rigid hindrance that limits the mean free path. Similar trends can be observed in HG rheology, with higher value of G" at 37 °C and 44 °C than HG-FLG, justified by the absence of graphene constraints.

The rheology sweep test (Figures 4.2.10B, 4.2.10C and 4.2.10D) evaluates also the

flow stress value, at which the contribution of G" is equal to G' (crossover point) and determines the value of the material damping tan(δ), representative of the internal friction between the hydrogel meshes in that condition. At low strain, G' and G" of FLG-HG and HG indicate a network of packed polymeric chains and the correlation with tan(δ) confirmed for both hydrogels a liquid-like response rather than a solid-like behavior. Moreover, the intersection of storage and loss moduli occurs at similar values in both samples at 37 °C (Figure 4.2.10C, at shear stress τ=16.8 Pa in FLG-HG and τ=14.8 Pa in HG) and 44 °C (Figure 4.2.10D, at shear stress τ= 16 Pa and τ=18.8 Pa), whereas at 25 °C the crossover is slower in graphene-laden samples (at shear stress τ=9.9 Pa) compared to standard hydrogel (at shear stress τ=17.6 Pa) indicating higher stiffness in the chemical network containing FLG.

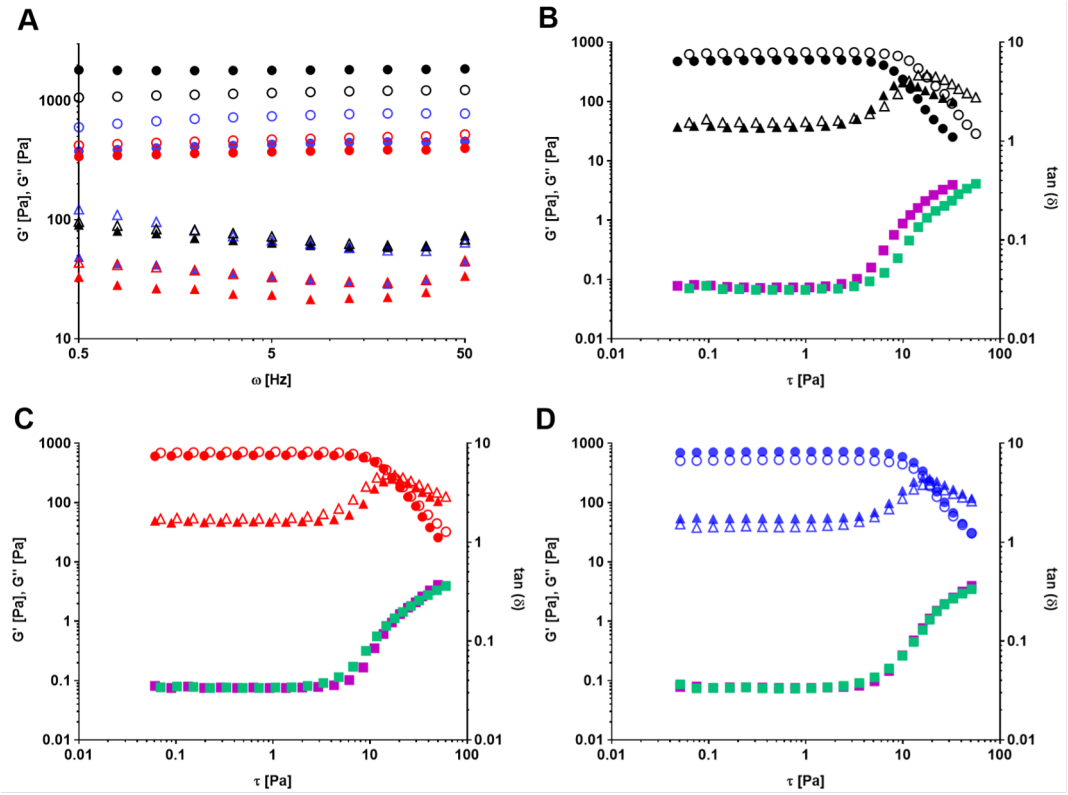

Figure 4.2.10: Rheological behavior of graphene-laden hydrogels at 25 °C (G´ • black, G″ ▲ black, tan(δ) ■ violet), at 37 °C (G´ • red, G″ ▲ red, tan(δ) ■ violet) and at 44 °C (G´ • blue, G″ ▲ blue, tan(δ) ■ violet) and hydrogels without graphene at 25 °C (G´ ∘ black, G″ △ black, tan(δ) ■ green), at 37 °C (G´ ∘ red, G″ △ red, tan(δ) ■ green) and at 44 °C (G´ ∘ blue, G″ △ blue, tan(δ) ■ green). A) G´ and G″ trends in frequency range 0.5–50 Hz; B) Crossover point at 25 °C; C) Crossover point at 37 °C; D) Crossover point at 44 °C

4.2.4 Drug release

Prior to the determination of drug release profile, the potential release of FLG from the hydrogel was ruled out.

The potential FLG release from the hydrogel meshes was investigated in order to check the stability of the physical interactions between the polymers and graphene over time, which, otherwise, could affect the following drug release. FLG release was studied at the different temperatures of 25 °C, 37 °C and 44 °C, in aqueous medium. The synthesized FLG-HG were placed in PBS solution (1 mL) and aliquots of 500 µL were collected at fixed time points. The removed volume was replaced by fresh solution, in order to prevent the equilibrium in mass transfer between the hydrogel and the surrounding environment. The amount of released FLG was estimated in percentage as the ratio of the released absolute amount in the aqueous media to the sum of the total amounts of the released and unreleased FLG. The experiments were repeated 3 times and the results were averaged. The released amounts were determined through UV-vis spectrophotometric analysis at wavelength λ= 268 nm [221] and determined referring to the standard calibration curve for FLG. The obtained results are showed in Figure 4.2.11.

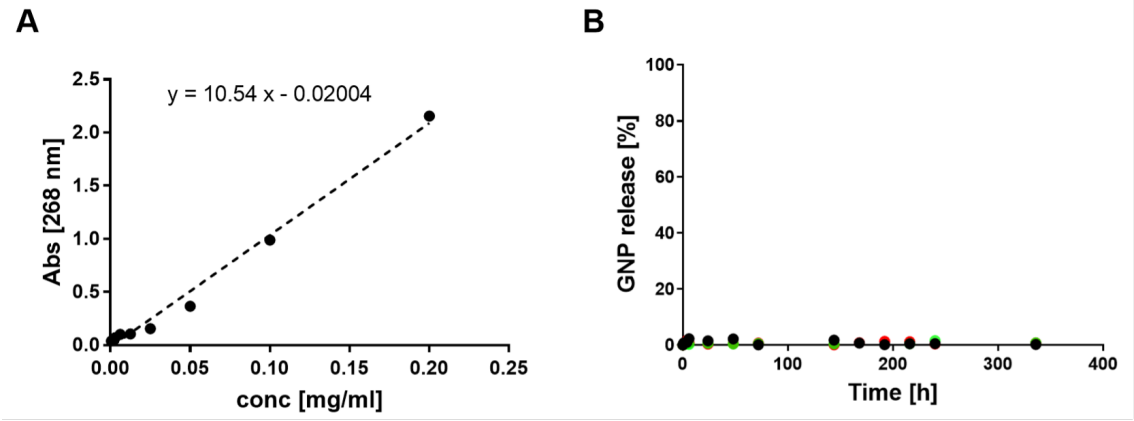

Figure 4.2.11: A) FLG calibration curve; B) FLG release at 25 °C (•, black), 37 °C (•, green) and 44 °C (•, red).

Moreover, the representative UV-vis spectra of FLG solution (red) and FLG release (black) are represented in Figure 4.2.12after 6 h, at 37 °C: in the latter the characteristic peak at 268 nm was not detectable confirming the stable entrapment of FLG within the hydrogel scaffolds. Similar spectra were recorded for the other time points and at all investigated temperatures.

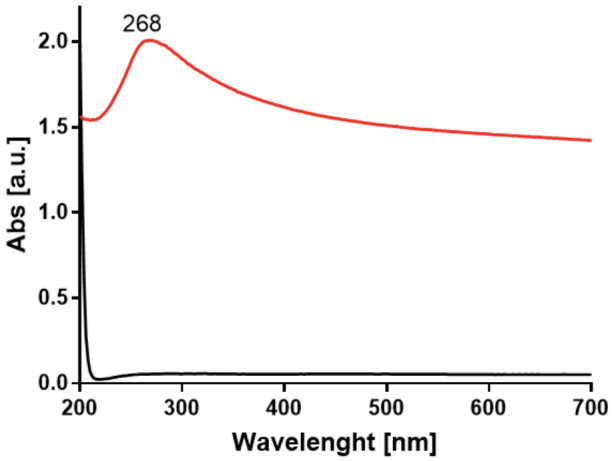

Figure 4.2.12: Representative UV-vis spectra of FLG solution (red) and FLG release (black) after 6 h, at 37 °C

Diclofenac was use as a drug. It is a nonsteroidal anti-inflammatory drug, derived from the phenylacetic acid class, with known analgesic and antipyretic properties, and commonly used in the treatments of a wide range of acute or chronic pain conditions [222, 223]. Its chemical structure involves a phenylacetic acid group and a phenyl ring containing two chlorine atoms and the resulting configuration ensures the maximal twisting of the phenyl ring and provides π-π binding with other molecules or substrates. The addition of diclofenac to the FLG aqueous suspension gave rise to strong medium-range interactions among π-orbitals of the aromatic substituents and resulted in physical adsorption of single drug molecules on FLG lattice. Moreover, the inner nature of pristine graphene with defects or vacancies [224] could promote hydrogen bonds, Van der Waals and hydrophobic interactions based on the bond interaction energy and polarizability, as widely discussed in the literature [225, 226, 227].

The concentration of Diclofenac was determined by the calibration curve. Diclofenac (5 mg, 17 μmol) was dissolved in 5 mL of distilled water. From the resulting 3.4 mM stock solution, the calibration solutions with concentration of 1.7 mM, 0.85 mM, 425 μM, 212.5 μM, 106.25 μM, 53.13 μM, 26.56 μM, 13.28 μM and 6.64 μM were prepared by diluting the stock solution with distilled water. UV-vis measurements were recorded for the calibration solutions. Its related calibration curve was obtained plotting absorbance at 276 nm versus concentration (Figure 4.2.13).

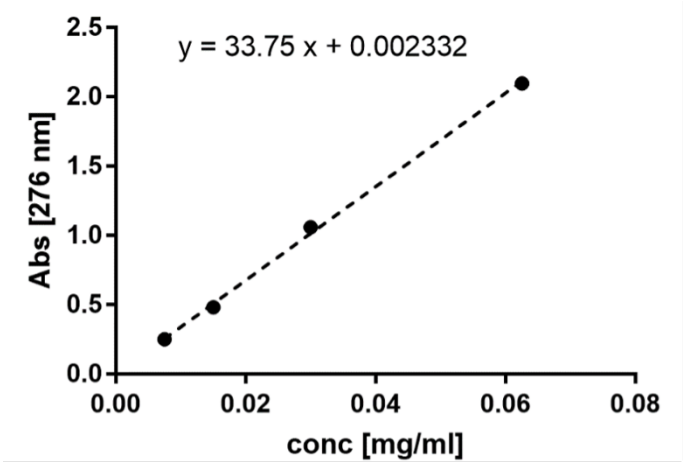

Figure 4.2.13: Calibration curve of diclofenac.

Exploiting the magnitude of π-π interactions, we investigated the potential effect of temperature in modulating drug release profile. Figure 4.2.14 shows the release profiles of diclofenac from FLG-HG and HG samples, at 25 °C, 37 °C and 44 °C.

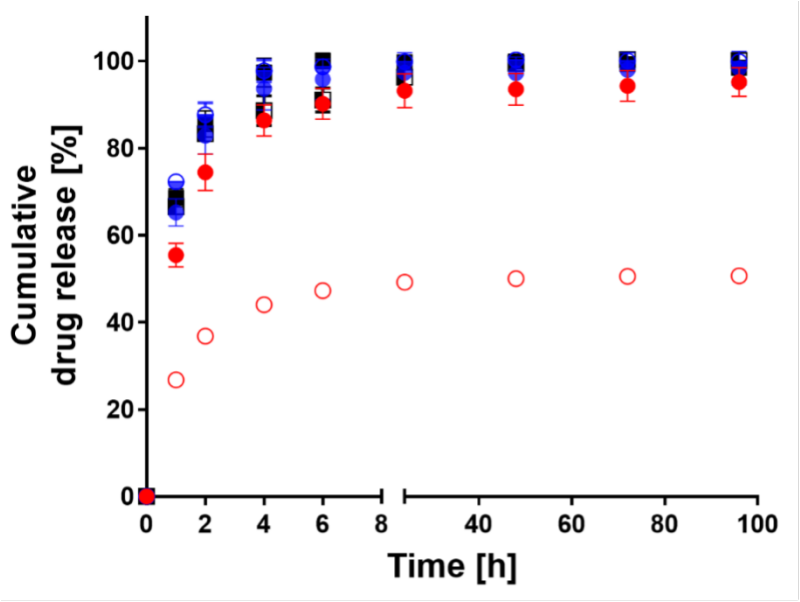

Figure 4.2.14: Diclofenac release profiles in FLG-HG samples at 25 °C (◯, red), at 37 °C (■ , black), at 44 °C (•, blue) and in HG samples at 25 °C (•, red), at 37 °C (■ , black), at 44 °C (•, blue).

The cumulative drug release from HG samples was approximately the same at each condition, defining a temperature-independent release kinetic. After 6 h, almost

the entire drug payload was released from the polymer meshes. This evaluation is in accordance with the increased molecular mobility and polymer elongation, which occur at temperature exceeding RT and promote the drug escape as driven by diffusion and concentration gradient [228]. Otherwise, the presence of FLG affected the amount of released drug over time: at 25 °C a plateau at 51% was reached, whereas at 37 °C and 44 °C complete release was achieved after 6 h. This means that FLG, preserving all its structural peculiar features, is able to establish physical interactions with diclofenac tuning its release in compliance with temperature: at RT the π orbitals of FLG and diclofenac are strongly connected, probably due to the reciprocal delocalization of π electrons, and in aqueous environment they are quite stable to limit the amount of escaped active principle. Increasing the temperature, a distortion of this physical set-up occurs, due to the increased molecular energy that overcomes the adsorption energies and enhances the dissipative forces [227]. It results in a drug desorption caused by the reduced stability of the π-π interactions. In addition, the drug release profiles within the first hours follow different trends (Figure 4.2.15): we observed that the higher is the temperature, the higher the percentage of released diclofenac. Thus, it is possible to modulate the drug release from FLG-HG heating up and therefore this material represents a promising tool for therapeutic thermal approach.

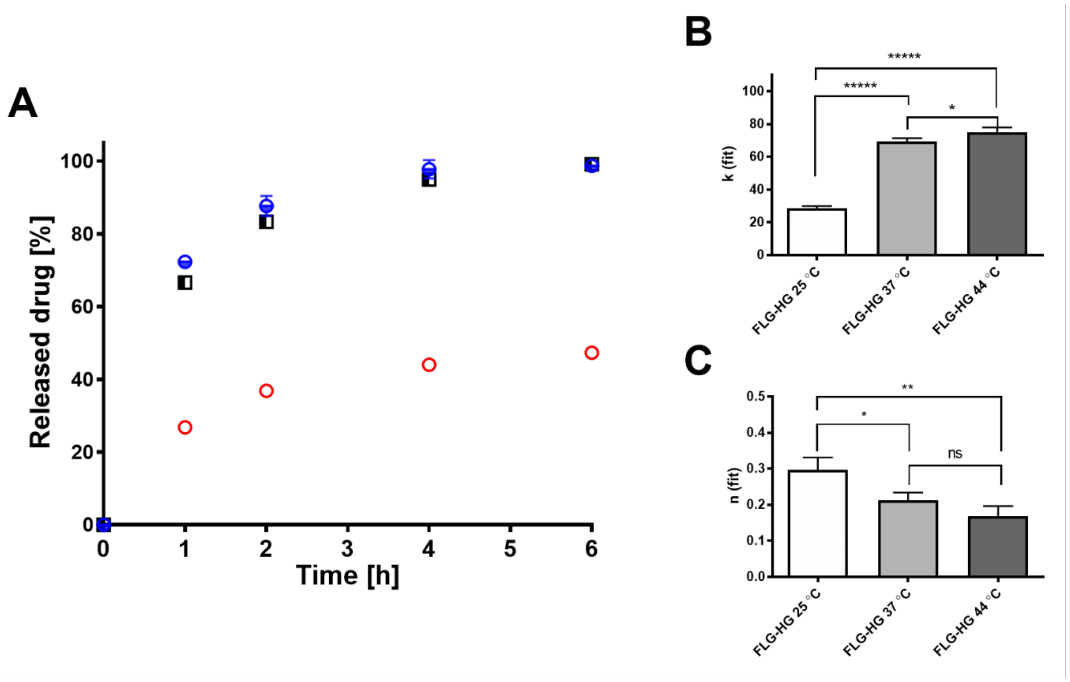

Figure 4.2.15: A) Focus on drug release profiles in FLG-HG samples within the first 6 h: 25 °C (○, red), 37 °C (■ , black) and 44 °C (●, blue). B, C) Evaluation of fitting parameters k and n: statistical analysis via one-way ANOVA.

Moreover, a simple expression of these behaviors can be heuristically written as the sum of the diffusion-controlled and relaxation-controlled drug delivery, referring to the well-known Peppas equation [229, 230] (Eq. 4.2.1):

$$\frac{M_t}{M_\infty} = kt^n \tag{4.2.1}$$

Where M_t represents the cumulative amounts of drug released at time$t$, and M_∞ is the total amount of drug in the system (release at infinite time), k is the constant of apparent release and n the diffusion exponent. This power law is extensively used to describe the trend of the release curves [231, 232]. The fitting of the FLG-HG experimental data shows significant differences trends in k and n values, confirming the thermal trigger effect of FLG.

In details the constant k shows different remarkable values comparing the experiments at 25 °C to those performed at 37 °C and 44 °C (in both cases, $p < 0.0001$) and a significant difference is visible also between 37 °C and 44 °C ($p < 0.05$). Furthermore, the fitted values of the diffusion differ each other, with a more marked difference at higher temperature than at RT, confirming the thermal π-π

effect FLG-drug in the diffusion regime. The presence of FLG affects the drug release diffusion regime naturally occurring in neat hydrogels, at all the investigated temperatures, tuning the amount of released diclofenac according to temperature increase, which led to overcome the binding energy of the attractive, noncovalent interactions between the aromatic rings. These differences in drug release profiles are not observable in HG specimens, where the trends are extremely similar at all temperatures; the influence of the graphene nanofiller is clearly detectable at 25 °C, while differences at 37 °C and 44 °C appear less marked. Overall, these data demonstrate that it is possible to perform a thermally triggered drug release without functionalization of graphene or its orthogonal grafting to specific chemical groups.

4.2.5 Cytotoxicity

The potential toxicity of synthetized HG and FLG-HG was assayed on hydrogel eluates in cell culture medium. Results in Figure 4.2.16 confirm the excellent biocompatibility for both formulations, with an overall cell viability above 90% for the highest extract concentration, that further rises to over 98% at 1:10 dilution.

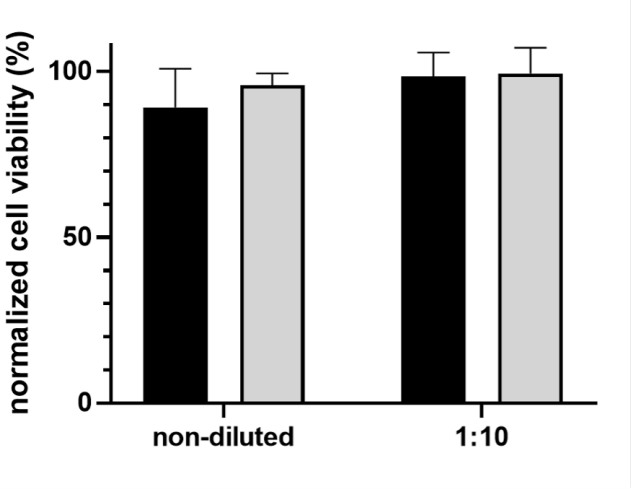

Figure 4.2.16: Results of MTT assay performed on BALB/3T3 cells supplemented with biomaterial extracts at different titers (FLG-HG in black, HG in grey). Cell viability was normalized to that of non-treated control cells.

4.2.6 Diclofenac: the effect on COX inhibition

The potential application of the proposed hydrogels could not be addressed without assessing the preservation of drug activity following its release. In particular, we studied its COX inhibition activity. COX is an enzyme responsible for the synthesis of prostanoids from arachidonic acid expressing peroxidase activity. In details, COX-1 is normally involved in cellular homeostasis and it is constitutive of different cell types, whereas COX-2 is expressed under acute inflammatory conditions [233, 234]. We compared the COX inhibition effect of the drug released by our hydrogels after 24 h to the activity of the same amount of neat diclofenac directly administered as aqueous solution (0.25 mg/mL), using a fluorometric COX inhibition assay. The results are reported in Figure 4.2.17.

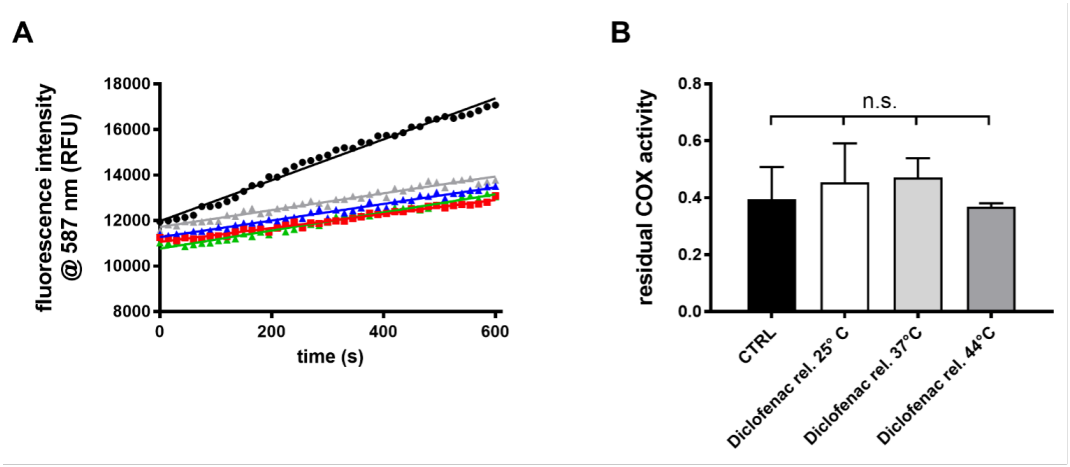

Figure 4.2.17: A) COX activity trends in lysate samples without inhibition (CTRL, • black) and with the addition of: neat diclofenac (■ red), released diclofenac at 25 °C (▲ blue), released diclofenac at 37 °C (▲ green) and released diclofenac at 44 °C (▲ grey). B) Residual COX activity after the drug administration and the use of COX Assay Kit: statistical analysis via one-way ANOVA.

The measurements of COX activity in the absence (hereinafter CTRL) and in the presence of the drug are plotted as RFU over time (Figure 4.2.17A) and the fitting of the recorded data shows significant variation in the slope of the regression line of CTRL respect to all other samples treated with diclofenac. In particular, no significant differences in terms of COX inhibitor capacity have been recorded comparing the use of pure diclofenac solution to the released drug at the different investigated temperatures (Figure 4.2.17B). This means that the interactions between the drug

and FLG did not affect the therapeutic properties of diclofenac and graphene could be considered as a useful filler to perform a thermally triggered drug release.

4.2.7 Discussion

In this work, we propose the formulation of graphene-laden hydrogels for thermally triggered drug release. In particular, graphene was used in its pristine form, without the need of oxidation/reduction processes to reach a homogeneous distribution within the hydrogel. The resulting material meets the criteria of biocompatibility for applications in the biomedical field and its drug release profile shows an amenable dependence on temperature in a physiologically relevant range. Furthermore, the possibility of modulating the drug delivery up to 44 °C defines these composite hydrogels as a promising tool for thermally triggered drug release in several healthcare scenarios. In light of their gelation mechanism and rheological behavior, the hydrogels may also be suitable for an application as injectable media, overcoming the main constraints related to the use of solid-like devices.

Chapter 5

Nanogel chemically functionalized

Nanotechnology is one of the most promising technologies of the 21st century, widely used in biomedical field to develop innovative therapeutic strategies. In the last years different types of nanosystems have been designed as potential therapeutic treatment in several healthcare scenarios, highlighting significant outcomes, especially in controlled drug delivery, demonstrating the chance of overcoming the main drawbacks related to the administration of drug in free form, such as rapid clearance, limited therapeutic effects and serious off-target toxic effects. Among nanomaterials, polymeric nanoscaffolds represent a promising system toward the design of innovative curative therapies, and in particular nanogels (NGs) play a relevant role due to their biocompatibility, blood stability, non-immunogenicity and possible biodegradability. A properly nanogel surface functionalization can influence interactions with cells, affecting the mechanism of their internalization with the cytosol. To date, the main approach to modulate the NGs-cell interactions towards a selective targeting, involves the use of polymer coating (e.g. PEG, chitosan). However, the potential effect of specific chemical moieties in tuning the internalization process is not widely investigated yet. In particular, the surface decoration with different aromatic groups represents a new scenario to discuss. The aim of this work is to evaluate how NGs with different aromatic coatings may affect biocompatibility, chemical-physical properties, drug loading, drug release and cell uptake in a specific disease scenario. Regarding the NGs internalization, following a preliminary evaluation through the conventional flow cytometry analysis, it was evaluated in vitro using an innovative approach based on the microfluidic system which mimics the effective condition on a potential in vivo administration and the obtained results were compared to the con-

ventional approach based on cell seeding in static conditions. The collected results showed how the selected aromatic coatings on NGs surface ensure a tunable drug delivery of the drug used, Sunitinib, and modulate the cellular internalization in T-786O cell line. Overall, these results demonstrated that through surface decoration with specific aromatic moieties it's possible to tune NG-cell interactions and the drug delivery performances, designing versatile nanosystems suitable for the definition of future therapeutic approaches.

5.1 Experimental

5.1.1 Materials

The NGs synthesis required the following polymers: polyethylene glycol 8000 (PEG; Mw = 8 kDa) and linear polyethylenimine 2500 (PEI; Mw = 2.5 kDa). NGs surface decoration was performed using the following aromatic molecules: 4-Butylbenzoic acid (BBA; Mw = 178.23 g/mol), Dymethilamino acid (DABA; Mw = 165,19 g/mol) and Pyreneacetic acid (PYR; Mw = 262,3 g/mol). The NGs were marked for in vitro traceability by the fluorescent dye Cyanine 5-azide (Cy5-azide; Mw 1035 Da) able to fluoresce in deep red (λex= 650 nm, λem= 670 nm).

5.1.1.1 Polyethylene glycol

Polyethylene glycol (PEG) is a synthetic, hydrophilic, biocompatibility and non-immunogenic polymer. PEG chemical structure is composed of repeat units $-O-CH_2-CH_2$- with $-OH$ as terminal groups.

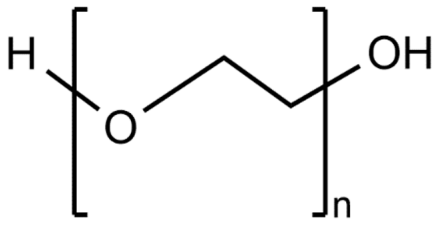

Figure 5.1.1: Chemical structure of PEG. Created with *ChemDraw*

A typical process used in biomedical applications is PEGylation by which PEG is bound to another molecule, which is promising in therapeutic methods. PEG can

hinder protein adsorption, which is essential in drug delivery to minimize protein corona [235].

5.1.1.2 Polyethylenimine

Polyethylenimine (PEI) is a synthetic, water soluble, linear or branched polymer. PEI chemical structure is composed of repeat units of amine groups and two carbon aliphatic spacers $-CH_2-CH_2-$. Linear PEI is a linear chain containing all secondary amines $-NH$ with $-OH$ and $-CH_3$ as terminal groups, in contrast to branched PEI which contains primary, secondary and tertiary amino groups.

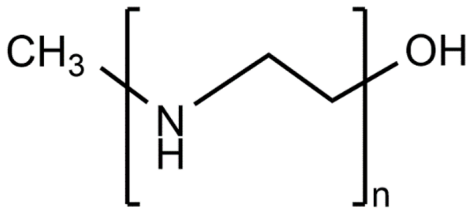

Figure 5.1.2: Chemical structure of linear PEI. Created with *ChemDraw*

The amine groups are protonated at physiological pH making PEI a positively charged polymer (cationic polymer) that promotes high loading efficiency for negatively charged molecules such as RNA and drugs [236]. Nevertheless, PEI suffers from high cytotoxicity effect [237], depending on its molecular weight and non-biodegradability, for that reason PEI is commonly associated with other polymers, such as polyethylene glycol (PEG) [238] to improve its safety while keeping its efficacy [239].

5.1.1.3 Aromatic molecules for NGs coating

Aromatic molecules are defined as organic compounds that contain one or more aromatic rings in their chemical structure and unlike other molecules are much more stable. Aromatic decorations used to NGs coating were based on:

- 4-Butylbenzoic Acid, constituted by $-CH_3-(CH_2)_3-$, an aromatic ring and a carboxylic acid group –$COOH$

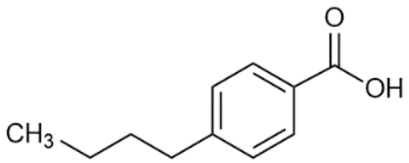

Figure 5.1.3: Chemical structure of 4-Butylbenzoic Acid. Created with *ChemDraw*

- Dimethylamino Benzoic Acid, composted of tertiary amine, an aromatic ring and a carboxylic acid group $-COOH$.

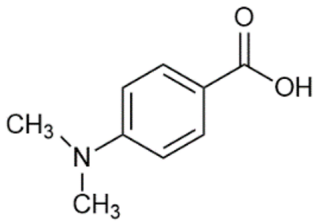

Figure 5.1.4: Chemical structure of Dimethylamino Benzoic Acid. Created with *ChemDraw*

- Pyreneacetic Acid is a molecule which chemical structure is assembled by 4-aromatic rings and a carboxylic acid group $-COOH$.

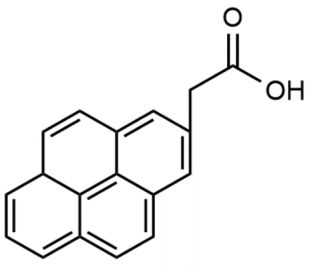

Figure 5.1.5: Chemical structure of Pyreneacetic Acid. Created with *ChemDraw*

5.1.2 Nanogels synthesis

As reported by Mauri et al. [240] the synthesis of NGs was performed by the emulsion-evaporation method and the final product was obtained involving four main steps: synthesis of PEG-CDI, synthesis of PEI-Propargyl, click-chemistry reaction PEI-Cy5 and synthesis of NGs-Cy5.

5.1.2.1 Synthesis of PEG-CDI

The synthesis of PEG-CDI consisted in bi-functionalizing PEG with the organic compound 1,1´-carbonyldiimidazole (CDI) in according to the procedure reported by Vinogradov et al. [241]. Specifically, the hydroxyl groups of PEG react with the imidazole of CDI to form PEG bifunctionalization.

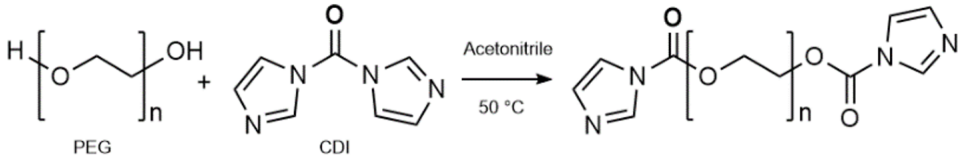

Figure 5.1.6: PEG bifunctionalization: PEG-CDI chemical reaction. Created with *ChemDraw*

In order to achieve PEG bifunctionalization, PEG (Mw=8 kDa, 3 g, 0.37 mmol) was dissolved in Acetonitrile (40 ml) then CDI (0.6 g, 3.7 mmol) was added to the solution. The obtained solution was maintained under stirring for 17h at 50 °C. The solvent was removed under pressure by evaporation using rotary evaporator. The opalescent residue of solution was dissolved in distiller water (15 ml), purified by membrane dialysis (Mw cut-off = 3.5 kDa) against distiller water (2l) for 48h and then freeze-dried. The final solid compound was stored at +4°C.

5.1.2.2 Synthesis of PEI-propargyl

Synthesis of PEI-propargyl consists in alkyne functionalization of linear PEI using propargyl bromide to obtain triple bonds on PEI polymer chain by which Cy5-azide fluorescence dye is bonded.

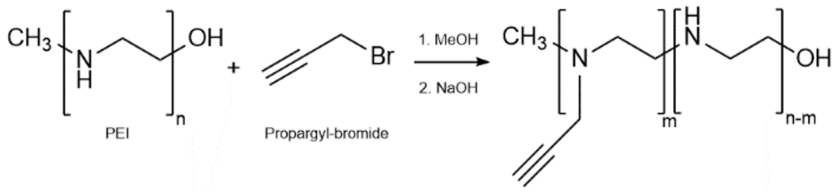

Figure 5.1.7: PEI functionalization: PEI-propargyl chemical reaction. Created with *ChemDraw*

This reaction was performed as suggested by Zhao et al. [242] and then subsequently reported by Mauri et al. [243]. PEI (Mw = 2.5 kDa, 300 mg, 0.12 mmol) was dissolved in methanol (4 ml) and then propargyl bromide solution in 80% toluene (194 µl, 1,5 mmol) was added dropwise at 0°. The resulting solution was maintained at room temperature for 48h under stirring condition. Subsequently, the solvent was removed by rotary evaporator, the residue was dissolved in distilled water (4 ml) and NaOH (1M) was added until pH = 10. The mixture was purified by extraction with ethyl acetate and then freeze-dried. The solid product was stored at +4°C.

5.1.2.3 Click-chemistry reaction PEI-Cy5

The term "click chemistry" was introduced for the first time in 2001 by K. B. Sharpless [244] to describe all those reactions that are fast, high yielding, create only by-products that can be removed without chromatography, stereospecific, simple to perform, and that can be conducted in easily removable or benign solvents [245].

The reaction that allows the bond between PEI-propargyl and Cy5-azide is called copper-catalyzed azide-alkyne cycloaddition (CuAAC), one of the main click-chemistry reaction. Azide-alkyne cycloaddition occurs between the azide group of Cy5-azide and the alkyne group of PEI-propargyl, forming a triazole.

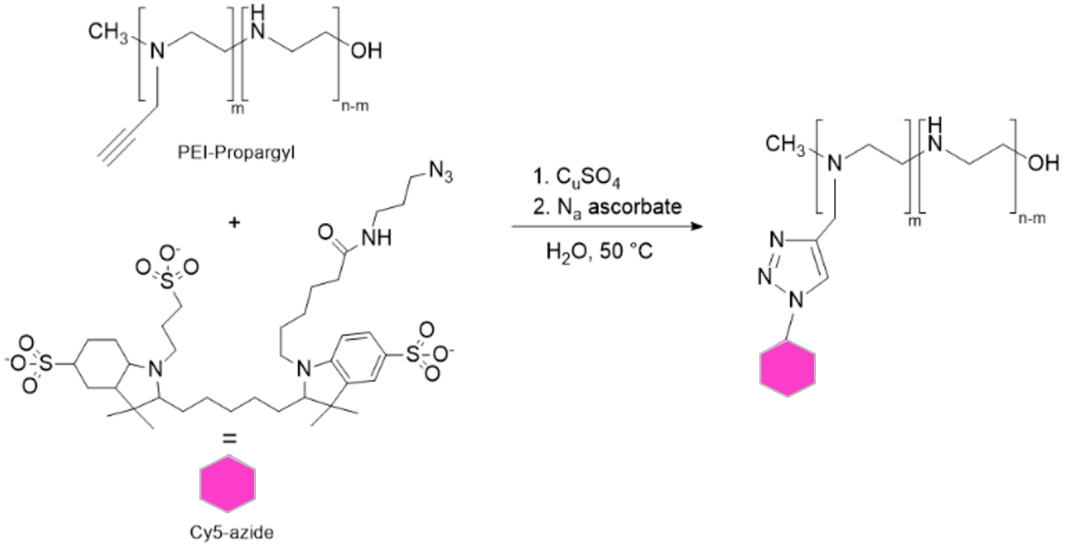

Figure 5.1.8: Azide-alkyne cycloaddition: PEI-propargyl - Cy5-azide. Created with *ChemDraw*

The click-reaction was achieved by the following procedure:

PEI-propargyl (60 mg, 24 µmol) was dissolved in distilled water (7 ml) and Cy5-azide dissolved in DMSO (2 mg/ml, 124 µl, 0.24 µmol) was added. Copper sulphate CuSO4 (12.77 µg, 0.08 µmol) as catalyst and sodium ascorbate (15.85 µg, 0.08 µmol), to avoid oxidation of CuSO4, were added. The resulting solution was kept at 50°C under stirring condition in the darkness for 36h. Subsequently, the mixture was purified for 48h by membrane dialysis (Mw cut-off = 100-500 Da) against distilled water (2l) where NaCl (11.2 g, 0.65 mmol) and HCl (1M, 200 µl) were dissolved and then freeze-dried. The final solid compound was stored at -20°C.

5.1.2.4 Synthesis of NGs-Cy5

Synthesis of NGs-Cy5 was realized by modified emulsion-evaporation method as reported by Vinogradov et al. [246].

PEG-CDI (57,6 mg, 7,2 µmol) was dissolved in dichloromethane CH2Cl2 (1,5 ml) and then added dropwise in an aqueous solution (2 ml) of PEI-Cy5 (12 mg, 4,8 µmol). The obtained solution was sonicated for 30 min at 40 Hz and then it was kept under vigorous stirring condition (1200 rpm) for 17h at room temperature to evaporate the organic solvent. The solution was purified for 48h by membrane dialysis (Mw cut-off = 6-8 kDa) against distilled water (2l), where NaCl (11,2 g, 0,65 mmol) was dissolved and then freeze-dried. The obtained NGs consisted in cross-linked polymeric matrices and they were stored at -20°C.

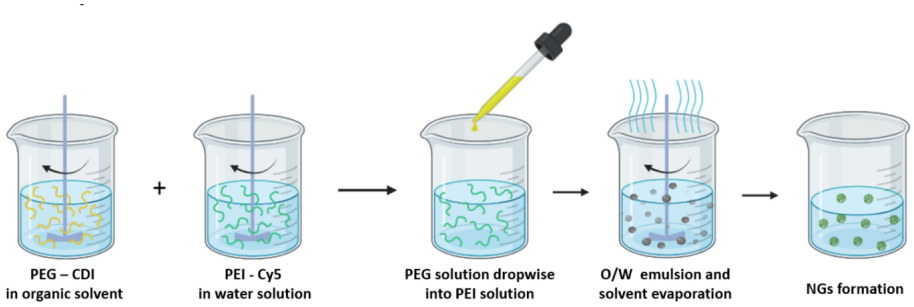

Figure 5.1.9: Schematic representation of emulsion-evaporation method. Created with *BioRender.com*

5.1.2.5 NGs coating

Once the NGs were synthesized, three different aromatic coatings were used to cover external NGs surface. NGs coating occurs by the bond between secondary amine

of PEI and carboxylic acid group on all the three aromatic molecules forming the amide group.

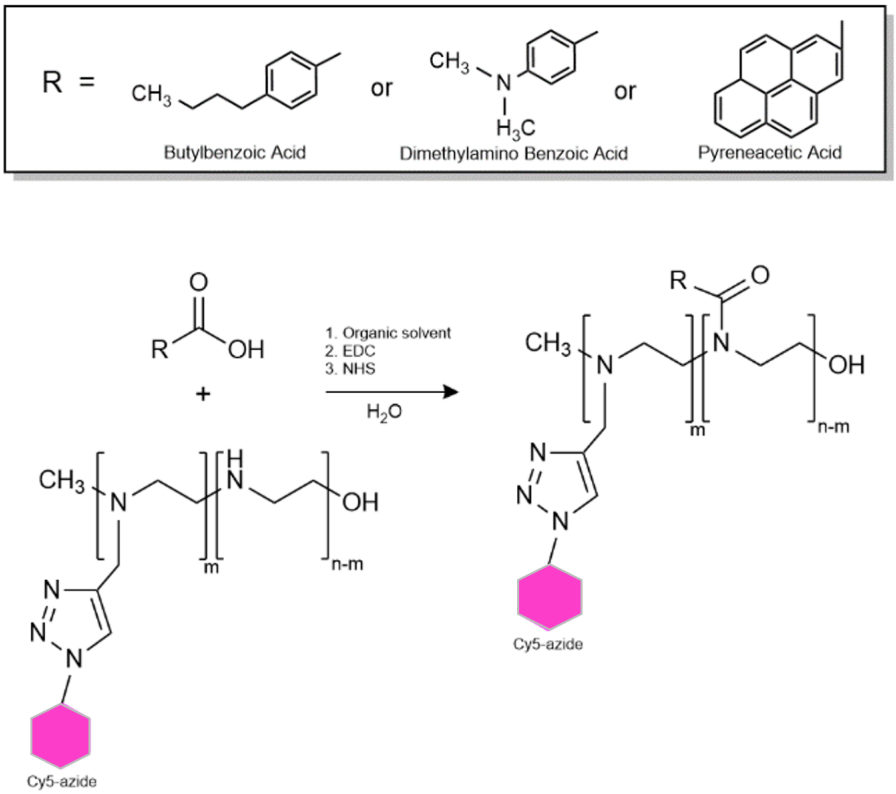

Figure 5.1.10: Chemical reaction between PEI-Cy5 and aromatic compound. Created with *ChemDraw*

The same procedure as well as catalysts were used for all three coatings, the differences consist in the type of coating used and the organic solvent in which it was dissolved.

The aromatic compound used for NGs coating was dissolved in an organic solvent (9mg/ml) with the coupling agents 1-Ethyl-3-(3-dimethylaminopropyl)carbodiimide (EDC) and N-Hydroxysuccinimide (NHS) and the solution was kept under stirring for 2h at room temperature.

The three different coating-solution are described below:

- Coating with Bytilbenzoic Acid - BBA

BBA (0.67 mg, 3.76 µmol) dissolved in (CH3)2SO (DMSO; 9mg/ml, 74.44 µl) and then EDC (0.87 mg, 5.64 µmol) and NHS (0.65 mg, 5.64 µmol) were added.

- Coating with Dimethylamino Benzoic Acid - DABA

DABA (0.62 mg, 3.75 µmol) was dissolved in CH2Cl2 (9mg/ml, 69 µl) and then EDC (0.87 mg, 5.64 µmol) and NHS (0.65 mg, 5.64 µmol) were added.

- Coating with Pyreneacetic Acid - PYR

Pyreneacetic Acid (1.96 mg, 7.54 µmol) was dissolved in CH2Cl2 (9mg/ml, 69 µl) and then EDC (1.75 mg, 11.29 µmol) and NHS (1.3 mg, 11.29 µmol) were added.

For each coating-solution, NGs (10 mg, 3,76 µmol) were dissolved in distilled water (1,5 ml) and the respective coating-solution was added into them dropwise keeping the mixture under vigorous stirring condition (1200 rpm) for 30h at room temperature. The resulting solution was purified by membrane dialysis (Mw cut-off = 6-8 kDa) against distilled water (2 l) for 48h and then freeze-dried. The coated NGs were store at -20°C. The resulting samples are labelled as NGs-BBA, NGs-DABA and NGs-PYR where the coatings were made respectively of BBA, DABA and PYR.

5.1.3 NGs characterization

The NGs physico-chemical characterization was performed by FT-IR (Fourier-transform Infrared) and DLS (Dynamic Light Scattering) in collaboration with Politecnico di Milano.

5.1.3.1 FT-IR analysis

FT-IR analysis is a technique based on the absorption of infrared radiation, the bonds between atoms that compose molecules are invested by an infrared radiation at specific frequencies corresponding to their respective vibrational energy levels. Different bonds vibrate in a molecule at different energy levels and therefore they absorb different wavelengths of infrared radiation. There are two fundamental ways in which the bonds can vibrate: stretching of the chemical bond (stretching) and deformation of the bond angle (bending). Based on stretching and bending, the synthetized NGS were chemically characterized to verify the presence of previously described chemical bonds using a Nicolet 8700 spectrophotometer (Thermo Fisher Scientific, Waltham, MA) equipped with a Golden GateMK II Single Reflection Diamond ATR system (Specac Ltd., Orpington, UK). Each spectrum (32 scans, 2 cm-1 resolution) was recorded in the wavenumber range 4000–800 cm-1).

5.1.3.2 DLS analysis

DLS analysis allows detection size of typically sub-micron molecules, nanoparticles or colloids. The sample is illuminated by a laser beam, and the intensity changes of the scattered light are measured as a function of time. At the same temperature and viscosity, 'small' particles move rapidly, creating rapid changes in scattering intensity while 'large' particles move slowly creating slow changes in intensity. The NGs size and the polydispersity index (PDI) were detected via DLS using a Zetasizer Nano ZS instrument (Malvern Panalytical, Malvern, UK).

5.1.4 NGs drug loading and drug release

The synthetized NGs were loaded with Sunitinib malate drug, an FDA approved drug to treat renal cell carcinoma [247]. Sunitinib malate was chosen as candidate drug thanks to its peculiar feature to inhibit tumor growth by acting in a more targeted and selective manner than traditional chemotherapy.

5.1.4.1 Drug loading

The drug was loaded through the sponge-like loading mechanism which exploits the peculiar swelling behaviour of NGs. Specifically, the drug was loaded into freeze-dried NGs to obtain a drug concentration of 500 µM and NGs concentration of 12.5 mg/ml in PBS. The drug concentration was selected on the linear tract of the calibration curve obtained in PBS medium (Figure 5.1.11).

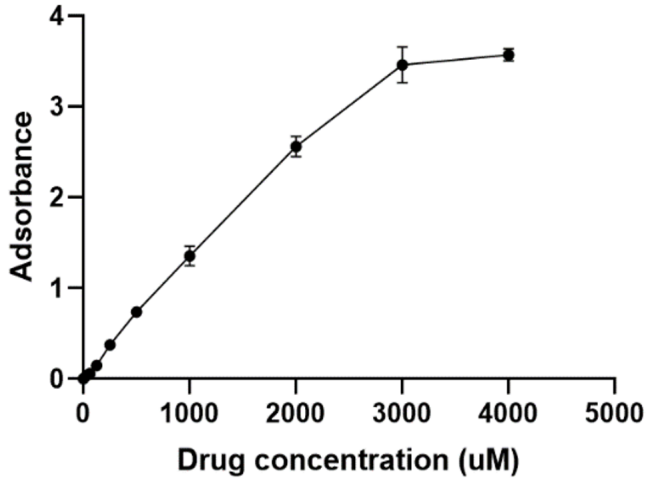

Figure 5.1.11: Calibration curve of Sunitinib malate.

Drug loading was performed on all NG specimens in the same following procedure:

Sunitinib malate solution (50 mM, 4 µl) was added to lyophilized sample (5 mg) and then it was diluted in PBS (196 µl) to achieve the desired drug concentration (1mM). The solution was kept for 10 min at room temperature to induce the drug adsorption.

Loading efficiency (% drug loading) was calculated based on the following equation:

$$\%drug\,loading = \frac{drug\,load_{t0} - drug_{Solv}}{drug\,load_{t0}} \cdot 100$$

where $drug\,load_{t0}$ (19.9 µg, 0.05 µmol) is the initial amount of Sunitinib malate loaded and $drug_{Solv}$ (depending on the analysed sample) is the amount of Sunitinib malate adsorbed on the NGs surface, released into release medium (PBS; 800 µl) in 10 min.

5.1.4.2 Drug release

The NGs-drug solution, previously described, was incorporated in a hydrogel matrix to evaluate the drug release profiles of NGs specimens.

In details, the hydrogel solution was obtained by dissolved carbomer 974p (100 mg, Mw = 700 kDa) in PBS (19.90 ml) under stirring condition for 30 min at room temperature. The polymeric solution was left to settle for 30 min and NaOH 1M

was added until pH = 7.8. The resulting solution was stored at +4 °C.

The polymerization of hydrogel solution occurred adding 8 mg of ultrapure agarose per 1ml of hydrogel solution and subjecting the solution to electromagnetic stimulation (500 W) which heats it up to 70 °C. When the latter solution decreased temperature around at 60 °C, it was 1:1 diluted with the loading solution (200 µl, 1 mM) to obtain for each hydrogel matrix a Sunitinib concentration of 500 µM and NGs concentration of 12.5 mg/ml. The ultimate solution was placed in cylindrical molds (100 µl per mold) in 24-multiwell plate, in order to have sample triplicate. Polymerization occurs in a few minutes. Cylindric gels were submerged in PBS (800 µl). In drug release trial the 24-multiwell plate was maintained at 37°C in 5% CO2.

In detail, four aliquots from the release medium (400 µl) were collected at defined timepoints, restoring the buffer volume to avoid mass transfer equilibrium with the surrounding environment. For each timepoints, the amount of released Sunitinib malate was determined by TECAN infinite M200-Pro (λ = 430 nm) and the absorbance values were fitted on the Sunitinib calibration curve to obtain the drug release profiles.

5.1.5 Cell culture

Primary renal carcinoma cells (T-786O) were cultured in RPMI 1640 cell medium supplemented with 10% fetal bovine serum (FBS), 1% penicillin/streptomycin and 1% L-glutamine (200 mM). Cells were maintained at 37°C in 5% CO2. After reaching confluency, the cells were trypsinized and used for experimental set-ups.

5.1.5.1 Cytotoxicity assay

The cytocompatibility of synthetized NGs was evaluated by VybrantTM Cytotoxicity Assay Kit (V-23111). Vybrant cytotoxicity assay commonly known as G6PD assay detects the cytosolic Glucose-6-phosphate dehydrogenase enzyme, through a two-step enzymatic process that leads to the reduction of resazurin in red fluorescent resorufin. The resulting fluorescence is proportional to the amount of G6PD released by apoptotic cells into the cell medium [248]. In details, T-786O cells were seeded in 96-well plate with a density of 2000 cells/well in 100 µl of complete RPMI 1640 medium and incubated at 37°C in 5% CO2. After the overnight incubation, each NGs sample at concentration of 5 µg/ml was placed in prolonged contact with the cells for 24h.

The $Vybrant^{TM}$ Cytotoxicity was performed by removing cell medium and incubating the cells with 50 µl of resazurin/reaction mixture at 37 °C in 5% CO2 for 10 min. The fluorescent resazurin was detected by a fluorescence spectrophotometer TECAN infinite M200-Pro at λabs= 530 nm, λem = 570 nm.

5.1.5.2 MTT assay

MTT assay was performed to evaluate the dose-responsive curve of Sunitinib and to investigate the impact of drug-loaded NGs. This colorimetric assay is based on the reduction of the yellow tetrazolium salt (3-(4,5-dimethylthiazol-2-yl)-2,5-diphenyltetrazolium bromide or MTT) to purple formazan crystals by metabolically active cells. Viable cells contain NAD(P)H-dependent oxidoreductase enzymes that reduce MTT to formazan. Insoluble formazan crystals are dissolved using a solubilization solution, and the resulting-coloured solution is quantified by measuring absorbance at 570 nm using a multi-well spectrophotometer [249].

Specifically, T-786O cells were seeded in 96-well plate at concentration of 2000 cells/well in 100 µl of complete RPMI 1640 medium at 37 °C in 5% CO2. After the cell incubation overnight, the medium was changed and drug-loaded NGs at concentration of 5 µg/ml were added. The selected Sunitinib concentration was 10 µM, a sublethal concentration in according to the obtained Dose-response curve of Sunitinib. The MTT assay was performed for three timepoints: 24h, 48h, 1w. For each timepoint, the cell medium was replaced with MTT solution (0,5 mg/ml) 1:10 diluted in cell medium and cells were incubated for 3h at 37 °C in 5% CO2. Then, the cell medium was removed and the formazan crystals were dissolved in DMSO (100 µl). The absorbance was read at λ = 570 nm using TECAN infinite M200-Pro. The procedure previously described was used also to evaluate dose-response curve of Sunitinib at 24h on T-786O cell line considering Sunitinib concentration ranging between 10 mM – 0 M.

5.1.6 NGs cell uptake

NGs-cells interaction in terms of cell uptake was evaluated using two different approaches: cytofluorimetry and microfluidic systems.

5.1.6.1 Flow cytometry

The flow cytometry is performed by cytofluorimeter, an instrument capable of identifying specific characteristics of cells through a laser system that produces scatter when it is focused on single cell. The characteristics may be physical as cell size and complexity or may depend on the signal generated by the dye intercepted by the laser. In this work, the flow cytometry was used to assess cellular uptake based on the Cy5-azide fluorescent dye bound to NGs. In particular, the NGs cellular internalization was estimated via Mean Fluorescence Intensity (MFI). The cell uptake was evaluated for three timepoints: 2h and 24h.

T-786O cells were seeded in 24-well plate at the density of 20.000 cells/well in 500 µl of complete RPMI 1640 medium and incubated overnight at 37 °C and 5% CO2. Cell medium was removed and replaced with NGs suspension at NGs concentration of 10 ug/ml of for each NGs samples. Cells were detached using TrypLETM (100 µl) and resuspended in PBS (200 µl) to perform flow cytometry analysis for each timepoints.

5.1.6.2 Microfluidic device

Microfluidic system was used to evaluate NGs cell uptake under dynamic conditions compared with the static condition always performed in the microfluidic system. This innovative approach aims at obtaining a potential tool by which the NGs-cell interaction can be evaluated simulating a potential in vivo administration.

5.1.6.3 Microfluidic device fabrication

The chip design, after drawing the CAD of the desired geometry, was obtained by two fundamental steps:

- Traditional photolithography to realize the silicon master with the impressed geometry used as silicon mold .
- Soft-lithography via Micro-Replica Molding (REM) to achieve a PDMS (polydimethylsiloxane) microfluid device.

The photolithography was performed using the photolithographic mask with geometry shown in Figure 5.1.12 inspired by the chip design developed by Donald E. Ingber et al. [250] composed of a central channel and two vacuum chambers (not

used in this application). The silicon master was realized using SU-8 3050 negative resist in order to realize a film thickness of 90 µm. After the silicon mold manufacturing, REM was realized. In details, PDMS (Sylgard-184) in a ratio of 10:1 w/w base: curing agent was mixed and degassed through planetary centrifugal mixer (Thinky Mixer) for 1 min at 2000 rpm and 30 s at 200 rpm and casted on the silicon master. Further degassing was performed for 5 min in dynamic vacuum and 3 min in static vacuum using a vacuum chamber. Subsequently, the chip was baked for 2h at 70°C and then peeled off from the silicon mold. An additional hour of baking at 100°C was executed complete the curing process. Once the solid PDMS was obtained, two reservoirs were realized with a puncher (d = 4 mm for dynamic condition, d = 6 mm for static condition) and cleaned with Kapton tape. The PDMS chip was bonded on a microscope glass slide by plasma oxygen exposure (1 mBar, 10% power for 0.6 s). The chip was ultimate with baking at 70 °C for 30 min.

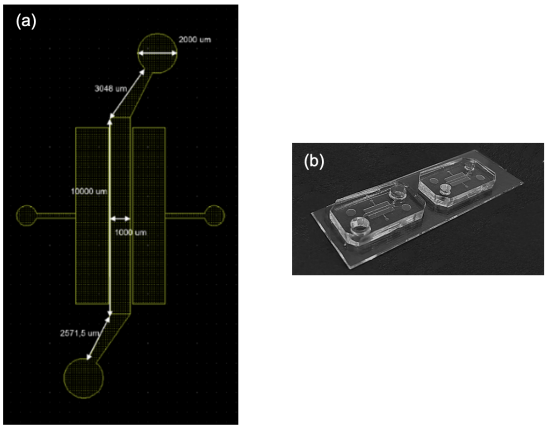

Figure 5.1.12: CAD of the silicon master's geometry realized by LayoutEditor (a); microfluidic systems used for the experimental set-up (b): static condition (left) and dynamic condition (right).

5.1.6.4 Cell culture in microfluidic device

Microfluidic devices were UV-sterilized for 20 min before cell seeding. T-786O cells were seeded in the central channel and a reproducible protocol to inject and seed cells was developed: ~ 20.000 cells were injected in the channel with a capacity of 3 µl. Twenty min after injection, the cells were attached to the glass and the cell medium was added into reservoirs. The PDMS chips were incubated overnight at 37°C in 5% CO_2.

5.1.6.5 Microfluidic-assisted NGs cell uptake

Microfluidic-assisted NGs cell uptake was evaluated in dynamic and static conditions. NGs were suspended in cell medium with a NGs concentration of 2,5 µg/ml and injected in the microfluidic systems, where T-786O cells were previously seeded. Specifically, in the microfluidic device used to analyse the static cell uptake, NGs suspension was injected in the central channel and the reservoirs at the ends of the channel were filled to ensure that the channel was always wet during the experiment.

To evaluate cell uptake under dynamic condition, NGs suspension was loaded into sterile syringe and connected to the inlet of the chip channel via sterile microfluidic tube. Another sterile microfluidic tube was connected to the end of the channel to collect the waste solution to allow continuous flow of NGs suspension. The syringe was actuated by the multichannel microfluidic syringe pump (Nemesys S) by which the flow rate was controlled. All the set-up is shown in Figure 5.1.13.

The experiment was performed using a flow rate of 5 µl/min [251] which fall in the range suitable to mimic the in vivo conditions of NG administration for 2h, 6h and 24h for each NGs samples. The microfluidic systems used to evaluate dynamic and static NGs cell uptake were maintained at 37°C in 5% CO_2 during the entire experiment.

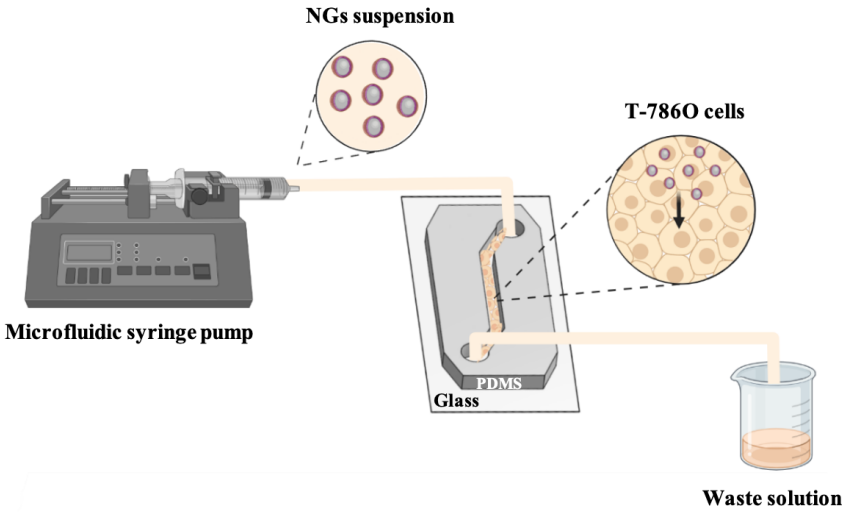

Figure 5.1.13: The dynamic experimental set-up used to evaluate NGs cell uptake under dynamic condition. Created with *BioRender.com*

The microfluidic-assisted NGs cell uptake images were analysed by mean fluor-

escence intensity (MFI) measurement through NIS Elementes AR Software suite (Nikon) keeping the laser parameters fixed during image acquisition via Nikon A1R+ confocal microscope (Nikon Instruments, Tokyo, Japan).

5.1.7 Cell staining

At the end of the NGs cell uptake experiments performed in plastic well-plate and microfluidic platform, cells were fixed in PFA (4% in PBS) and stained. In details, after some rises in PBS, cells were incubated in PFA for 20 min and then maintained in PBS at +4°C. The cell staining aimed to dye the nucleus with DAPI and the cytoskeleton with phalloidin, the procedure was performed at room temperature. Cell membranes were permeabilized with Triton X-100 (0,1% in PBS) for 10 min and rise with PBS, then cells were incubated with blocking solution (2% BSA + 22 mg/ml glycine in PSBT; PSBT: PBS + 0.1% Tween20) for 30 min. After PBS rinsing, the phalloidin diluted 1:400 in PBS was added and maintained in the darkness for 1h. Washed-off phalloidin with PBS, DAPI diluted 1:1000 in PBS was added for 10 min. The cells were copious rinsed and viewed under a confocal microscope.

5.2 Results and discussion

5.2.1 NGs chemical characterization

NGs chemical characterization was performed by FT-IR analysis. The characteristic signals of PEG-PEI chemical crosslinking and covalent grafting of the aromatic motifs are reported in Figure 5.2.1.

In detail, the characteristic peaks of PEG and PEI chains were recognized: PEG chain, C-N stretching and C-H bending of PEI at 1470÷800 cm^{-1} and N-H bending of PEI around 1600 cm^{-1}. The characteristic C=O stretching of the carbamate bond, related to the PEG-PEI bond, is detected around 1750 cm^{-1}. The N-H and C-H stretch of the polymers are showed at 2700 cm^{-1} and 2900 cm^{-1} respectively. In addition, the peak of the triazole bonding of PEI-Cy5 is observed at 1558 cm^{-1}.

The presence of characteristic signals of the aromatic structures used for the superficial functionalization was, also, detected. The aromatic grafting is related to C=O stretching of amide bond in the different decoration approaches around 1700 cm^{-1} while C-H bending of aromatic rings is detected ranging between 950-1000

cm^{-1} as shown in NGs-PYR, NGs-BBA and NGs-DABA spectra.

Figure 5.2.1: FT-IR spectra of NGs-Cy5, NGs-BBA, NGs-DABA and NGs-PYR.

5.2.2 NGs physical characterization

The NGs physical proprieties such as diameter and polydispersity index (PDI) were evaluated by DLS analysis. Despite the aromatic coatings, NGs do not exceed 258 nm preserving a size suitable for nanoparticles aimed to biomedical applications, which are characterized by a diameter value in the range 1-1000 nm

Nanogel type	Diameter [nm]	PDI [-]
NGs-Cy5	229	0,04
NG-BBA	232	0,01
NGs-DABA	222	0,19

Table 5.2.1: NGs physical characterization

5.2.3 Drug loading and drug release

Drug loading and drug release performances were estimated using Sunitinib malate, an FDA-approved drug to the treatment of kidney cancer [252].

5.2.3.1 Drug loading

The drug loading, as shown in Table 5.2.2, showed high encapsulation efficiency (EE) in all NG specimens, thanks to the peculiar swelling behaviour of NGs, which, exploiting the transition dried-hydrated state, absorb a high amount of drug solution. In particular, NGs-PYR encapsulated the highest amount of drug: this can be attributed to high π-π stacking interactions between the 4 aromatic rings that compose the chemical structure of PRY and Sunitinib. In addition, a comparable behaviour was exhibited by NGs-BBA due to π -π stacking interactions between the aromatic ring and Sunitinib. Instead, NGs-DABA showed a reduced level of drug EE due to the protonation of the amino group of DABA and Sunitinib that induces a repulsion with the amino groups reducing the drug encapsulation.

Nanogel type	EE %
NGs-Cy5	85,15 %
NG-BBA	85,92 %
NGs-DABA	67,27 %

Table 5.2.2: NGs encapsulation efficiency.

5.2.3.2 Drug release

Drug release was evaluated as reported in Figure 5.2.2 as percentage of drug cumulative release vs time. All selected NGs samples, loaded with Sunitinib malate (500 µM) considering a NGs concentration of 12,5 mg/ml in PBS, release the drug until to 14 days. The drug release profiles, as shown in Figure 35 are modulated by the presence of aromatic coating layers appreciable especially up to 24h.

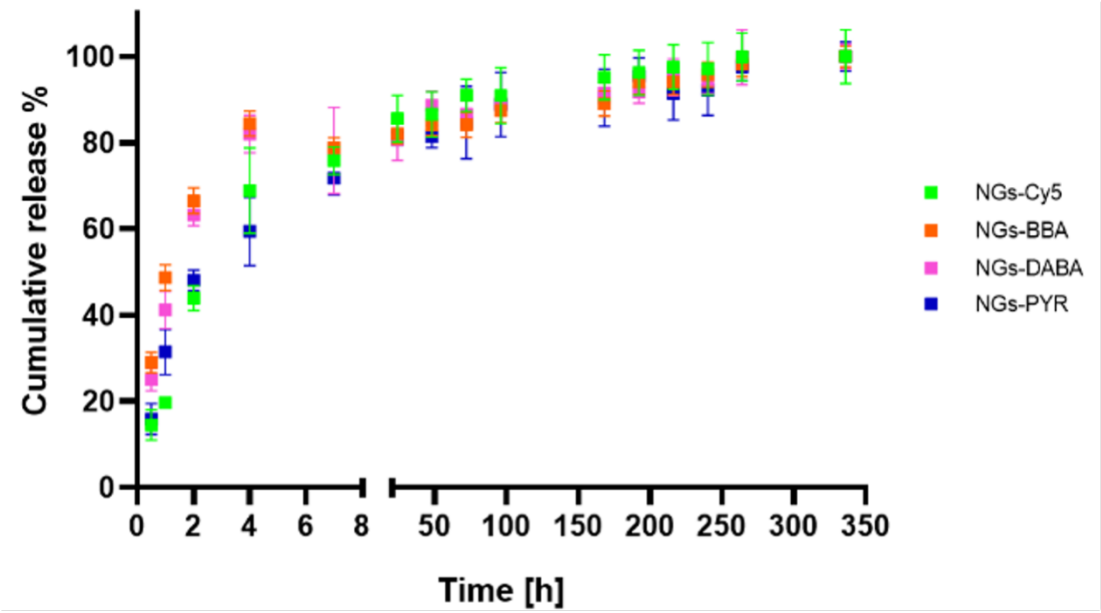

Figure 5.2.2: Cumulative Sunitinib release profile for each NGs sample.

All NGs specimens release around 75% of loaded drug within 7h then continue to release more gradually after 24h until 14 days following different trends.

In particular, a faster drug release was observed in NGs-BBA, a slight slowdown compared to NGs-BBA was detected in NGs-DABA and a slower drug was exhibited by NGs-PYR. NGs-PYR exhibited a more sustained release due to the π-π stacking interaction between the 4 aromatic rings of PYR and the aromatic component of Sunitinib. In NGs-DABA, the π-π stacking interaction between the aromatic ring of DABA and Sunitinib is counterbalanced by the repulsion between protonated amino groups, inducing a faster drug release compared to NGs-PRY. A further remarkable difference was detected in NGs-BBA where the drug release is modulated not only by π-π stacking interaction between BBA and Sunitinib but also by the presence of the aliphatic moiety of BBA.

The π-π stacking interaction effects introduced by aromatic moieties increase the stability and drug loading capacity as reported by Hennink et al. [253] and in fact, according to the collected data, NGs-PYR showed the highest EE and the most controlled drug release between NGs specimen.

Further analyses of the drug release profiles were performed by plotting cumulative release percentage against second to the power of 1/2.3 (Figure 36), which is the typical exponent used for spherical geometries, according to the Higuchi and Korsmeyer-Peppas model [254, 255]. In the representation, in Figure 5.2.3, the linearity of data is representative of a Fickian diffusion regime, and the y-axis intercept value is an indication of the burst release, which is assumed to be equal to zero for an ideal controlled release system [256]. The collected data showed good linearity, confirming that Sunitinib release was mediated by the Fickian regime. In particular, a double-diffusion regime with different slopes was detected in all investigated conditions. The transition and duration of the two regimes could be ascribed to the nature of the predominant interactions of the drug-NGs over time. The first diffusion trend, occurring in the first 7h, could be associated with the adsorbed Sunitinib at the NG/water interface, released at a faster rate. The second regime could be due to the drug—NGs interactions in the nanoscaffold core and aromatic surface decoration.

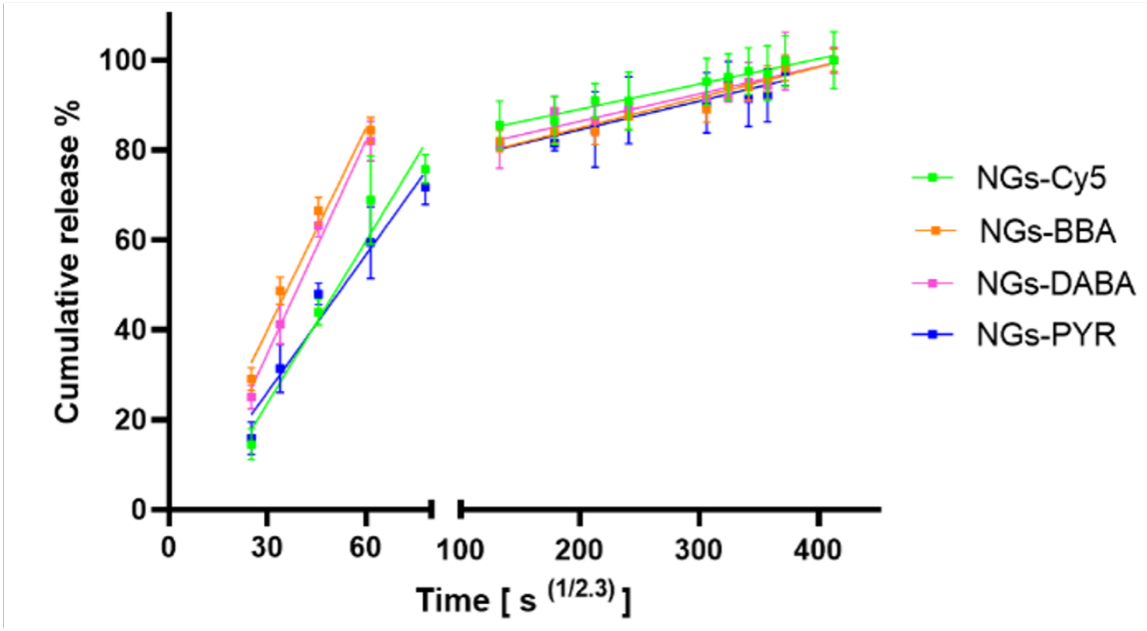

Figure 5.2.3: Cumulative Sunitinib release profile for each NGs samples according to the Higuchi and Korsmeyer-Peppas model.

5.2.4 Biocompatibility

NGs biocompatibility was investigated by VybrantTM Cytotoxicity Assay Kit (V-23111) known as G6PD assay. After 24h of prolonged contact between T-786O cells (2000 cell/well) and NGs (5 µg/ml), cell viability levels were close to 99% in each specimen (Figure 5.2.4). Therefore, the aromatic-decorated NGs provide high biocompatibility as well as uncoated NGs without any cytotoxic effect.

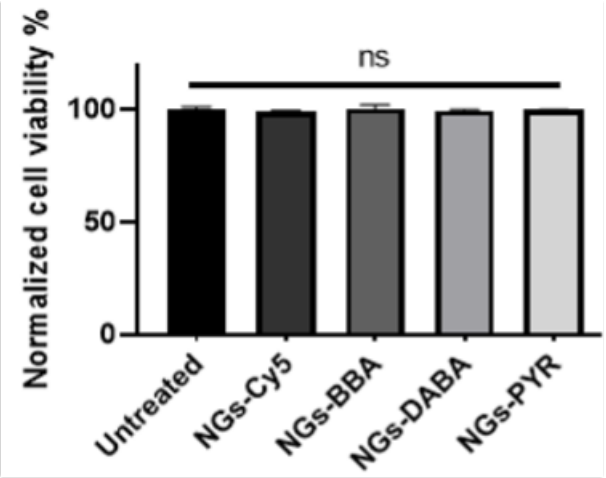

Figure 5.2.4: Cell viability by cytotoxicity assay (G6PD assay).

5.2.5 MTT assay

Cell metabolic activity on T-786O cell line was investigated by MTT assay to evaluate the therapeutic effect of Sunitinib loaded into NGs. MTT was performed using the drug-loaded NGs at sublethal concentration of 10 µM showed by the red dashed line in Figure 5.2.5.

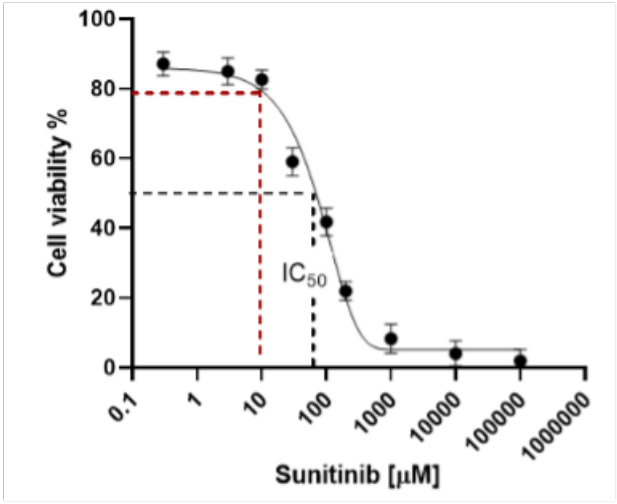

Figure 5.2.5: Dose-response curve of Sunitinib: IC_{50} level in black dashed line and the sublethal Sunitinib concentration used in red dashed line.

As shown in the Figure 5.2.6, there were no static differences between the NGs samples and the free drug and the cell metabolic activity is around 80% at 24h, while the difference between the free drug and the drug loaded in the NGs became more significant at 48h. Moreover, after 1 week of treatment, the advantages of administering drug loaded into NGs began to be appreciated. Hence, administering drug through the NGs increased the therapeutic effect compared to the free drug despite the chosen concentration did not completely reduce cell metabolic activity.

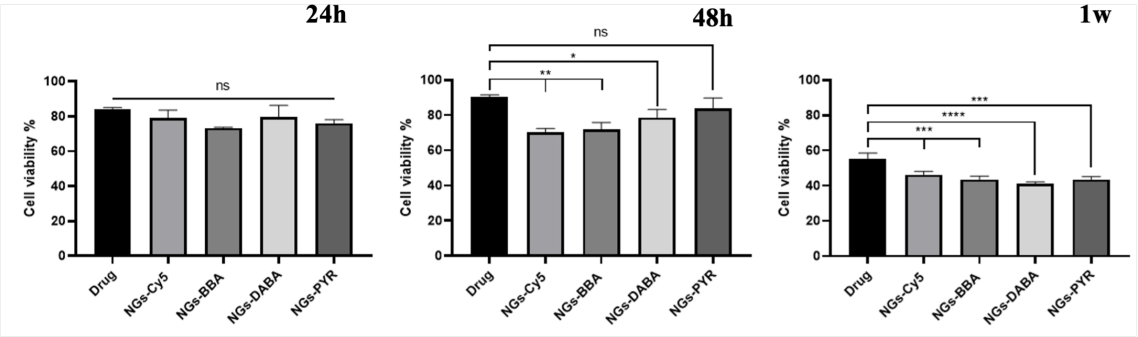

Figure 5.2.6: MTT results at 24h, 48h and 1w to evaluate the therapeutic effect comparing free drug against drug-loaded-NGs

5.2.6 Citofluorimetry

NG internalization was evaluated via flow cytometry (CytoFLEX flow cytometer, Beckman Coulter, Brea, CA) and recorded in the allophycocyanin (APC-A700) channel using CytoExpert software and quantified as median fluorescence intensity MFI fold change. The aromatic coatings modulated cell uptake and, as shown in Figure 5.2.7, the uncoated NGs (NGs-Cy5) were internalized in T-786O cells faster than coated NGs by reaching the fold increase equal to 301 at 24h and 56 at 2h compared to untreated cell (CTR). Instead, NGs-DABA had the slowest cellular internalization than the other NGs samples with a fold increase equal to 15 at 2h and 69 at 24h. An intermediate behaviour was represented by NGs-BBA and NGs-PYR with a fold increase equal to, respectively, 32; 17 at 2h and 136; 84 at 24h (Figure 5.2.7, B).

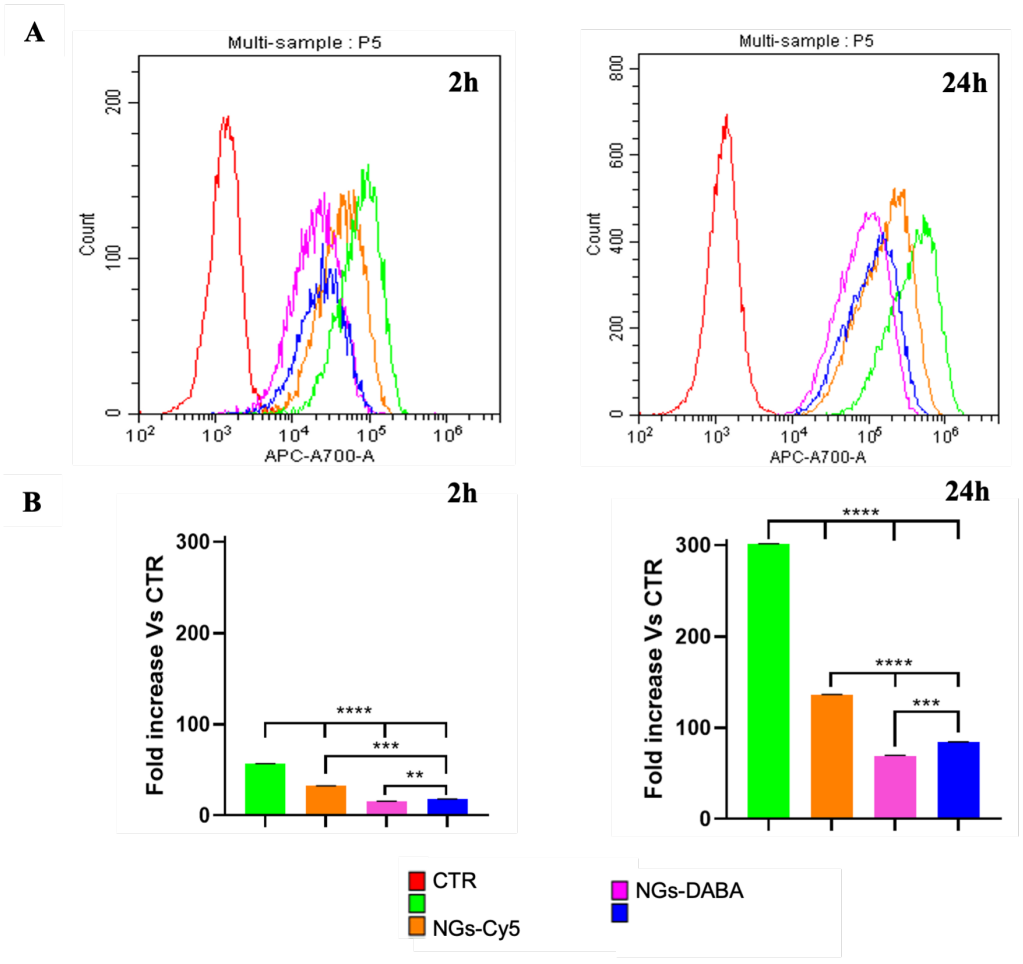

Figure 5.2.7: The NGs cellular internalization: fold increase for all nanogel types at timepoints 2h and 24h.

The behaviours previously described can be observed more intuitively through the graphs in Figure 5.2.7, A where cell uptake is identified by all curves shifted to the left of control curve (in red) and for each timepoint the cellular internalization was achieved by all NG types.

A confirmation of NGs internalization was obtained by confocal micrographs, following the cell staining after NG administration: NGs are clearly detectable in the cell cytosol thanks to their labelling with Cy5-azide. These results demonstrated that through surface decoration with specific aromatic moieties it's possible to tune NGs-cell interactions. In particular, maintaining equal laser setting, NGs-Cy5, that showed the fastest uptake, has the highest fluorescence intensity that is proportional to the amount of internalized NGs (B, F Figure 5.2.8) while NGs-BBA, that was internalized more slowly, has the lowest fluorescence intensity (D, H Figure 5.2.8).

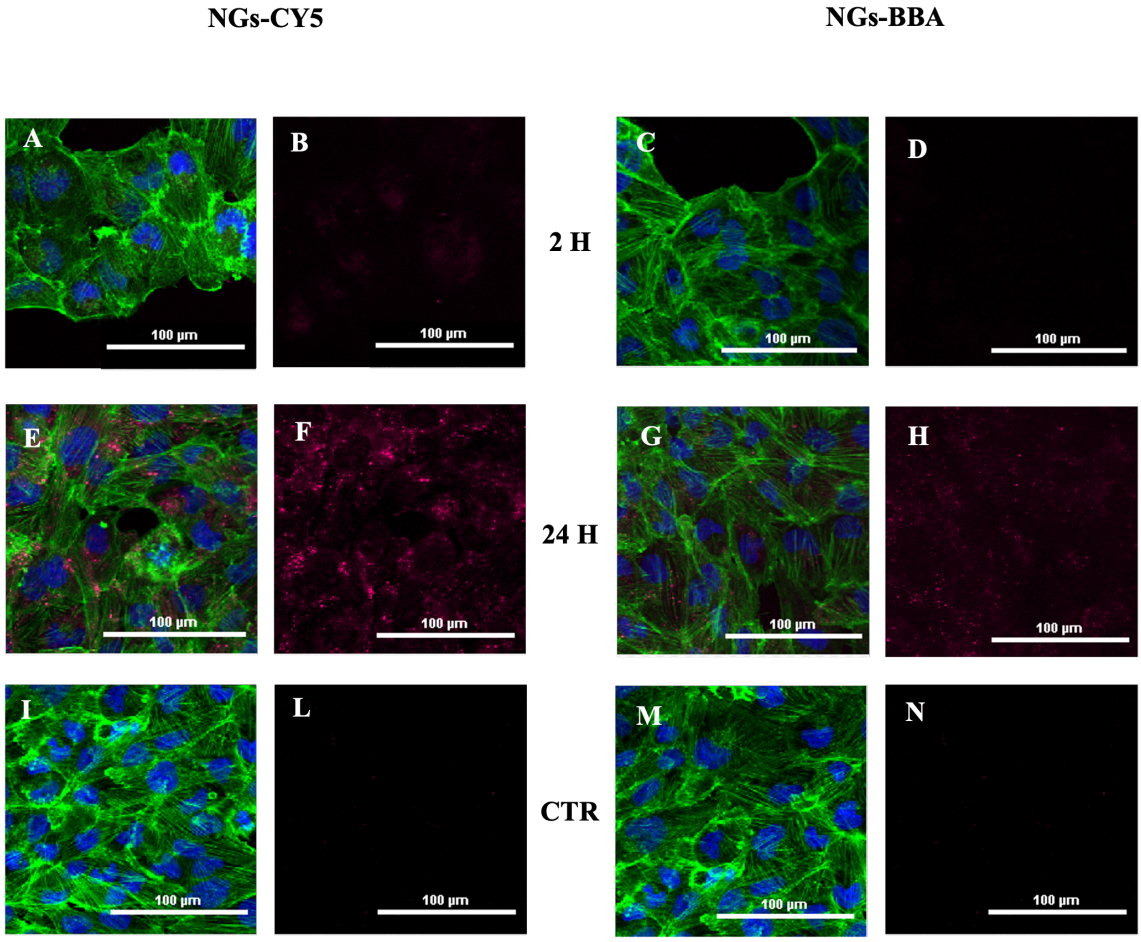

Figure 5.2.8: NGs cell internalization on plate of NGs-Cy5 and NGs-BBA compared to untreated cells (CTR) at 2h and 24h.

In addition, NGs-DABA and NGs- BBA also differed in terms of uptake as is shown in the Figure 5.2.9.

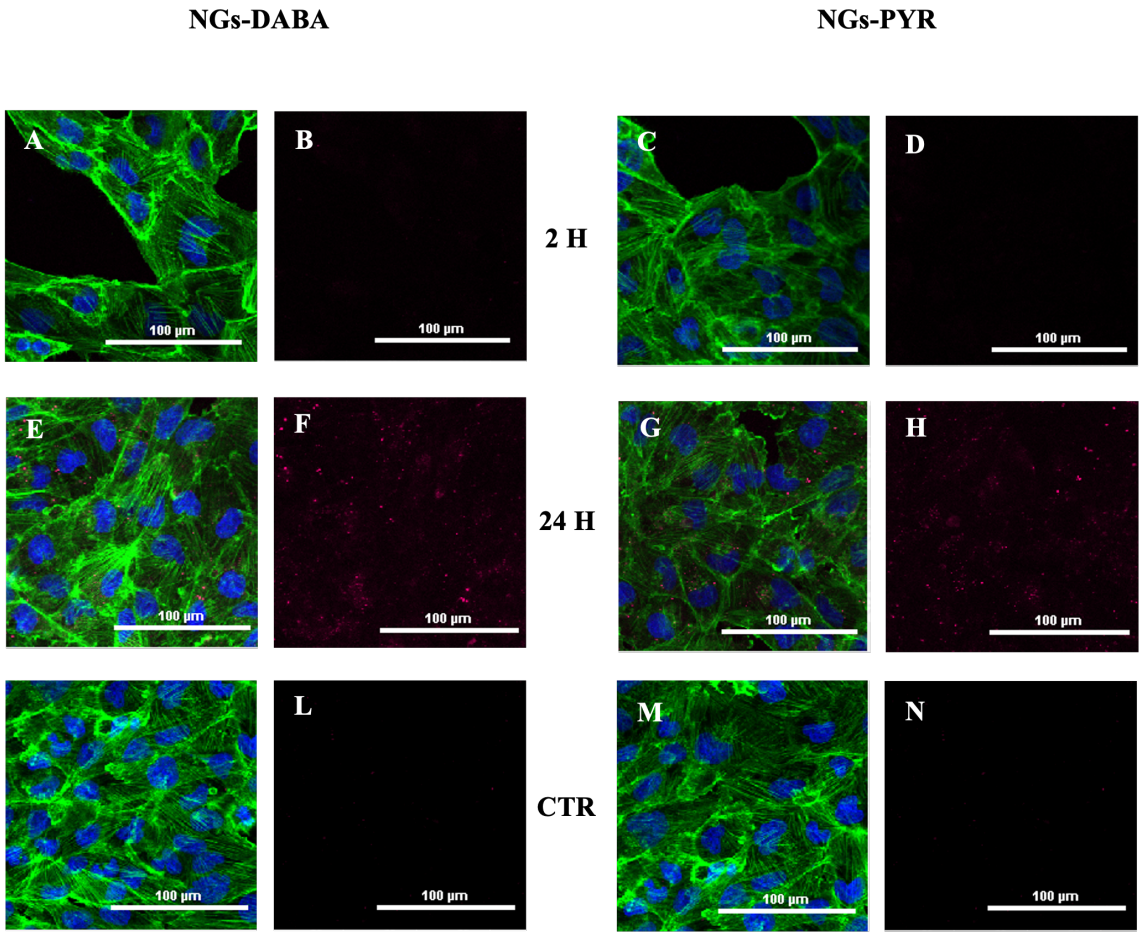

Figure 5.2.9: NGs cell internalization on plate of NGs-DABA and NGs-PYR compared to untreated cells (CTR) at 2h and 24h.

5.2.7 Microfluidic-assisted NGs cell uptake

NGs cell uptake in static condition, performed through the microfluidic platform, confirmed the trend obtained with the traditional flow cytometry as shown in Figure 5.2.10. Therefore, the microfluidic system can be a potential innovative tool on which to evaluate NGs uptake as an alternative to the traditional approach.

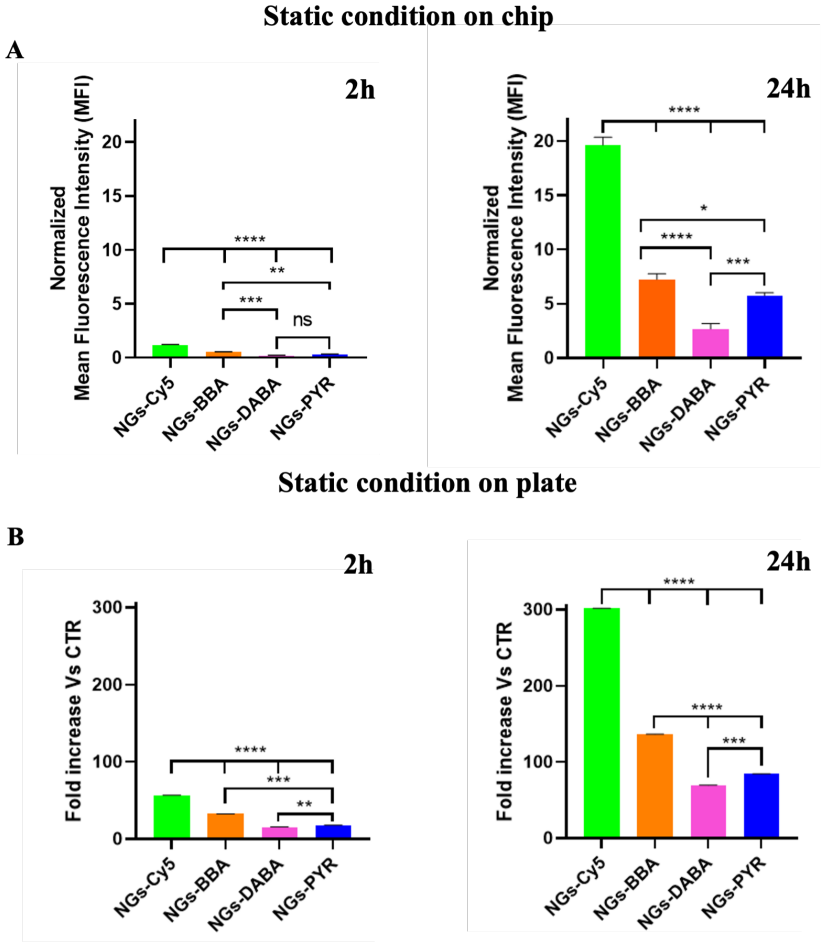

Figure 5.2.10: NGs cell uptake performed on chip in static condition at 2h and 24h (A); NGs cell uptake performed on plate at 2h and 24h (B).

The microfluidic-assisted NGs cell uptake, estimated as MFI, showed a statistically different cell uptake under dynamic condition *vs.* static condition, highlighting a higher NGs intracellular distribution closer to the *in vivo* setting.

In particular, all NGs specimens showed, in dynamic condition, a higher cell uptake compared to static condition as shown in Figure 5.2.11. Therefore, NGs-PYR compared to NGs-BBA and NGs-DABA showed a faster cell internalization for each time point, probably attributable to the π-π stacking continuous interaction between the coating PYR and cell membrane.

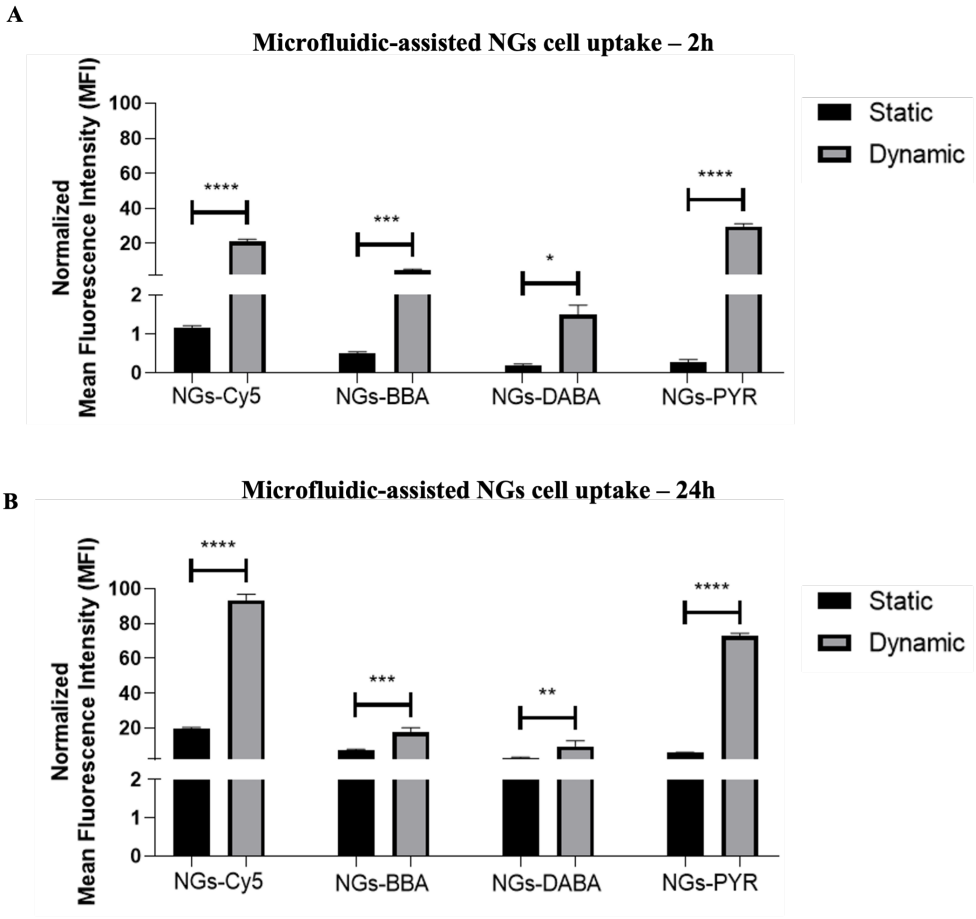

Figure 5.2.11: Microfluidic-assisted NGs cell uptake performed in static and dynamic conditions at 2h (A), Microfluidic-assisted NGs cell uptake performed in static and dynamic conditions at 24h (B).

This variation between static and dynamic conditions could be ascribed to the different diffusion regime occurring in the two microfluidic set-ups. In static conditions, the mutual interaction NGs-cells takes place within the diffusional boundary layer around cells, limiting the mass of nanoparticles overall provided for the cellular internalization. On the other hand, the sustained diffusion regime occurring in dynamic conditions ensure a continuous turnover of the NGs expose to cells.

Observing the confocal micrographs, NGs cell internalization is favoured under dynamic condition particularly for NGs-Cy5 and NGs-PYR as shown in Figure 5.2.12 and Figure 5.2.13.

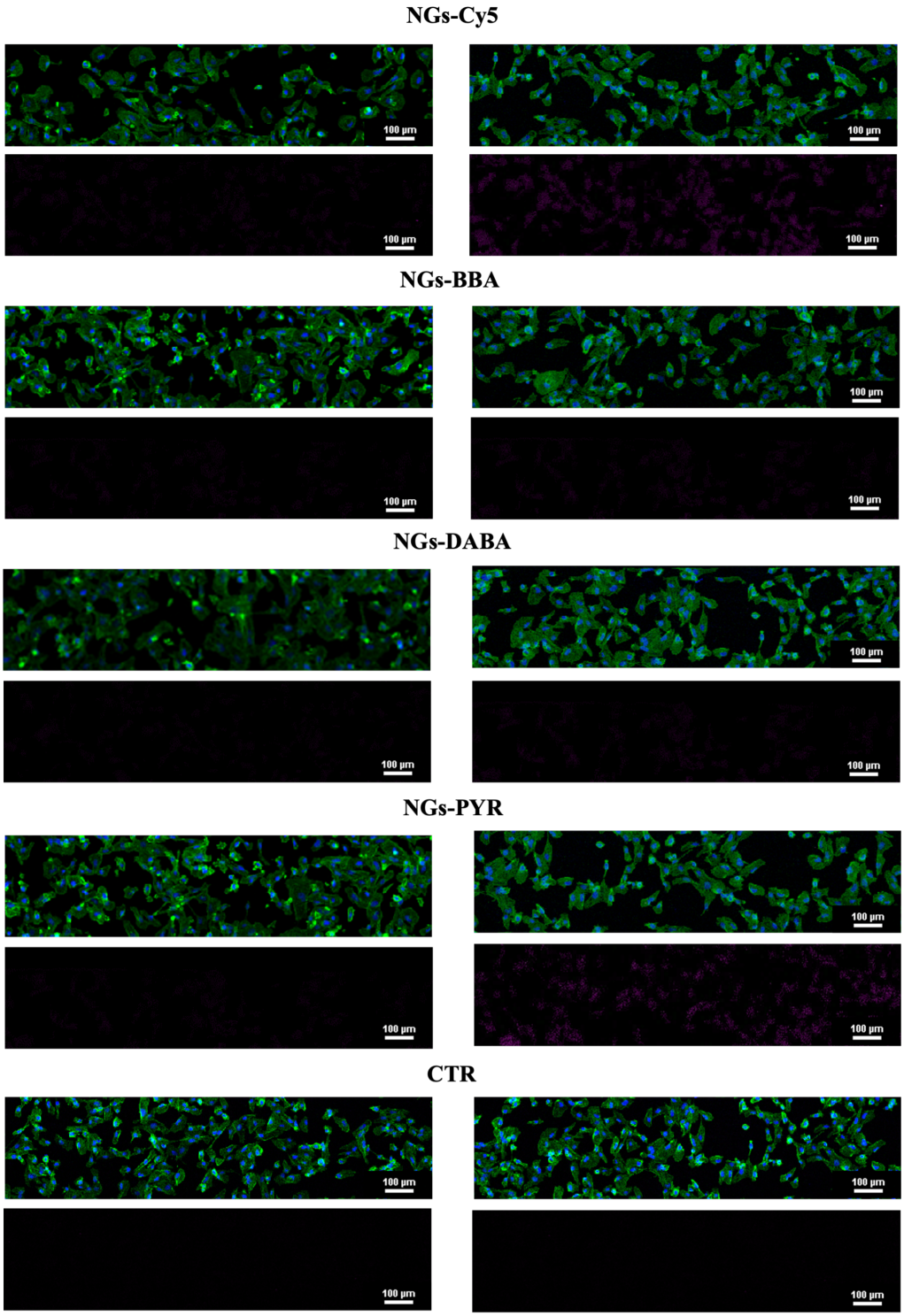

Figure 5.2.12: NGs cell internalization in static and dynamic condition performed on the microfluidic platform at 2h.

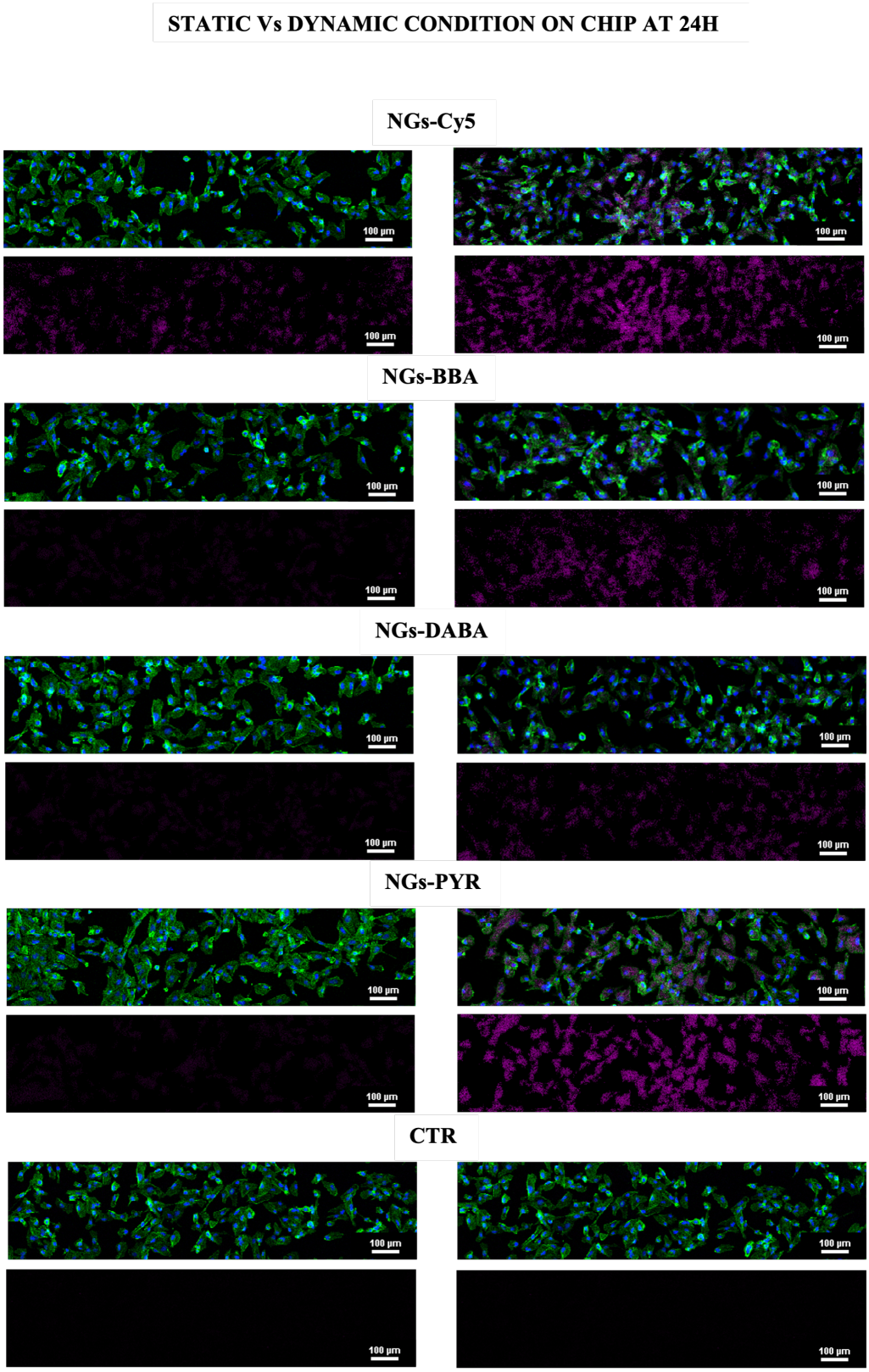

Figure 5.2.13: NGs cell internalization in static and dynamic condition performed on the microfluidic platform at 24h.

5.2.8 Discussion

Thus we demonstrated that the selected aromatic coatings on NGs surface ensure a tunable drug delivery of Sunitinib and modulate the cellular internalization in T-786O cell line. Regarding the latter, the evaluation of NGs cell uptake in flow condition through the microfluidic system has revealed a different trend from the traditional approach, more similar to the effective injection-like condition, suggesting the potential of this approach to study the NG internalization process. Overall, these results demonstrated that through aromatic surface decoration it's possible to tune NG-cell interaction and drug delivery.

Chapter 6

Conclusions and future directions

In this PhD thesis we proposed the synthesis of hydrogel systems with physical functionalization and of nanogel chemically functionalized.

As it concerns the first part we propose the synthesis of graphene-based hydrogels as thermo-sensitive carriers for controlled drug release. For this work, hydrogels were obtained via microwave-assisted condensation reaction between branched polyacrylic acid and agarose, and pristine nano-layered graphene (few layered graphene, FLG) was used as a nanofiller to investigate the graphene thermal effect in the drug release scenario. The FLG stabilization was obtained through the dispersion of exfoliated graphite in isopropyl alcohol to induce the intercalation of the solvent molecules into the graphitic interlayer spaces, providing a material with increased water dispersibility. This approach ensures the sol-gel transition in aqueous media, avoiding the use of organic solvents. Moreover, the synthetized hybrid scaffolds preserve all the peculiar features of pristine graphene, without distortions related to the oxidation processes. We investigated the drug release profile at different temperatures: 25 °C, 37 °C and 44 °C. Diclofenac, an anti-inflammatory molecule commonly used to treat musculoskeletal and systemic inflammations, was chosen as a candidate drug. Results showed tunable diclofenac release over time, according to the temperature increase. This response is not observed in polymeric scaffolds without FLG, suggesting that the thermal conductivity and the π-conjugated structure affect the vibration frequency of the nanofiller and, consequently, the electrostatic interactions with drug and the release kinetic. In particular, increasing temperature, the diclofenac release becomes faster. Furthermore, we evaluated the anti-inflammatory performance of released drug, in terms of cyclooxygenase (COX) inhibition, reporting an efficiency compar-

able to diclofenac in aqueous medium, and proving that the interactions with FLG did not affect the properties of the drug. According to ISO 10993-5, these graphene hybrid hydrogels present high biocompatibility, that confirms their potential application for thermally triggered drug release in several biomedical applications. In future studies, the graphene-based hydrogels shall be investigated as pH-sensitive carriers by acting on the charge of the system in order to be able to release the drug by exploiting the basic or acidic environment of the site of interest. For instance, in order to release a drug in the intestine, which is slightly more basic than the blood, one can exploit hydrogels that modify their structure leading to the desorption of the drug in an alkaline environment, or on the other hand, it is possible to exploit this feature to release an anticancer drug in the characteristic acidic environment of cancerous masses.

With regard to chemical functionalized nanocarriers, NGs composed of PEI-PEG were synthesized by emulsion-evaporation method then subsequently a surfacial coating was realised using three different aromatic coatings: BBA, DABA and PYR to obtain respectively NGs-BBA, NGs-DABA and NGs-PYR. Uncoated NGs (NGs-Cy5) was compared to aromatic-decorated NGs. In particular, NGs were chemically characterized by FT-IR to evaluate chemical bonding and verify NG formation and coatings. Following a preliminary evaluation of NGs cytocompatibility and physicochemical features. Then, the nanocarriers were validated as controlled drug delivery system using Sunitinib as therapeutic treatment for renal cell carcinoma T-786O. In particular, different drug release profiles were obtained for each aromatic coating confirming the possibility of using the nanomaterial for intracellular controlled drug delivery. NGs-PYR showed the slower drug release profile over time compared to NGs-BBA and NGs-DABA that exhibited a faster drug release demonstrating how aromatic-coating can modulate drug release. In addition, NGs cell uptake was evaluated using a microfluidic system in static and dynamic condition. The NGs-cell interaction in flow condition was performed to obtain a potential tool capable of mimicking the in vivo administration. The collected results showed how the selected aromatic coatings on NGs surface ensure a tunable drug delivery of Sunitinib and modulate the cellular internalization in T-786O cell line. Regarding the latter, the evaluation of NGs cell uptake in flow condition through the microfluidic system has revealed a different trend from the traditional approach, more similar to the effective injection-like conditions, suggesting the potential of this approach to study the NG internalization process. In conclusion, NGs-PYR seemed to be a promising

aromatic-decorated NGs due to high drug EE and a more controlled drug release over time than the other investigated NGs. Moreover, under dynamic conditions, it also showed higher uptake than in static condition improving NGs-cell interaction in injection-like condition. Overall, these results demonstrated that through surface decoration with specific aromatic moieties it's possible to tune NG-cell interactions and the drug delivery performances, designing versatile nanosystems suitable for the definition of future therapeutic approaches. In future studies, it could be investigated the behaviour of the same aromatic coatings by varying the ratio of NGs and coating, to assess how the surface layer can interfere in the processes already evaluated in the present work. Moreover, NGs cell uptake was investigated considering the primary renal cancer cells T-786O and it could be evaluated using metastatic cancer cells and healthy cell to investigate a selective NGs cell uptake to promote a targeted therapy approach. Considering the microfluidic device, NGs cell uptake could be assessed via a tumor-on-chip system. In detail, a microfluidic system should be developed composing of a region where cells are embedded in a gel matrix in order to create a 3D tumor and a channel where to inject NGs suspension. Specifically, the 3D tumor and NGs suspension should be connected through multi-microchannels allowing only transverse diffusion of NGs, simulating the NGs cell uptake in tumor side.

List of Figures

Bibliography

[1] N. I. o. B. I. a. Bioengineering, Drug Delivery Systems, 2018

[2] A. K. Bajpai and S. K. Shukla, "Responsive Polymers in Controlled Drug Delivery." Progress in Polymer Science, vol. 33, no. 11, pp. 1088-1118, 2008.

[3] R. A. Siegel and M. J. Rathbone, "Overview of controlled release mechanisms." Fundamentals and Applications of Controlled Release Drug Delivery, Springer US, pp. 9-43, 2012.

[4] S. Mura, J. Nicolas and P. Couvreur, "Stimuli-responsive nanocarriers for drug delivery." Nature Materials volume , vol. 12, pp. 991-1003, 2013.

[5] T.R. Hoare, D.S. Kohane, Polymer, 49 (2008) 1993-2007.

[6] Enas M. Ahmed. "Hydrogel: Preparation, characterization, and applications: A review". In: Journal of Advanced Research 6.2 (2015), pp. 105– 121. issn: 20901232.

[7] S. J. Owonubi et al. "Characterization and in vitro release kinetics of anti-malarials from whey protein-based hydrogel biocomposites". In: International Journal of Industrial Chemistry 9.1 (2018), pp. 39–52.

[8] Guochao Liao et al. "Preparation, properties, and applications of graphene-based hydrogels". In: Frontiers in Chemistry 6.SEP (2018), pp. 1–5.

[9] Mina Sattari et al. "Thermoresponsive graphene oxide - Starch micro/nano-hydrogel composite as biocompatible drug delivery system". In: BioImpacts 7.3 (2017), pp. 167–175.

[10] Dinesh K. Patel, Yu Ri Seo e Ki Taek Lim. "Stimuli-responsive graphene nano-hybrids for biomedical applications". In: Stem Cells International 2019 (2019).

[11] Alekha K. Dash e Greggrey C. Cudworth. “Therapeutic applications of implantable drug delivery systems”. In: Journal of Pharmacological and Toxicological Methods 40.1 (1998), pp. 1–12.

[12] O Okay. “Hydrogel Sensors and Actuators”. In: Hydrogel Sensors and Actuators 6 (2010), pp. 1–15.

[13] Li Jianyu e David J Mooney. Designing hydrogels for controlled drug delivery. Rapp. tecn. 2016, pp. 1–38.

[14] Paul Calvert. “Hydrogels for soft machines”. In: Advanced Materials 21.7 (2009), pp. 743–756. issn: 09359648.

[15] Kazunobu Arakaki et al. “Artificial cartilage made from a novel double- network hydrogel: In vivo effects on the normal cartilage and ex vivo evaluation of the friction property”. In: Journal of Biomedical Materials Re- search - Part A 93.3 (2010), pp. 1160–1168.

[16] Mayer et al. “NIH Public Access”. In: Bone april.12(4) (2012), pp. 276– 285.

[17] Abdullah A. Ghawanmeh et al. “Graphene oxide-based hydrogels as a nanocarrier for anticancer drug delivery”. In: Nano Research 12.5 (2019), pp. 973–990.

[18] Zhe Yang et al. “Crystallization behavior of poly(ε-caprolactone)/layered double hydroxide nanocomposites”. In: Journal of Applied Polymer Science 116.5 (2010), pp. 2658–2667.

[19] Libo Yang, James S. Chu e Joseph A. Fix. “Colon-specific drug delivery: New approaches and in vitro/in vivo evaluation”. In: International Journal of Pharmaceutics 235.1-2 (2002), pp. 1–15.

[20] Zhai Maolin et al. “The swelling behavior of radiation prepared semi-interpenetrating polymer networks composed of polyNIPAAm and hydrophilic polymers”. In: Radiation Physics and Chemistry 58.4 (2000), pp. 397–400.

[21] Mark W. Tibbitt e Kristi S. Anseth. “Hydrogels as extracellular matrix mimics for 3D cell culture”. In: Biotechnology and Bioengineering 103.4 (2009), pp. 655–663.

[22] Lin Yu e Jiandong Ding. “Injectable hydrogels as unique biomedical materials”. In: Chemical Society Reviews 37.8 (2008), pp. 1473–1481.

[23] Vladimir P Torchilin. “Targeted pharmaceutical nanocarriers for cancer therapy and imaging”. In: 9.2 (2007), pp. 128–147.

[24] Latorre, N., J. F. Silvestre, and A. F. Monteagudo. "Allergic contact dermatitis caused by formaldehyde and formaldehyde releasers." Actas Dermo-Sifiliográficas (English Edition) 102.2 (2011): 86-97.

[25] Meng, Hao, et al. "Hydrogen peroxide generation and biocompatibility of hydrogel-bound mussel adhesive moiety." Acta biomaterialia 17 (2015): 160-169.

[26] Sherwood, Noble P. “The Effect of Various Chemical Substances on the Hemolytic Reaction [with Discussion].” The Journal of Infectious Diseases 20, no. 2 (1917): 185–200.

[27] Hebling, Josimeri, et al. "Cytotoxicity of dimethyl sulfoxide (DMSO) in direct contact with odontoblast-like cells." Dental Materials 31.4 (2015): 399-405.

[28] Yi, Xiaoyang, et al. "Toxic effects of dimethyl sulfoxide on red blood cells, platelets, and vascular endothelial cells in vitro." FEBS open bio 7.4 (2017): 485-494.

[29] Sturla, Shana J., et al. "Systems toxicology: from basic research to risk assessment." Chemical research in toxicology 27.3 (2014): 314-329.

[30] Salleh, Kushairi Mohd, et al. "Hydrogel-and aerogel-based composites: Biodegradable hydrogel and aerogel polymer blend-based composites." Biodegradable Polymers, Blends and Composites. Woodhead Publishing, 2022. 355-388.

[31] Samadian, Hadi, et al. "Natural polymers-based light-induced hydrogels: Promising biomaterials for biomedical applications." Coordination Chemistry Reviews 420 (2020): 213432.

[32] Uyanga, Kindness A., et al. "Citric acid crosslinked natural bi-polymer-based composite hydrogels: Effect of polymer ratio and beta-cyclodextrin on hydrogel microstructure." Reactive and functional polymers 154 (2020): 104682.

[33] Teo, Pei Yun, et al. "Hydrophobic modification of low molecular weight polyethylenimine for improved gene transfection." Biomaterials 34.32 (2013): 7971-7979.

[34] Poncin-Epaillard, Fabienne, et al. "Surface treatment of polymeric materials controlling the adhesion of biomolecules." Journal of functional biomaterials 3.3 (2012): 528-543.

[35] Drobota, Mioara, Stefan Ursache, and Magdalena Aflori. "Surface functionalities of polymers for biomaterial applications." Polymers 14.12 (2022): 2307.

[36] Kurapati, Rajendra, et al. "Covalent chemical functionalization enhances the biodegradation of graphene oxide." 2D Materials 5.1 (2017): 015020.

[37] Hintze, Vera, Matthias Schnabelrauch, and Sandra Rother. "Chemical modification of hyaluronan and their biomedical applications." Frontiers in chemistry 10 (2022): 39.

[38] Puppi, Dario, et al. "Nano/microfibrous polymeric constructs loaded with bioactive agents and designed for tissue engineering applications: a review." Journal of Biomedical Materials Research Part B: Applied Biomaterials 102.7 (2014): 1562-1579.

[39] Cantone, Sara, et al. "Efficient immobilisation of industrial biocatalysts: criteria and constraints for the selection of organic polymeric carriers and immobilisation methods." Chemical Society Reviews 42.15 (2013): 6262-6276.

[40] Kim, Chulgu, et al. "Cyclodextrin functionalized agarose gel with low gelling temperature for controlled drug delivery systems." Carbohydrate polymers 222 (2019): 115011.

[41] J. Tan, Q. Wang and K. Tam, “Control of burst release from nanogels via layer by layer assembly.” Journal of Controlled Release, vol. 128, pp. 248-254, 2008.

[42] E. Cauchetier, M. Deniau, H. Fessi, A. Astier and M. Paul, “Atovaquone-loaded nanocapsules: influence of the nature of the polymer on their in vitro characteristics.” International Journal of Pharmaceutics, vol. 250, pp. 273-281, 2003.

[43] J. Crank, "The mathematics of diffusion.", Clarendon Press, Oxford , 1975.

[44] K. Shah, D. Umalkar, K. Rajesh, M. Patel and V. Chauhan, "Sustained release drug delivery systems." Elixir Pharmacy, vol. 35, pp. 2809-2815, 2011.

[45] C. T. Huynh and D. S. Lee, "Controlled Release." Encyclopedia of Polymeric Nanomaterials, pp. 1-12, 2014.

[46] R. Langer and N. Peppas, "Chemical and Physical Structure of Polymers as Carriers for Controlled Release of Bioactive Agents: A Review." Journal of Macromolecular Science, vol. 23, no. 1, pp. 61-126, 1983.

[47] S. Herrlich, S. Spieth, S. Messner and R. Zengerle, "Osmotic micropumps for drug delivery." Advanced drug delivery reviews, vol. 64, no. 14, pp. 1617-1627, 2012.

[48] P. Colombo, "Swelling-controlled release in hydrogel matrices for oral route," Advanced Drug Delivery Reviews, vol. 11, no. 1-2, pp. 37-57, 1993.

[49] C. C. Lin and A. T. Metters, "Hydrogels in controlled release formulations: network design and mathematical modeling." Advanced drug delivery reviews, vol. 58, no. 12, pp. 1379-1408, 2006.

[50] N. Kamaly, B. Yameen, J. Wu and O. C. Farokhzad, "Degradable Controlled-Release Polymers and Polymeric Nanoparticles: Mechanisms of Controlling Drug Release." Chemical Reviews, vol. 116, no. 4, p. 2602–2663., 2016.

[51] W. Lee and I. Chu, "Preparation and degradation behavior of polyanhydrides nanoparticles." Journal of Biomedical Materials Research, vol. 84, no. 1, pp. 138-146, 2008.

[52] V. B. F., L. Schedl and A. Göpferich, "Why degradable polymers undergo surface erosion or bulk erosion." Biomaterials, vol. 23, no. 21, pp. 4221-4231, 2002.

[53] S. Medina, M. Chevliakov, G. Tiruchinapally, Y. Durmaz, S. Kuruvilla and M. ElSayed, " Enzyme-activated nanoconjugates for tunable release of doxorubicin in hepatic." Biomaterials, vol. 34, pp. 4655-4666. , 2013.

[54] C. Chang, H. Wei, C. Quan, Y. Li, J. Liu, Z. Wang, S. Cheng, X. Zhang and Z. R. , "Fabrication of thermosensitive PCL-PNIPAAm-PCL triblock copolymeric micelles for drug delivery." Journal of Polymer Science Part A: Polymer Chemistry, vol. 46, pp. 3048-3057, 2008.

[55] C. Chang, H. Wei, D. Wu., B. Yang, N. Chen, S. Cheng, X. Zhang and R. Zhuo, "Thermo-responsive shell cross-linked PMMA-b-P(NIPAAm-co-NAS) micelles for drug." International Journal of Pharmaceutics, vol. 420, pp. 333-340, 2011.

[56] S. Abouelmagd, H. Hyun and Y. Yeo, "Extracellularly activatable nanocarriers for drug delivery to tumors." Expert Opinion on Drug Delivery, vol. 11, no. 10, pp. 1601-168, 2014.

[57] K. Min, J. Kim, S. Bae, H. Shin, M. Kim, S. Park, H. Lee, R. Park and I. Kim, "Tumoral acidic pH-responsive MPEG-poly(β-amino ester) polymeric micelles for cancer targeting therapy." Journal of Controlled Release, vol. 144, pp. 259-266, 2010.

[58] J.Q. Liu, L. Cui, D. Losic, Acta Biomater, 9 (2013) 9243-9257.

[59] S. Javanbakht, H. Namazi, Mater Sci Eng C, 87 (2018) 50-59.

[60] X. Sun et al., "Carbon nanotubes reinforced hydrogel as flexible strain sensor with high stretchability and mechanically toughness," Chem. Eng. J., vol. 382, p. 122832, 2020.

[61] A. Alam et al., "Electrically conductive, mechanically robust, pH-sensitive graphene/polymer composite hydrogels," Compos. Sci. Technol., vol. 127, pp. 119–126, 2016.

[62] Y. Y. Lv, Z. J. Huang, H. Z. Chi, X. Zheng, H. Qin, and F. Yan, "Preparation of manganese oxide/graphene oxide hydrogel for capacitive energy storage," Electrochim. Acta, vol. 330, p. 135330, 2020.

[63] S. Syama, P.V. Mohanan, Nano-Micro Lett, 11 (2019) 6.

[64] M.R. Rezapour, C.W. Myung, J. Yun, A. Ghassami, N. Li, S.U. Yu, A. Hajibabaei, Y. Park, K.S. Kim, ACS Appl Mater Interfaces, 9 (2017) 24393-24406.

[65] M. Kakran, L. Li, Key Eng Mater 508 (2012) 76-80.

[66] L. Nilewski, W. Sikkema, E. Samuel, A. Jalilov, K. Mendoza, R. Zhang, R. Huq, C. Beeton, M. Sharpe, D. Baskin, T. Kent, J. Tour, Abstr Pap Am Chem Soc, 253 (2017).

[67] L.Z. Feng, Z.A. Liu, Nanomedicine-Uk, 6 (2011) 317-324.

[68] B.M. Zhang, Y. Wang, G.X. Zhai, Mater Sci Eng C, 61 (2016) 953-964.

[69] F. Zheng, R. Li, Q. He, K. Koral, J. Tao, L. Fan, R. Xiang, J. Ma, N. Wang, Y. Yin, Z. Huang, P. Xu, H. Xu, Mater Sci Eng C, 109 (2020) 110560.

[70] A.A. Ghawanmeh, G.A.M. Ali, H. Algarni, S.M. Sarkar, K.F. Chong, Nano Res, 12 (2019) 973-990.

[71] B. Liu, C.X. Li, Z.Y. Cheng, Z.Y. Hou, S.S. Huang, J. Lin, Biomater Sci-Uk, 4 (2016) 890-909.

[72] M. Nurunnabi, K. Parvez, M. Nafiujjaman, V. Revuri, H.A. Khan, X. Feng, Y.-k. Lee, RSC Adv, 5 (2015) 42141-42161.

[73] S.J. Cheng, H.Y. Chiu, P.V. Kumar, K.Y. Hsieh, J.W. Yang, Y.R. Lin, Y.C. Shen, G.Y. Chen, Biomater Sci-Uk, 6 (2018) 813-819.

[74] U. Dembereldorj, M. Kim, S. Kim, E.-O. Ganbold, S.Y. Lee, S.-W. Joo, J Mater Chem, 22 (2012) 23845-23851.

[75] C. Wang, X. Wang, T. Lu, F. Liu, B. Guo, N. Wen, Y. Du, H. Lin, J. Tang, L. Zhang, RSC Adv, 6 (2016) 22461-22468.

[76] Z. Cheng, B. Landish, Z. Chi, C. Nannan, D. Jingyu, L. Sen, L. Xiangjin, Mater Sci Eng C, 82 (2018) 244-252.

[77] J.M. González-Domínguez, C. Martín, Ó.J. Durá, S. Merino, E. Vázquez, ACS Appl Mater Interfaces, 10 (2018) 1987-1995.

[78] I. Mellal, A. Oukaira, E. Kengne, A. Lakhssassi, Thermal Therapy Modalities for Cancer Treatment: A Review and Future Perspectives, 2017.

[79] S. Jha, P.K. Sharma, R. Malviya, Achiev Life Sci, 10 (2016) 161-167.

[80] J.M.C. Bull, Int J Hyperther, 34 (2018) 840-852.

[81] A.L. Bredlau, M.A. McCrackin, A. Motamarry, K. Helke, C. Chen, A.-M. Broome, D. Haemmerich, Crit Rev Biomed Eng, 44 (2016) 443-457.

[82] O. Ashraf, N.V. Patel, S. Hanft, S.F. Danish, World Neurosurg, 112 (2018) 166-177.

[83] M. Hernández, M. del M. Bernal, R. Verdejo, T. A. Ezquerra, and M. A. López-Manchado, "Overall performance of natural rubber/graphene nanocomposites," Compos. Sci. Technol., vol. 73, no. 1, pp. 40–46, 2012.

[84] HP Boehm, R Setton e E Stumpp. Nomenclature and terminology of graphite intercalation compounds. 1986.

[85] Kian Ping Loh et al. "The chemistry of graphene". In: Journal of Materials Chemistry 20.12 (2010), pp. 2277–2289.

[86] T. Kuila, S. Bose, A. K. Mishra, P. Khanra, N. H. Kim, and J. H. Lee, "Chemical functionalization of graphene and its applications," Prog. Mater. Sci., vol. 57, no. 7, pp. 1061–1105, 2012.

[87] I. M. Afanasov et al., "Preparation, electrical and thermal properties of new exfoliated graphite-based composites," Carbon N. Y., vol. 47, no. 1, pp. 263–270, 2009.

[88] K. R. Nandanapalli, D. Mudusu, and S. Lee, "Functionalization of graphene layers and advancements in device applications," Carbon N. Y., vol. 152, pp. 954–985, 2019.

[89] Fereshte Taherian et al. "What is the contact angle of water on graphene?" In: Langmuir 29.5 (2013), pp. 1457–1465.

[90] Lingyan Feng, Li Wu e Xiaogang Qu. "New horizons for diagnostics and therapeutic applications of graphene and graphene oxide". In: Advanced Materials 25.2 (2013), pp. 168–186.

[91] Andre K Geim e Konstantin S Novoselov. "The rise of graphene". In: Nanoscience and technology: a collection of reviews from nature journals. World Scientific, 2010, pp. 11–19.

[92] Cuili Fu e Xiaoning Yang. “Molecular simulation of interfacial mechanics for solvent exfoliation of graphene from graphite”. In: Carbon 55 (2013), pp. 350–360.

[93] Catriona McCallion et al. “Graphene in therapeutics delivery: Problems, solutions and future opportunities”. In: European Journal of Pharmaceutics and Biopharmaceutics 104 (2016), pp. 235–250.

[94] Tapas Kuila et al. “Chemical functionalization of graphene and its applications”. In: Progress in Materials Science 57.7 (2012), pp. 1061–1105.

[95] Ö. Güler and N. Bağci, “A short review on mechanical properties of graphene reinforced metal matrix composites,” J. Mater. Res. Technol., no. 6, pp. 1–26, 2020.

[96] Z. Guo, L. Song, C. G. Boay, Z. Li, Y. Li, and Z. Wang, “A new multiscale numerical characterization of mechanical properties of graphene-reinforced polymer-matrix composites,” Compos. Struct., vol. 199, pp. 1–9, 2018.

[97] S. Song et al., “Biomedical application of graphene: From drug delivery, tumor therapy, to theranostics,” Colloids Surfaces B Biointerfaces, vol. 185, p. 110596, 2020.

[98] F. Chen et al., “Graphene quantum dots in biomedical applications: Recent advances and future challenges,” Front. Lab. Med., vol. 1, no. 4, pp. 192–199, 2017.

[99] A. L. Rivera-Briso, F. L. Aachmann, V. Moreno-Manzano, and Á. Serrano-Aroca, “Graphene oxide nanosheets versus carbon nanofibers: Enhancement of physical and biological properties of poly(3-hydroxybutyrate-co-3-hydroxyvalerate) films for biomedical applications,” Int. J. Biol. Macromol., vol. 143, no. xxxx, pp. 1000–1008, 2020.

[100] S. S. Sumit Goenka, Vinayak Sant, “Graphene-based nanomaterials for drug delivery and tissue engineering,” J. Control. Release, 2013.

[101] C. M. Amado, C. J. Minahk, E. Cilli, G. Oliveira, and F. G. Dupuy, “Effects of grain dimensions and edge states on the thermal conductivity of graphene ribbons,” BBA - Biomembr., p. 183135, 2019.

[102] A. V. Savin, E. A. Korznikova, A. M. Krivtsov, and S. V. Dmitriev, "Longitudinal stiffness and thermal conductivity of twisted carbon nanoribbons," Eur. J. Mech. A/Solids, vol. 80, p. 103920, 2020.

[103] D. Sharma, S. Kanchi, M. I. Sabela, and K. Bisetty, "Insight into the biosensing of graphene oxide: Present and future prospects," Arab. J. Chem., vol. 9, no. 2, pp. 238–261, 2016.

[104] A. Ashery, A. A. M. Farag, M. A. Moussa, and G. M. Turky, "Enhancement of electrical and dielectrically performance of graphene-based promise electronic devices," Synth. Met., vol. 261, no. November 2019, p. 116303, 2020.

[105] M. Chakraborty and M. S. J Hashmi, Potential of Graphene for Miniature Sensors and Conducting Devices for Biomedical Applications. Elsevier Ltd., 2018.

[106] J. Li, X. Liu, J. M. Crook, and G. G. Wallace, "Electrical stimulation-induced osteogenesis of human adipose derived stem cells using a conductive graphene-cellulose scaffold," Mater. Sci. Eng. C, vol. 107, p. 110312, 2020.

[107] Tapas Kuila et al. "Chemical functionalization of graphene and its applications". In: Progress in Materials Science 57.7 (2012), pp. 1061–1105.

[108] Rahul Raveendran Nair et al. "Fine structure constant defines visual transparency of graphene". In: Science 320.5881 (2008), pp. 1308–1308.

[109] Peter Blake et al. "Graphene-based liquid crystal device". In: Nano letters 8.6 (2008), pp. 1704–1708.

[110] Yanwu Zhu et al. "Graphene and graphene oxide: synthesis, properties, and applications". In: Advanced materials 22.35 (2010), pp. 3906–3924.

[111] Jun Yao et al. "Chemistry, physics and biology of graphene-based nanomaterials: new horizons for sensing, imaging and medicine". In: Journal of Materials Chemistry 22.29 (2012), pp. 14313–14329.

[112] Jumana Abdul Jaleel, S Sruthi e K Pramod. "Reinforcing nanomedicine using graphene family nanomaterials". In: Journal of Controlled Release 255 (2017), pp. 218–230.

[113] Jinzhao Liu et al. “Graphene-based nanomaterials and their potentials in advanced drug delivery and cancer therapy”. In: Journal of Controlled Re- lease 286.July (2018), pp. 64–73. issn: 0168-3659.

[114] Cuili Fu e Xiaoning Yang. “Molecular simulation of interfacial mechanics for solvent exfoliation of graphene from graphite”. In: Carbon 55 (2013), pp. 350–360.

[115] Catriona McCallion et al. “Graphene in therapeutics delivery: Problems, solutions and future opportunities”. In: European Journal of Pharmaceutics and Biopharmaceutics 104 (2016), pp. 235–250.

[116] Liming Zhang et al. “Enhanced chemotherapy efficacy by sequential delivery of siRNA and anticancer drugs using PEI-grafted graphene oxide”. In: Small 7.4 (2011), pp. 460–464.

[117] Lingyan Feng, Li Wu e Xiaogang Qu. “New horizons for diagnostics and therapeutic applications of graphene and graphene oxide”. In: Advanced Materials 25.2 (2013), pp. 168–186.

[118] Kapil D Patel, Rajendra K Singh e Hae-Won Kim. “Carbon-based nanomaterials as an emerging platform for theranostics”. In: Materials Horizons 6.3 (2019), pp. 434–469.

[119] Xinchao Yang, Nana Zhao e Fu-Jian Xu. “Biocleavable graphene oxide basednanohybrids synthesized via ATRP for gene/drug delivery”. In: Na- noscale 6.11 (2014), pp. 6141–6150.

[120] Xiaoying Yang et al. “High-efficiency loading and controlled release of doxorubicin hydrochloride on graphene oxide”. In: The Journal of Physical Chemistry C 112.45 (2008), pp. 17554–17558.

[121] Xinxing Ma et al. “A functionalized graphene oxide-iron oxide nanocomposite for magnetically targeted drug delivery, photothermal therapy, and magnetic resonance imaging”. In: Nano Research 5.3 (2012), pp. 199–212.

[122] Liangzhu Feng et al. “Polyethylene glycol and polyethylenimine dual-functionalized nano-graphene oxide for photothermally enhanced gene delivery”. In: Small 9.11 (2013), pp. 1989–1997.

[123] Stefano Fusco et al. “Shape-switching microrobots for medical applications: The influence of shape in drug delivery and locomotion”. In: ACS applied materials & interfaces 7.12 (2015), pp. 6803–6811.

[124] R. P. Feynman, “There’s plenty of room at the bottom. An invitation to enter a new field of physics.” Engineering and Science magazine, California Institute of Technology, vol. 23, pp. 22-36, 1960.

[125] K. Drexlr, “Engine of Creation: The coming era of nanotechnology.” Anchor book, 1986.

[126] K. E. Drexler, C. Peterson and G. Pergamit, “Unbounding the Future: The Nanotechnology Revolution.” Book, 1991.

[127] R. A. Freitas, "Nanomedicine.", Springer, 1999.

[128] Lancet, “Nanomedicine: grounds for optimism, and a call for papers.” Lancet, vol. 362, no. 9385, 2003.

[129] D. F. Emerich and G. Thanos C., “Nanotechnology and medicine.” Expert Opinion on biological theraphy, vol. 3, no. 4, pp. 655-663, 2003.

[130] V. Wagner, B. Hüsing and S. Gaisser, “Nanomedicine: Drivers for development and possible impacts.” JRC Scientific and Technical Reports, pp. 1-116, 2008.

[131] V. Wagner, A. Dullaart, A. K. Bock and A. Zweck, “The emerging nanomedicine landscape.” Nature biotechnology, vol. 24, pp. 1211-1217, 2006.

[132] K. McNamara and S. A. M. Tofail, “Nanoparticles in biomedical applications.” Advances in Physics: X, vol. 2, pp. 54-88, 2017.

[133] J. Tiwari, R. Tiwari and S. K. Kim, “Zero-dimensional, one-dimensional, two-dimensional and three-dimensional nanostructured materials for advanced electrochemical energy devices.” Progress in Materials Science, vol. 57, no. 4, pp. 724-803, 2012.

[134] P. Couvreur and C. Vauthier, “Nanotechnology: Intelligent Design to Treat Complex Disease.” Pharmaceutical Research, vol. 23, no. 7, pp. 1417-1450, 2006.

[135] O. C. Farokhzad and R. Langer, " Impact of Nanotechnology on Drug." ASC Nano, vol. 3, no. 1, p. 16–20, 2009.

[136] A. Bangham, M. Standish and J. Watkins, "Diffusion of univalent ions across the lamellae of swollen phospholipids." Journal of Molecular Biology, vol. 13, no. 1, pp. 238-252 , 1965.

[137] M. Alavi, N. Karimi and M. Safaei, "Application of various types of liposomes in drug delivery systems." Advanced pharmaceutical bulletin, vol. 7, no. 3, pp. 3-9, 2017.

[138] G. Husseini and W. G. Pitt, "Micelles and Nanoparticles for Ultrasonic Drug and Gene Delivery." Advanced Drug Delivery reviews, vol. 60, no. 10, pp. 1137-152, 2008.

[139] H. L. Wong, R. Bendayan, A. M. Rauth, Y. Li and X. Y. Wu, "Chemotherapy with anticancer drugs encapsulated in solid lipid nanoparticles." Advanced Drug Delivery reviews, vol. 59, no. 6, pp. 491-504, 2007.

[140] S.-G. S. and J. Yarema K., "Dendrimers in Cancer Treatment and Diagnosi." Nanotechnologies for the Life Sciences, vol. 5, 2007.

[141] B. Klajnert and M. Bryszewska, "Dendrimers: properties and applications." Acta Biochimica Polonica, vol. 48, pp. 199-208, 2001.

[142] E. Abbassi, S. F. Aval, A. Akbarzadeh, M. Milani, H. T. Nasrabadi, S. W. Joo, Y. Hanifehpour, K. Nejati-Koshki and R. Pashaei-Asl, "Dendrimers: synthesis, applications, and properties." Nanoscale Research Letters , vol. 9, pp. 1-10, 2014.

[143] L. P. Mendes, J. Pan and V. P. Torchilin, "Dendrimers as nanocarriers for nucleic acid and drug delivery in cancer therapy." Molecules, vol. 22, no. 9, 2017.

[144] M. Nikzamir, A. Akbarzadeh, Y. Hanifehpour and Y. Panahi, "Applications of Dendrimers in Nanomedicine and Drug Delivery: A Review." Journal of Inorganic and Organometallic Polymers and Materials , vol. 31, no. 12, pp. 1-26, 2021.

[145] S. Svenson, "Carrier-Based Drug Delivery." Dendritic NanoTechnologies, pp. 1-22, 2004.

[146] N. Nishiyama and K. Kataoka, "Current state, achievements, and future prospects of polymeric micelles as nanocarriers for drug and gene delivery." Pharmacology & Therapeutics , vol. 112, no. 3, pp. 630-648, 2016.

[147] Y. Zhang, Y. Huang and S. Li, "Polymeric micelles: Nanocarriers for cancer-targeted drug delivery." AAPS PharmSciTech, vol. 15, no. 4, pp. 862-871, 2014.

[148] Z. P. Aguilar, "Nanomaterials for Medical Applications." in Chapter 5 - Targeted Drug Delivery, 2013, pp. 181-234.

[149] Y. Zhao, X. Li, X. Zhao, Y. Yang, H. Li, X. Zhou and W. Yuan, "Asymmetrical polymer vesicles for drug delivery and other applications." Frontiers in Pharmacology, vol. 8, no. 374, 2017.

[150] J. Petit, I. Polenz, J. C. Baret, S. Herminghaus and O. Bäumchen, "Vesicles-on-a-chip: A universal microfluidic platform for the assembly of liposomes and polymersomes." The European Physical Journal , vol. 39, no. 6, 2016.

[151] B. E. K. A. Vinogradov S, "Poly(ethylene glycol)-polyethyleneimine NanoGel(TM) particles: novel drug delivery systems for antisense oligonucleotides.for antisense oligonucleotides." Colloids Surfaces Biointerfaces, vol. 16, no. 1-4, p. 291–304 , 1999.

[152] E. Mauri, S. M. Giannitelli, M. Trombetta and A. Rainer, "Synthesis of Nanogels: Current Trends and Future Outlook." Gels, vol. 7, no. 36, pp. 1-23, 2021.

[153] S. K. Soni, S. S. Desale and T. K. and Bronich, "Nanogels: an overview of properties, biomedical applications and obstacles to clinical translation." Journal of Controlled Release, vol. 240, pp. 109-126, 2015.

[154] M. Hamidi, P. Rafiei, A. Azadi and S. Mohammadi-Samani, "Encapsulation of valproate-loaded hydrogel nanoparticles in intact human erythrocytes: a novel nano-cell composite for drug delivery." Journal of pharmaceutical sciences, vol. 100, no. 5, pp. 1702-1711, 2011.

[155] H. Cho, U. Jammalamadaka and K. Tappa, "Nanogels for Pharmaceutical and Biomedical Applications and Their Fabrication Using 3D Printing Technologies." Materials, vol. 11, no. 2, 2018.

[156] K. Raemdonck, J. Demeester and S. De Smedt, "Advanced nanogel engineering for drug delivery." Soft Matter, vol. 5, no. 4, pp. 707-715, 2009.

[157] I. Neamtu, A. G. Rusu, A. Diaconu, L. E. Nita and A. P. Chiriac, "Basic concepts and recent advances in nanogels as carriers for medical applications." Drug Delivery, vol. 24, pp. 539-557, 2017.

[158] E. Mauri, G. Perale and F. Rossi, "Nanogel functionalization: a versatile approach to meet the challenges of drug and gene delivery." ACS Applied Nano Materials, vol. 1, p. 6526–6541, 2018.

[159] F. Pinelli, O. F. Ortolà, P. Makvandi, G. Perale and F. Rossi, "In vivo drug delivery applications of nanogels: a review." Nanomedicine, vol. 15, no. 27, 2020.

[160] H. C. Huang, Barua, S., G. Sharma, S. K. Dey and K. Rege, "Inorganic nanoparticles for cancer imaging and therapy." Journal of Controlled Release , vol. 155, no. 3, pp. 344-357, 2011.

[161] T. Kim and T. Hyeon, "Applications of inorganic nanoparticles as therapeutic agents." Nanotechnology, vol. 25, no. 1, 2013.

[162] N. Erathodiyil and J. Y. Ying, "Functionalization of Inorganic Nanoparticles for Bioimaging Applications." Accounts of chemical research, vol. 44, no. 10, p. 925–935, 2011.

[163] A. Oberlin, M. Endo and T. Koyama, "Filamentous growth of carbon through benzene decomposition." Journal of Crystal Growth, vol. 32, no. 3, pp. 335-349, 1976.

[164] J. Chen, S. Chen, X. Zhao, L. V. Kuznetsova, S. S. Wong and I. Ojim, "Functionalized single-walled carbon nanotubes as rationally designed vehicles for tumor-targeted drug delivery." Journal of the American Chemical Society, vol. 130, no. 49, p. 16778–16785, 2008.

[165] K. H. Son, J. H. Hong and J. W. Lee, "Carbon nanotubes as cancer therapeutic carriers and mediators." International Journal of Nanomedicine, vol. 11, p. 5163–5185, 2016.

[166] D. Maiti, X. Tong, X. Mou and K. Yang, "Carbon-Based Nanomaterials for Biomedical Applications: A Recent Study." Frontiers in Pharmacology, vol. 9, no. 1401, pp. 1-16, 2019.

[167] N. Kobayashi, H. Izumi and Y. Morimoto, "Review of toxicity studies of carbon nanotubes." Jornal of occupational health, vol. 59, no. 5, p. 394–407, 2017.

[168] J. Shi, H. Zhang, L. Wang, L. Li, H. Wang, Z. Wang, Z. Li, C. Chen, L. Hou, C. Zhang and Z. Zhang, "PEI-derivatized fullerene drug delivery using folate as a homing device targeting to tumor." Biomaterials, vol. 34, pp. 251-261, 2013.

[169] R. Partha, L. Mitchell, R., J. Lyon, L., P. P. Joshi and J. L. Conyers, "Buckysomes: Fullerene-Based Nanocarriers for Hydrophobic Molecule Delivery." ACS Nano, vol. 2, no. 9, p. 1950–1958, 2008.

[170] I. Rašović, "Water-soluble fullerenes for medical applications" Materials Science and Technology, vol. 33, no. 7, pp. 777-794, 2017.

[171] V. A. Chistyakov, Y. O. Smirnova, E. V. Prazdnova and A. V. Soldatov, "Possible Mechanisms of Fullerene C60 Antioxidant Action." BioMed Research International, pp. 1-5, 2013.

[172] F. Kong, J. W. Zhang, R. F. Li, Z. X. Wang, W. J. Wang and W. Wang, "Unique roles of gold nanoparticles in drug delivery, targeting and imaging application." Molecules, vol. 22, no. 9, 2017.

[173] T. V. Verissimo, N. T. Santos, J. R. Silva, R. B. Azevedo, A. J. Gomes and C. N. Lunardi, "In vitro cytotoxicity and phototoxicity of surface-modified gold nanoparticles associated with neutral red as a potential drug delivery system in phototherapy." Materials Science and Engineering: C, Materials for Biological Applications, vol. 1, no. 65, pp. 199-204, 2016.

[174] S. Zeng, K. T. Yong, I. Roy, X. Q. Dinh, X. Yu and F. Luan, "A Review on Functionalized Gold Nanoparticles for Biosensing Applications." Plasmonics, vol. 6, no. 491, 2011.

[175] J. Huang and A. E. Mostafa, "Gold nanoparticles: Optical properties and implementations in cancer diagnosis and photothermal therapy." Journal of Advanced Research, vol. 1, no. 1, pp. 13-28, 2010.

[176] D. Bobo, K. J. Robinson, J. Islam and K. J. Thurecht, "Nanoparticle-based medicines: a review of FDA-approved materials and clinical trials to date." Pharmaceutical Research , vol. 33 , p. 2373–2387, 2017.

[177] A. Mashhadi Malekzadeh, A. Ramazani, S. Tabatabaei Rezaei and H. Niknejad, "Design and construction of multifunctional hyperbranched polymers coated magnetite nanoparticles for both targeting magnetic resonance imaging and cancer therapy." Journal of Colloid and Interface Science, vol. 490, p. 64–73, 2017.

[178] L. S. Arias, J. P. Pessan, A. P. M. Vieira, T. M. Toito de Lima, A. C. Botazzo Delbem and D. R. Monteiro, "Iron Oxide Nanoparticles for Biomedical Applications: A Perspective on Synthesis, Drugs, Antimicrobial Activity, and Toxicity." Antibiotics, vol. 7, no. 2, 2018.

[179] C. Rümenapp, B. Gleich and A. Haase, "Magnetic nanoparticles in magnetic resonance imaging and diagnostics." Pharmaceutical Research, vol. 29, p. 1165–1179, 2012.

[180] N. J. Halas, "Nanoscience under glass: the versatile chemistry of silica nanostructures." ACS Nano, vol. 2, pp. 179-183, 2008.

[181] S. Angelos, M. Liong, E. Choi and J. I. Zink, "Mesoporous silicate materials as substrates for molecular machines and drug delivery." Chemical Engineering Journal, vol. 137, pp. 4-13, 2008.

[182] C. Coll, L. Mondragòn, R. Martínez-Máñez, F. Sancenòo, D. Marcos. M., J. Soto, P. Amoròs and E. Pèrez-Payà, "Enzyme-mediated controlled release systems by anchoring peptide sequences on mesoporous silica supports." Angewandte Chemie International Edition, vol. 50, no. 9, pp. 2138-2140, 2011.

[183] C. Y. Lai, B. G. Trewyn, D. M. Jeftinija, K. Jeftinija, S. Xu, S. Jeftinija and V. S. Y. Lin, "A Mesoporous Silica Nanosphere-Based Carrier System with Chemically Removable CdS Nanoparticle Caps for Stimuli-Responsive

Controlled Release of Neurotransmitters and Drug Molecules." Journal of the American Chemical society , vol. 125, no. 15, p. 4451–4459, 2003.

[184] A. Bitar, N. M. Ahmad, H. Fessi and A. Elaissari, "Silica-based nanoparticles for biomedical applications." vol. 17, no. 19, pp. 1147-1154, 2012.

[185] A.A. Balandin, S. Ghosh, W.Z. Bao, I. Calizo, D. Teweldebrhan, F. Miao, C.N. Lau, Nano Lett, 8 (2008) 902-907.

[186] U.N. Temel, K. Somek, M. Parlak, K. Yapici, J Therm Anal Calorim, 133 (2018) 907-918.

[187] A. Dabrowska, S. Bellucci, A. Cataldo, F. Micciulla, A. Huczko, Phys Status Solidi B, 251 (2014) 2599-2602.

[188] A. Maffucci, F. Micciulla, A. Cataldo, G. Miano, S. Bellucci, Nanotechnology, 27 (2016).

[189] L. Pierantoni, D. Mencarelli, M. Bozzi, R. Moro, S. Moscato, L. Perregrini, F. Micciulla, A. Cataldo, S. Bellucci, Ieee T Microw Theory, 63 (2015) 2491-2497.

[190] D. Iannazzo, A. Pistone, C. Celesti, C. Triolo, S. Patane, S.V. Giofre, R. Romeo, I. Ziccarelli, R. Mancuso, B. Gabriele, G. Visalli, A. Facciola, A. Di Pietro, Nanomaterials-Basel, 9 (2019).

[191] A. Chutia, F. Cimpoesu, H. Tsuboi, A. Miyamoto, Chem. Phys. Lett. 503 (2011) 91–96.

[192] M. Potenza, A. Cataldo, G. Bovesecchi, S. Corasaniti, P. Coppa, S. Bellucci, AIP Adv, 7 (2017).

[193] N.A. Nebogatikova, I.V. Antonova, V.A. Volodin, V.Y. Prinz, Physica E, 52 (2013) 106-111.

[194] L. Rodriguez-Perez, M.A. Herranz, N. Martin, Chem Commun, 49 (2013) 3721-3735.

[195] L. Ferrigno, A. Cataldo, S. Sibilia, A. Maffucci, S. Bellucci, Nanotechnology 31 (2019) 075701.

[196] A.V. Kukhta, A.G. Paddubskaya, P.P. Kuzhir, S.A. Maksimenko, S.A. Vorobyova, S. Bistarelli, A. Cataldo, S. Bellucci, Synth. Met. 222 (2016) 192–197.

[197] A. Sacchetti, E. Mauri, M. Sani, M. Masi, F. Rossi, Tetrahedron Lett, 55 (2014) 6817-6820.

[198] C. Tang, L. Yin, J. Yu, C. Yin, Y. Pei, J. Appl. Polym. Sci. 104 (2007) 2785–2791.

[199] G. Calixto, A.C. Yoshii, H. Rocha e Silva, B. Stringhetti Ferreira Cury, M. Chorilli, Pharm Dev Technol, 20 (2015) 490-496.

[200] G. Perale, F. Rossi, E. Sundstrom, S. Bacchiega, M. Masi, G. Forloni, P. Veglianese, ACS Chem Neurosci, 2 (2011) 336-345.

[201] P. Zarrintaj, S. Manouchehri, Z. Ahmadi, M.R. Saeb, A.M. Urbanska, D.L. Kaplan, M. Mozafari, Carbohydr Polym, 187 (2018) 66-84.

[202] V. Georgakilas, M. Otyepka, A.B. Bourlinos, V. Chandra, N. Kim, K.C. Kemp, P. Hobza, R. Zboril, K.S. Kim, Chem. Rev. 112 (2012) 6156–6214.

[203] M. Santoro, P. Marchetti, F. Rossi, G. Perale, F. Castiglione, A. Mele, M. Masi, J. Physl. Chem. B, 115 (2011) 2503-2510.

[204] F. Rossi, G. Perale, G. Storti, M. Masi, J. Appl. Polym. Sci., 123 (2012) 2211-2221.

[205] A.S.K. Kumar, N. Rajesh, RSC Adv., 3 (2013) 2697-2709.

[206] M. Hayyan, A. Abo-Hamad, M.A. AlSaadi, M.A. Hashim, Nanoscale Res. Lett., 10 (2015) 324.

[207] S.M.K. Hasan, R. Li, Y. Wang, N. Reddy, W. Liu, Y. Qiu, Q. Jiang, Nanomaterials (Basel), 9 (2019) 918.

[208] F. Rossi, M. Santoro, T. Casalini, P. Veglianese, M. Masi, G. Perale, Int J Mol Sci, 12 (2011) 3394-3408.

[209] L.A. Belyaeva, P.M.G. van Deursen, K.I. Barbetsea, G.F. Schneider, Adv Mater, 30 (2018) 1703274.

[210] C. Mart-N, S. Merino, J.M. Gonzalez-Dominguez, R. Rauti, L. Ballerini, M. Prato, E. Vazquez, Sci Rep-Uk, 7 (2017).

[211] B. Bahaya, D. Johnson, C. Yavuzturk, On the Effect of Graphene Nanoplatelets on Water–Graphene Nanofluid Thermal Conductivity, Viscosity, and Heat Transfer Under Laminar External Flow Conditions, 2017.

[212] Q. Chai, Y. Jiao, X. Yu, Gels 3 (2017) 6.

[213] M.C. Catoira, L. Fusaro, D. Di Francesco, M. Ramella, F. Boccafoschi, J. Mater. Sci. Mater. Med. 30 (2019) 115.

[214] S. Ganguly, D. Ray, P. Das, P.P. Maity, S. Mondal, V.K. Aswal, S. Dhara, N.C. Das, Ultrason Sonochem, 42 (2018) 212-227.

[215] M. Bastiurea, M.S. Rodeanu, D. Dima, M. Murarescu, G. Andrei, Dig J Nanomater Bios, 10 (2015) 521-533.

[216] A.A. Balandin, Nat Mater, 10 (2011) 569.

[217] E. Fernández, D. López, C. Mijangos, M. Duskova-Smrckova, M. Ilavsky, K. Dusek, J Polym Sci Pol Phys, 46 (2008) 322-328.

[218] B. Mao, T. Divoux, P. Snabre, J Rheol, 60 (2016) 473-489.

[219] F. Rossi, G. Perale, G. Storti, M. Masi, J Appl Polym Sci, 123 (2012) 2211-2221.

[220] J. Shen, B. Yan, T. Li, Y. Long, N. Li, M. Ye, Soft Matter, 8 (2012) 1831-1836.

[221] Z. Çiplak, N. Yildiz, A. Çalimli, Fuller Nanotub Car N, 23 (2015) 361-370.

[222] R. Altman, B. Bosch, K. Brune, P. Patrignani, C. Young, Drugs, 75 (2015) 859-877.

[223] J. Kołodziejska, M. Kołodziejczyk, Reumatologia, 56 (2018) 174-183.

[224] L. Liu, M. Qing, Y. Wang, S. Chen, J Mater Sci Technol, 31 (2015) 599-606.

[225] H. Tang, Y. Zhao, S. Shan, X. Yang, D. Liu, F. Cui, B. Xing, Environ Sci Nano, 5 (2018) 2357-2367.

[226] A. Rochefort, J.D. Wuest, Langmuir, 25 (2009) 210-215.

[227] S.M. Kozlov, F. Viñes, A. Görling, Carbon, 50 (2012) 2482-2492.

[228] Y. Fu, W.J. Kao, Expert Opin Drug Del, 7 (2010) 429-444.

[229] C. Mircioiu, V. Voicu, V. Anuta, A. Tudose, C. Celia, D. Paolino, M. Fresta, R. Sandulovici, I. Mircioiu, Pharmaceutics, 11 (2019).

[230] N.A. Peppas, Pharm Acta Helv, 60 (1985) 110-111.

[231] M.V. Ghica, M. Hirjau, D. Lupuleasa, C.E. Dinu-Pirvu, Molecules, 21 (2016).

[232] C. Ferrero, A. Munoz-Ruiz, M.R. Jimenez-Castellanos, Int J Pharm, 202 (2000) 21-28.

[233] W.L. Xie, J.G. Chipman, D.L. Robertson, R.L. Erikson, D.L. Simmons, Proc Natl Acad Sci USA, 88 (1991) 2692-2696.

[234] I. Morita, Prostag Oth Lipid M, 68-9 (2002) 165-175.

[235] M. Abdolmaleki, T. Tavakoli, O. M. Jazani and R. Saeb M., "Blend membranes based on polyurethane and polyethylene glycol: exploring the impact of molecular weight and concentration of the second phase on gas permeation enhancement." Journal of Polymer Engineering, vol. 36, pp. 513-519, 2015.

[236] D. C. Arruda, C. Hoffmann, C. Charrueau, P. Bigey and V. Escriou, "Innovative nonviral vectors for small-interfering RNA delivery and therapy." Nanostructures for Novel Therapy, vol. Chapter 26, pp. 713-740, 2017.

[237] S. V. Vinogradov, A. D. Zeman, V. Batrakova E. and V. Kabanov A., "Polyplex Nanogel PEG-PEI formulations for drug delivery of cytotoxic nucleoside analogs." Journal of Controlled Release, vol. 107, no. 1, pp. 143-157, 2005.

[238] J. Sung S., H. Min S., K. Y. Cho, S. M. Y. J. Lee, Y. I. Yeom and J. K. Park, "Effect of polyethylene glycol on gene delivery of polyethylenimine." Biological and Pharmaceutical Bulletin, vol. 26, p. 492–500, 2003.

[239] C. Ganta, A. Shi, S. K. Battina, M. Pyle, S. Rana, D. H. Hua, M. Tamura and D. Troyer, "Combination of Nanogel Polyethylene glycol-Polyethylenimine

and 6 (hydroxymethyl)-1,4-anthracenedione as an Anticancer Nanomedicine." Journal of Nanoscience and Nanotechnolog, vol. 8, no. 5, p. 2334–2340, 2008.

[240] E. Mauri, E. Moroni, L. Magagnin, M. Masi, A. Sacchetti and F. Rossi, "Comparison between Two Different Click Strategies to Synthesize Fluorescent Nanogels for Therapeutic Applications." Reactive and Functional polymers, vol. 105, pp. 35-44, 2016.

[241] S. Vinogradov, E. Batrakova and A. Kabanov, "Poly(ethylene glycol)-polyethyleneimine NanoGel(TM) particles: Novel drug delivery systems for antisense oligonucleotides." Colloids and Surfaces B: Biointerfaces, vol. 16, no. 1-4, pp. 291-304, 1999.

[242] N. Zhao, S. Roesler and T. Kissel, " Synthesis of a new potential biodegradable disulfide containing poly(ethylene imine)-poly(ethylene glycol) copolymer cross-linked with click cluster for gene delivery." International Journal of Pharmaceutics, vol. 411, no. 1-2, pp. 97-205, 2011.

[243] E. Mauri, E. Moroni, L. Magagnin, M. Masi, A. Sacchetti and F. Rossi, "Comparison between two different click strategies to synthesize fluorescent nanogels for therapeutic applications." Reactive and Functional Polymers, vol. 105, pp. 35-44, 2016.

[244] H. Kolb, M. Finn and k. B. Sharpless, "Click chemistry: diverse chemical function from a few good reactions." Angewandte Chemie International Edition, vol. 40, pp. 2004-2021, 2001.

[245] C. D. Hein, X. M. Liu and D. Wang, "Click chemistry, a powerful tool for pharmaceutical sciences." Pharmaceutical research, vol. 25, no. 10, pp. 2216-2230, 2008.

[246] S. Vinogradov, E. Batrakova and A. Kabanov, "Poly(ethylene glycol)-polyethyleneimine NanoGel(TM) particles: Novel drug delivery systems for antisense oligonucleotides." Colloids and Surfaces B: Biointerfaces, vol. 16, no. 1-4, pp. 291-304, 1999.

[247] L. Wood, "Sunitinib malate for the treatment of renal cell carcinoma." Expert Opinion on Pharmacotherapy, vol. 13, no. 9, pp. 1323-1336, 2012.

[248] M. probes, "VybrantTM Cytotoxicity Assay Kit (V-23111)".

[249] J. V. Meerloo, G. J. L. Kaspers and J. Cloos, "Cell sensitivity assays: the MTT assay." Mthods in molecular biology , pp. 237-245, 2011.

[250] D. Huh, H. J. Kim, J. P. Fraser, E. D. Shea, M. Khan, A. Bahinski, G. A. Hamilton and D. E. Ingber, "Microfabrication of human organs-on-chips." Nature America, Inc, vol. 8, no. 11, pp. 2135-2157, 2013.

[251] A. Malek, S. Alper and S. Izum, Journal of the American Medical Association (JAMA), vol. 282, p. 2035–2042, 1999.

[252] E. P. Rock, V. Goodman, J. X. Jiang, K. Mahjoob, S. L. Verbois, D. Morse, R. J. R. Dagher and R. Pazdur, "Food and Drug Administration Drug Approval Summary: Sunitinib Malate for the Treatment of Gastrointestinal Stromal Tumor and Advanced Renal Cell Carcinoma." The Oncologist Regulatory Issues: FDA, vol. 12, pp. 107-113, 2007.

[253] Y. Shi, M. J. Van Steenbergen, E. A. Teunissen, L. Novo, S. Gradmann, M. Baldus, C. F. Van Nostrum and W. E. Hennink, "Π-π stacking increases the stability and loading capacity of thermosensitive polymeric micelles for chemotherapeutic drugs." Biomacromolecules, vol. 14, no. 6, pp. 1826-1837, 2013.

[254] J. Siepmanna and N. A. Peppas, "Higuchi equation: Derivation, applications, use and misuse." International Journal of Pharmaceutics, vol. 418, pp. 6-12, 2011.

[255] G. Singhvi and M. Singh, "Review: in-vitro drug release characterization models." International Journal of Pharmaceutical Studies and Research , vol. 2, pp. 77-84, 2011.

[256] E. Mauri, M. Gori, S. M. Giannitelli, A. Zancla, P. Mozetic, F. Abbruzzase, N. Merendino, G. Gigli, F. Rossi, M. Trombetta and A. Rainer, "Nanoencapsulation of hydroxytyrosol into formulated nanogels improves therapeutic effects against hepatic steatosis: An in vitro study." Materials Science & Engineering C, vol. 124, pp. 1-11, 2021.

[257] J. H. Lee and Y. Yeo, "Controlled drug release from pharmaceutical nanocarriers." Chemical engineering science, vol. 125, pp. 75-84, 2015.